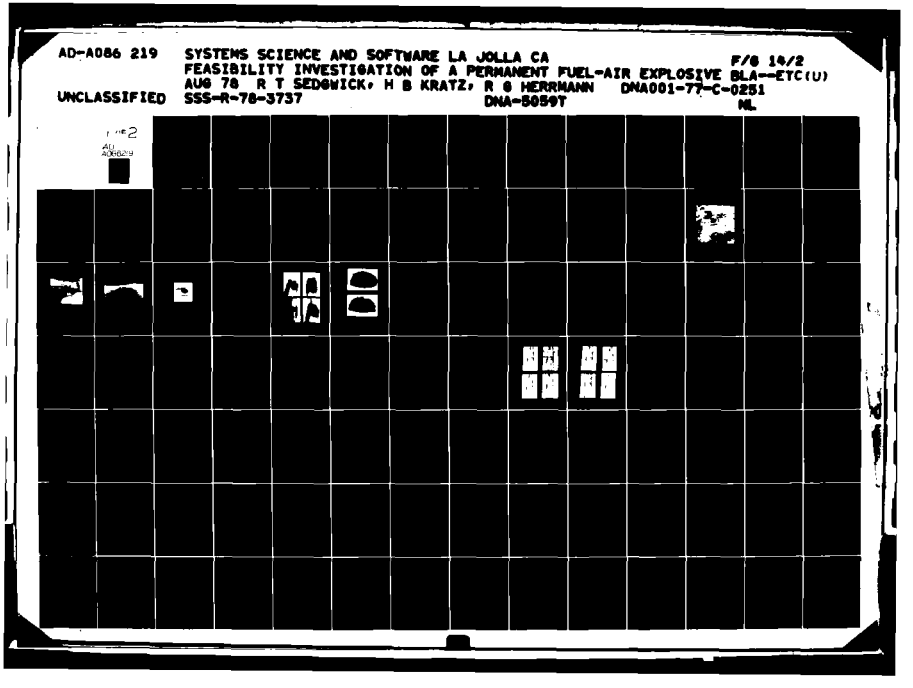
AD-A086 219
SYSTEMS SCIENCE AND SOFTWARE LA JOLLA CA
FEASIBILITY INVESTIGATION OF A PERMANENT FUEL-AIR EXPLOSIVE BLA--ETC(U)
AUG 78 R T SEDGWICK, H B KRATZ, R G HERRMANN DNA001-77-C-0251
UNCLASSIFIED SSS-R-78-3737 DNA-5059T
F/G 19/2
NL

(12) LEVEL II

AD-E300812*

DNA 5059T

FEASIBILITY INVESTIGATION OF A PERMANENT FUEL-AIR EXPLOSIVE BLAST SIMULATOR

R. T. Sedgwick
H. B. Kratz
R. G. Herrmann

Systems, Science and Software, Inc.
P.O. Box 1620
La Jolla, California 92038

9 August 1978

Topical Report for Period 9 May 1977—9 August 1978

CONTRACT No. DNA 001-77-C-0251

APPROVED FOR PUBLIC RELEASE;
DISTRIBUTION UNLIMITED.

THIS WORK SPONSORED BY THE DEFENSE NUCLEAR AGENCY
UNDER RDT&E RMSS CODE B344077464 Y99QAXSD07034 H2590D.

Prepared for
Director
DEFENSE NUCLEAR AGENCY
Washington, D. C. 20305

Destroy this report when it is no longer needed. Do not return to sender.

PLEASE NOTIFY THE DEFENSE NUCLEAR AGENCY, ATTN: STTI, WASHINGTON, D.C. 20305, IF YOUR ADDRESS IS INCORRECT, IF YOU WISH TO BE DELETED FROM THE DISTRIBUTION LIST, OR IF THE ADDRESSEE IS NO LONGER EMPLOYED BY YOUR ORGANIZATION.

UNCLASSIFIED

SECURITY CLASSIFICATION OF THIS PAGE *(When Data Entered)*

REPORT DOCUMENTATION PAGE

READ INSTRUCTIONS BEFORE COMPLETING FORM

1. REPORT NUMBER: DNA 5059T	2. GOVT ACCESSION NO.: AD-A086 219
3. RECIPIENT'S CATALOG NUMBER:	
4. TITLE *(and Subtitle)*: FEASIBILITY INVESTIGATION OF A PERMANENT FUEL-AIR EXPLOSIVE BLAST SIMULATOR.	5. TYPE OF REPORT & PERIOD COVERED: Topical Report for Period 9 May 77—9 Aug 78
	6. PERFORMING ORG. REPORT NUMBER: R-78-3737
7. AUTHOR(s): R. T. Sedgwick, H. B. Kratz, R. G. Herrmann	8. CONTRACT OR GRANT NUMBER(s): DNA 001-77-C-0251
9. PERFORMING ORGANIZATION NAME AND ADDRESS: Systems, Science & Software, Inc., P.O. Box 1620, La Jolla, California 92038	10. PROGRAM ELEMENT, PROJECT, TASK AREA & WORK UNIT NUMBERS: Subtask Y99QAXSD070-34
11. CONTROLLING OFFICE NAME AND ADDRESS: Director, Defense Nuclear Agency, Washington, D.C. 20305	12. REPORT DATE: 9 August 1978
	13. NUMBER OF PAGES: 150
14. MONITORING AGENCY NAME & ADDRESS *(if different from Controlling Office)*	15. SECURITY CLASS *(of this report)*: UNCLASSIFIED
	15a. DECLASSIFICATION DOWNGRADING SCHEDULE

16. DISTRIBUTION STATEMENT *(of this Report)*

Approved for public release; distribution unlimited.

17. DISTRIBUTION STATEMENT *(of the abstract entered in Block 20, if different from Report)*

18. SUPPLEMENTARY NOTES

This work sponsored by the Defense Nuclear Agency under RDT&E RMSS Code B344077464 Y99QAXSD07034 H2590D.

19. KEY WORDS *(Continue on reverse side if necessary and identify by block number)*

Fuel-Air Explosive
Airblast
Dissemination
Detonation
Nuclear Blastwave Simulation
Propylene Oxide
Permanent Blastwave Simulation
Reuseable Blastwave Simulation

20. ABSTRACT *(Continue on reverse side if necessary and identify by block number)*

Initial results from an investigation to determine the feasibility of using fuel-air-explosives (FAE) to simulate the airblast from a 1 KT nuclear blast are reported. A small scale blast facility was developed and tested. Up to 22.7 kg (50 lbs) of fuel such as propylene oxide can be disseminated through a hemispherical nozzle head containing 600 nozzles to form 9.14 m (30 ft) diameter hemispherical clouds which are subsequently detonated. The measured pressure history and impulse from

DD FORM 1 JAN 73 1473 EDITION OF 1 NOV 65 IS OBSOLETE

UNCLASSIFIED

SECURITY CLASSIFICATION OF THIS PAGE *(When Data Entered)*

20. ABSTRACT (Continued)

several experiments were scaled and compared with 1 KT nuclear blastwave data. These initial results indicate that FAE can be used to simulate nuclear blastwaves and that continued effort to develop the technology required to design a permanent, reuseable 1 KT FAE nuclear blastwave facility is therefore warranted.

TABLE OF CONTENTS

I. INTRODUCTION

The development of a permanent reusable fuel-air-explosive (FAE) blast facility would greatly facilitate the simulation of free-air blast waves from nuclear events for yields as high as 1 KT. The work reported herein was performed for the purpose of investigating the feasibility of such an FAE blast simulator.

The technical program was divided into two phases. The objective of Phase I was to demonstrate the use of FAE for simulating nuclear blast waves. To accomplish this objective, a test facility was developed for small-scale fuel dissemination and detonation experiments. The facility consisted of a fuel dispenser with a hemispherical nozzle head which was pressurized to force fuel through nozzles to form 9.1-m (30-ft) diameter hemispherical FAE clouds. After sufficient delay for fuel-air mixing, the clouds were detonated. The test pad was instrumented with gauges for measuring both side-on (static) and stagnation pressures. These gauges, together with high-speed photography, provided sufficient data to determine cloud detonability, cloud symmetry, and detonation efficiency. The blast waveforms generated in this manner were scaled and compared with nuclear blast wave data. The agreement between the FAE data and the nuclear data indicated that the use of FAE as a nuclear blast wave simulator is indeed feasible, at least on the small scale.

The Phase II portion of the program involved investigating the feasibility and practicability of a reusable FAE blast facility. This program phase was more engineering oriented than was the Phase I portion and dealt with various problem areas associated with the development and operation of an actual blast facility including hardware configuration, fuel dispersal techniques, initiation and cloud detonation, fuel

efficiency, repeatability, safety, and construction and life-cycle costs. While all of these facility-oriented problems were addressed to some degree, the Phase I portion of the program received greater emphasis during the performance of the contract.

Section II of this report contains a general discussion of FAE blast simulation. The specific FAE blast simulator concept under study is then presented in Section III. In Section IV the technical program for determining the feasibility of the FAE blast simulator is discussed in detail and specific areas of investigation in both the Phase-I and Phase-II portions of the program are outlined. In Section V the FAE test facility is described in detail, the test program is outlined, and results from the experimental program are presented and discussed. In Section VI scaling laws and FAE-nuclear equivalences are discussed, followed by a comparison of scaled FAE experimental results with nuclear data in Section VII. Details of the proposed full-scale simulator are then described in Section VIII and Section IX presents conclusions and recommendations.

While several problems remain to be solved, the results of this study indicate that it is possible to scale the fuel dispensers to a size sufficient to disseminate fuel into 160-m (524-ft) diameter hemispherical clouds, which should be sufficient to simulate nuclear blasts for yields up to 1 KT.

The advantages of such a blast facility include: the absence of cratering, ejecta and significant ground shock; a short turnaround time between blast wave experiments; and relatively lower costs per experiment when compared with other means of blast simulation. These advantages, along with results from the feasibility study, lead to our recommendation for continued developmental work towards the construction of a large-scale FAE blast simulator. The existence of such

a simulator should greatly enhance the state-of-the-art of blast wave simulation and provide a means for accelerating our knowledge of blast wave-structural interactions.

II. FAE BLAST SIMULATION

Prior to the current effort, there existed some indication that FAE could be used for nuclear blast simulation. Comparisons between nuclear data and existing FAE data, both experimental and theoretical, had been made and generally reasonable agreement between the nuclear and FAE data was noted. Since the data used in these comparisons were generated under various programs, none of which had as an objective the comparison of FAE and nuclear blast wave data, the detailed comparisons needed to determine the feasibility of FAE as a nuclear blast simulator were not available. This lack of detailed information gave rise to the Phase-I portion of the current program, the objective of which was to perform experiments for the specific purpose of collecting sufficient data to determine the feasibility of FAE for nuclear blast simulation. In this section, FAE blast simulation is discussed in general and some of the background which led to the formulation of the Phase-I portion of the current program is presented.

Figure 1 is a plot of static overpressure versus range in which experimental FAE data obtained at the Naval Weapons Center have been scaled according to the "cube-root law." The scale factor applied to the range was the cube root of the ratio of the energy yield of an FAE cloud equivalent to a 1-KT nuclear yield to the yield of the FAE cloud tested. These scaled FAE data are then compared with the static overpressure range curve from a 1-KT nuclear shot. It is seen in Figure 1 that while there is some scatter in the FAE data, agreement with the nuclear curve is generally good. An additional point is plotted on the curve in Figure 1 from an FAE finite difference calculation involving the detonation of an ideal hemispherical cloud formed from 136,000 kg (300,000 lb) of propylene oxide homogeneously mixed with air

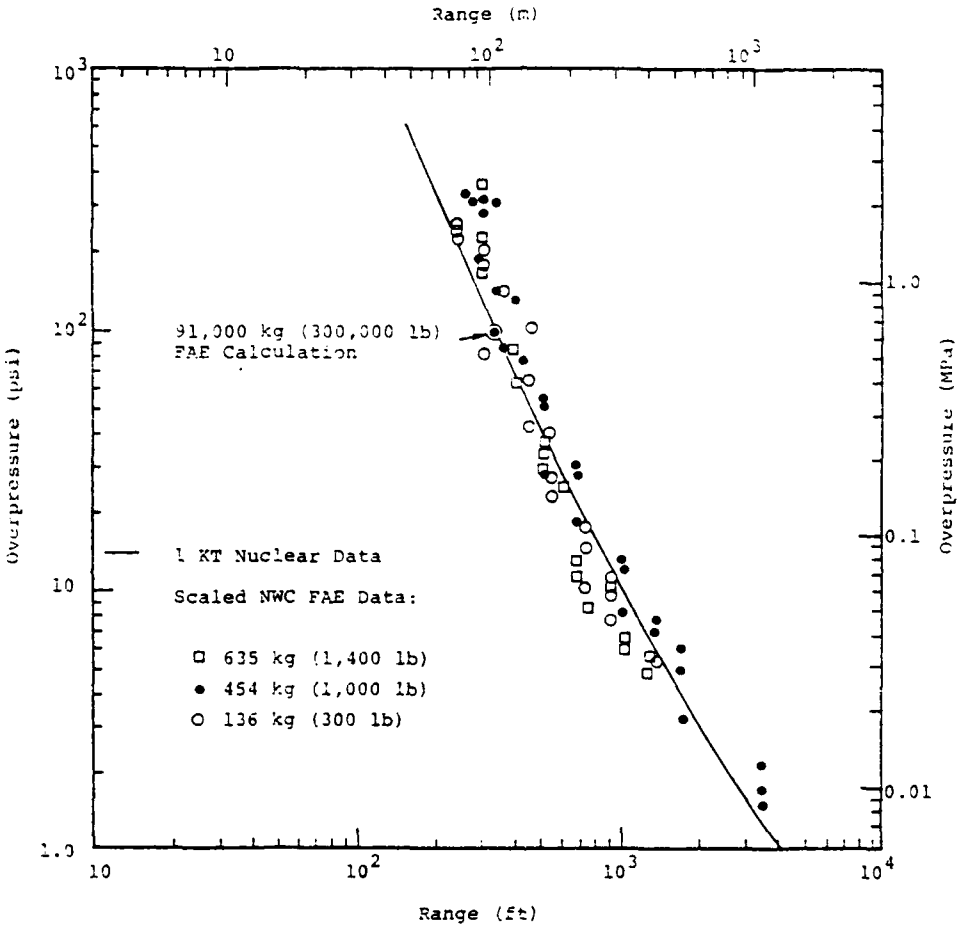

Figure 1. Peak overpressure as a function of range from a 1-KT nuclear blast compared with scaled peak overpressures from FAE data collected at the Naval Weapon Center (NWC). A single point from a hydrodynamic calculation involving 136,000 kg (300,000 lb) of fuel dispersed homogeneously into a 90-m (295 ft) radius cloud is shown for comparison.

and initiated at the center. It is seen in the figure that agreement between the calculation and both the FAE and nuclear data is good.

In order to simulate nuclear blast phenomena, however, it is necessary that the waveform, i.e., static overpressure as a function of time at a given range, be in agreement with similar data from a nuclear blast. Figure 2 is a plot of the blast waveform from a 1-KT nuclear event at a range of 113 m (370 ft). The peak static overpressure at that range is 0.68 MPa (100 psi). The FAE finite difference calculation predicted a value of that peak overpressure at a range of 105 m (345 ft). The calculated FAE blast waveform at that range is also shown in Figure 2. It is seen that agreement between the FAE and nuclear waveforms is reasonable, especially since the nuclear curve, which was generated by Brode's equation[1], predicts a slightly lower value of pressure in this pressure range.

If indeed the peak pressure and blast waveforms from an FAE blast of given weight of fuel and a given range agree with similar blast waveforms from a nuclear event of given yield and given range, the question that remains to be answered in order to use FAE as a simulator is: What is the nature of the transformation from the FAE data to the nuclear data? Thus, a curve such as the one shown in Figure 3, relating the scaled range, r, on the blast simulator using a yield, W, to the scaled range, R, of a nuclear event of yield, Y, must be generated. Such a curve is the locus of all points for which the FAE and nuclear blast waveforms are in good agreement. Once such a curve is established, it will be possible to simulate the blast waveform at a range, R, from a nuclear event of yield, Y, by locating on Figure 3 the ordinate, $z_o = r/W^{1/3}$ which corresponds to the scaled range, $Z_o = R/Y^{1/3}$.

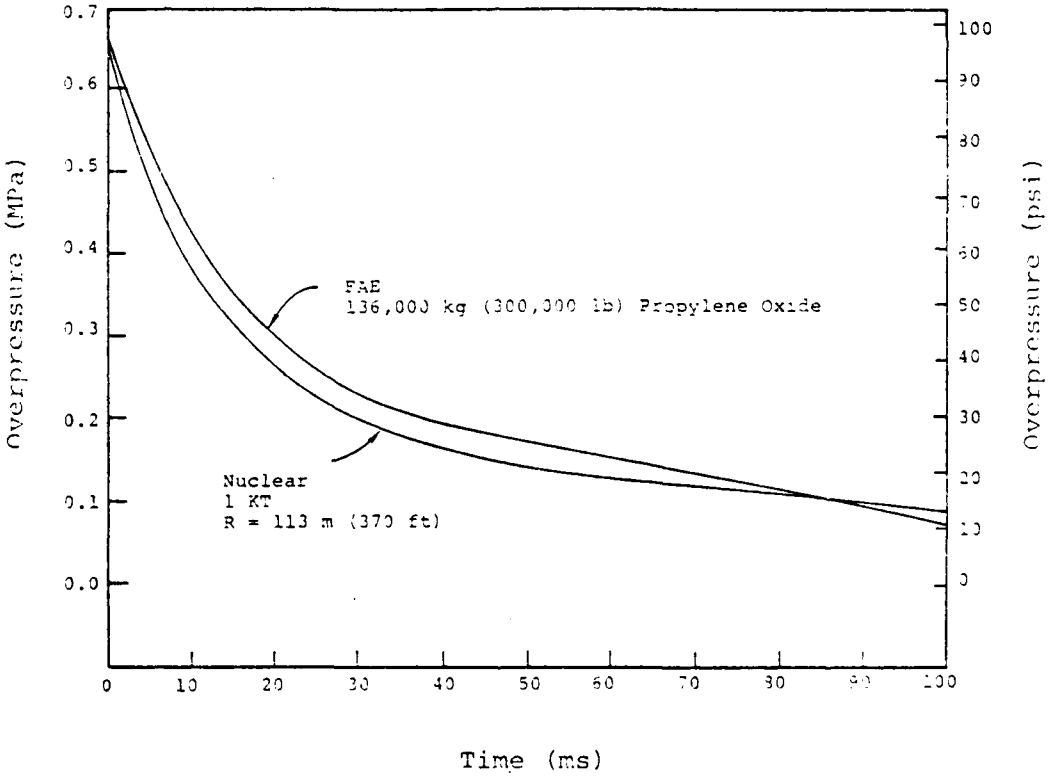

Figure 2. Comparison of predicted nuclear and FAE overpressure as a function of time. The 1-KT nuclear blast waveform is that predicted by Brode's equation [1] at a range of 113 m. The FAE blast waveform is predicted by a finite difference hydrodynamic code at a range of 105 m from the center of a homogeneous, hemispherical propylene oxide/air cloud. The ranges at which the comparison was made was chosen on the basis of equal peak overpressures of 0.68 MPa (100 psi).

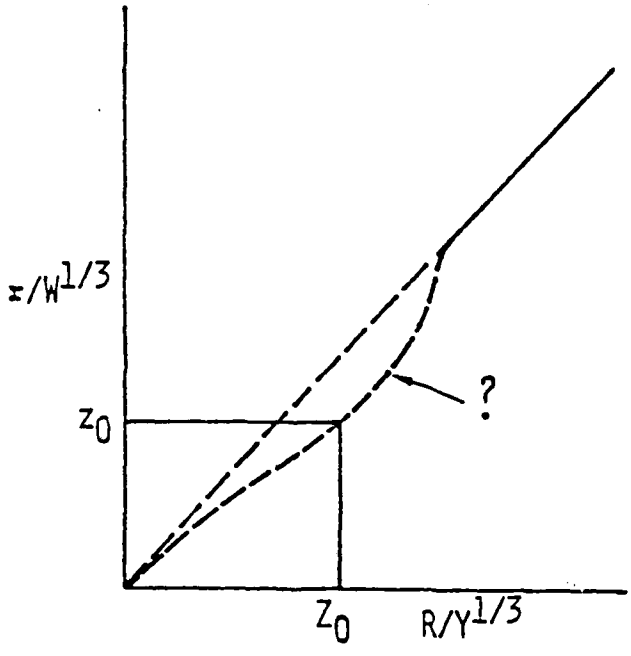

Figure 3. Schematic indicating a possible curve relating scaled nuclear data to scaled FAE data. The curve is the locus of all points at which the nuclear and FAE blast waveforms and impulses are in good agreement. The dashed portion of the curve is currently unknown; however, it is expected that at long ranges the curve should asymptotically approach a straight line.

Any value of z_o for which the curve is valid, gives a combination of fuel weight and range on the blast simulator pad that simulates the nuclear blast waveform of interest. Gauges and test structures could then be placed at that range on the pad. To facilitate the simulation process, a computer program could be developed to provide the dynamic quantities of interest at that range. These quantities would include the peak pressures, the waveform and the static and dynamic impulses associated with the nuclear event, as well as similar quantities from scaled FAE calculations and experimental data.

A procedure has been outlined for generating the FAE scaled nuclear range curve shown in Figure 3. A simple computer program has been developed following the flowchart shown in Figure 4. It will generate both the FAE-nuclear scaled range curve as well as the predicted and measured FAE blast waveforms and nuclear blast data for the specific value of z_o of interest. As seen in the flowchart, a given range, r_o, is chosen and plots of peak static overpressure and impulse from an FAE experiment involving a yield, W_o, are plotted at that range. From digitized nuclear blast data involving peak pressures within, say, ten percent of the measured peak pressure, values of scaled range as well as scaled pressure-time histories and impulses are generated. Statistical methods are then employed to select the particular set of scaled nuclear curves that are in best agreement with the FAE blast data. The value of the scaled nuclear range associated with the best set of scaled nuclear curves is then plotted versus the scaled FAE range to give a single point on the FAE-nuclear scaled range curve (Figure 3). The process is then repeated until a sufficient number of ranges has been selected to provide a complete curve. As new experimental data are gathered, the data base stored in the computer program can be expanded and a more accurate FAE-nuclear scaled range curve can be obtained. In addition, the data base containing the theoretical FAE blast waveforms, as well

Given: (1) Static overpressure and impulse histories $P_i^e(t)$ and $I_i^e(t)$ at ranges, r_i, from an FAE experiment of yield, W.

(2) Static overpressure and impulse histories $P^n(Z,t)$ and $I^n(Z,t)$ for all scaled ranges $Z = R/Y^{1/3}$ from nuclear data.

The following procedure, applied to a particular FAE range, r_i, determines one point on the curve in Figure 3.

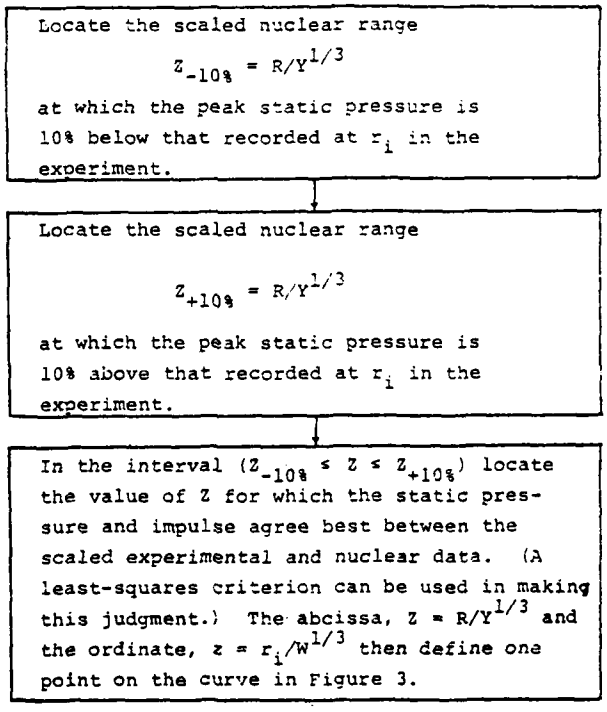

Figure 4. Flowchart outlining the procedure for generating the curve of Figure 3 for relating scaled FAE ranges to scaled nuclear ranges.

as the nuclear blast waveform data, can also be expanded so that eventually the program will be a tool that can be used in conjunction with the final blast wave facility to provide the user with the necessary data for designing blast wave-structural interaction tests.

III. FAE BLAST SIMULATOR CONCEPT

The blast simulator concept under investigation here involves the use of a central fuel dispenser made up of several pressurized dispenser units which will disseminate fuel through nozzle heads into hemispherical clouds 160 m (524 ft) in diameter. A sketch of the proposed simulator is shown in Figure 5. Each dispenser unit must be capable of projecting the fuel out to an 80-m (262-ft) reach and fill a solid angle of the hemispherical cloud. It is envisioned that propellants will be used to pressurize the dispensers and that the pressure will be tailored to fill the desired volume.

It is anticipated that the full-scale facility will consist of a cluster of dispenser units each having a capacity of approximately 3,000 kg (6608 lbs) of fuel for a total facility capability of 119,000 kg (262,000 lb) of fuel. These dispenser units will be below ground so that the nozzle heads will be close to the ground surface. The cluster of dispenser units is expected to be approximately 18.3 m (60 ft) in depth and about 4.6 m (15 ft) in radius. The radius of the dispenser is, therefore, small compared to the radius of the FAE cloud and the dispenser can thus be considered a point disseminator.

The full-scale blast simulator facility will be instrumented with pressure gauges located at various ranges both inside and outside the cloud radius. These gauges will measure both side-on and stagnation pressures. In addition, several high-speed cameras will be placed at various locations in order to get a relative measure of detonation efficiency.

To design a blast wave simulation test on an actual structure, the user must first choose the yield of the nuclear blast being simulated and the range from that blast at which he wishes to place the structure. The FAE-nuclear scaled

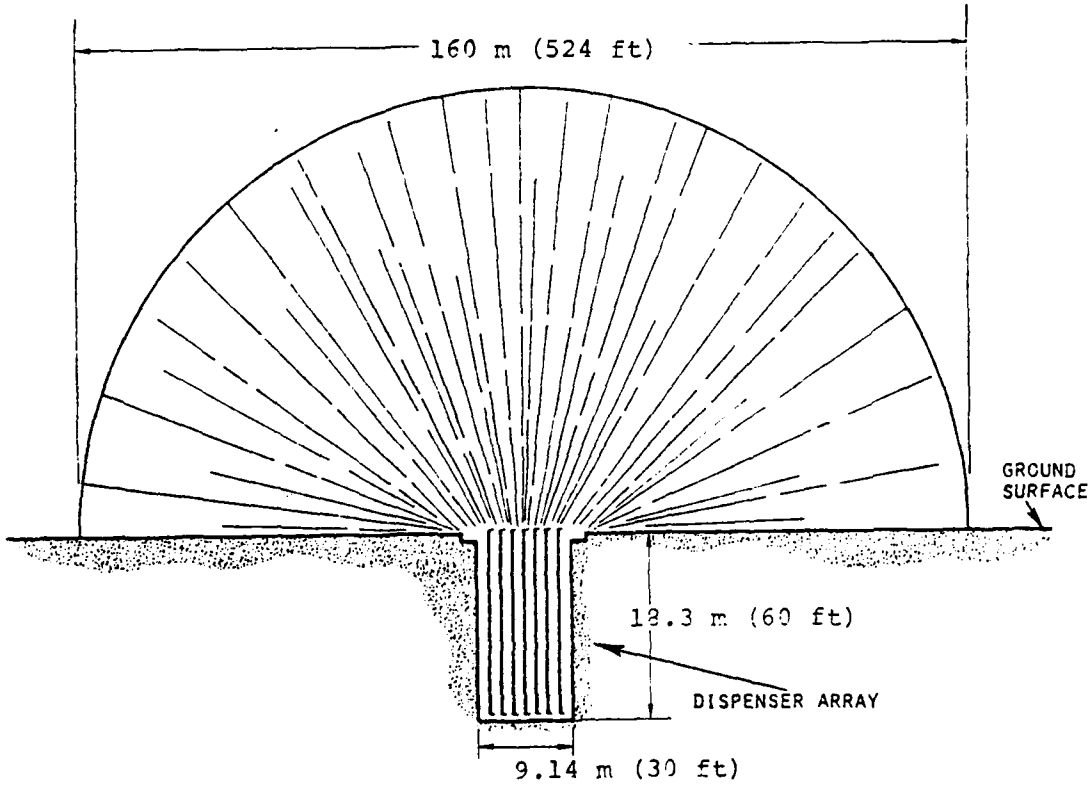

Figure 5. Schematic diagram showing clustered array of fuel dispensers for disseminating a 160-m (524-ft) diameter fuel-air explosive cloud.

range curve of Figure 3 will then provide the user with the scaled range at which the structure must be placed on the blast simulator pad. A computer program will be available to provide the user with the expected static overpressure time curve at that scaled range.

The details of the proposed full-scale blast wave simulator will be discussed in greater detail in Section VIII.

IV. TECHNICAL PROGRAM

The technical program that was outlined to perform the feasibility investigation of the particular full-scale blast wave simulator concept discussed in the last section has been divided into two phases. The objective of the Phase-I portion of the program was to investigate the feasibility of using FAE as a nuclear blast simulator. To demonstrate this feasibility, a small-scale fuel disseminator facility was developed. This facility was used to disseminate fuel, detonate the resulting FAE clouds and measure pressure-time histories at various ranges. Both side-on and stagnation pressures were measured at various ranges from the center of the facility, and the following blast wave quantitites were either directly measured or determined from the measured values:

- $P(t)$
- $P_{max}(r)$
- $I_p = \int_o^{t+} P(t)\, dt$
- $q(t) = \frac{1}{2} \rho u^2$
- $I_q = \int_o^{t+} q(t)\, dt$

where P is static overpressure, ρ is mass density, u is particle velocity, q is dynamic pressure and I_p and I_q are respectively the positive phase static and dynamic impulses.

The Phase-II portion of the program involves investigating to some degree the following engineering-oriented aspects of the proposed blast simulator:

- Facility hardware configuration
- Fuel dispersal techniques
- Initiation/detonation
- Fuel efficiency and safety
- Repeatability
- Construction and life-cycle costs

In addition to the above considerations, the question of scaling to the large-scale blast facility must also be addressed. While it is known that the blast waveforms from two clouds similar in shape will scale according to the cube-root law, i.e., the ratio of the yields to the one-third power, the scaling laws governing the dissemination process are not completely understood. Thus, even if the small-scale blast simulator demonstrates the feasibility of using FAE to simulate nuclear blast wave phenomena, it must be shown that the proposed full-scale blast simulator concept can indeed disseminate fuel into a homogeneous detonable cloud of 80-m (262-ft) radius. As part of Phase II, therefore, several single nozzle tests were performed in which both water and propylene oxide were disseminated to determine the extent of the plume formed. The results to date of the single-nozzle tests will be discussed in Section V.

V. EXPERIMENTAL INVESTIGATION

5.1 U-TUBE TEST FACILITY

In order to measure the pressure-time histories from FAE blast waves, an experimental test facility was developed for the purpose of disseminating 22.7 kg (50 lb) of propylene oxide fuel into a 9.1-m (30-ft) diameter hemispherical fuel-air cloud. The facility involves a U-tube with a nozzle head on one leg and a pressure supply on the other. As shown in Figure 6, the pressure supply end of the U-tube contains water which when pressurized drives a piston and forces fuel through the nozzle head to form the fuel-air cloud. Figure 7 is a photograph of the facility showing both the nozzle end and pressurized end of the U-tube. A typical nozzle head for disseminating hemispherical fuel-air clouds is shown and is composed of an 8-inch diameter hemispherical shell having a thickness of 7.9 mm (0.31 in). Originally, 605 2.4-mm (3/32-in) diameter holes were drilled in the nozzle head shown. During the course of the investigation, however, it was found that a more nearly hemispherical cloud could be formed if the holes near the center of the nozzle were larger than those near the periphery.

A plan view of the test pad is shown in Figure 8. The location of the nozzle head is shown along with the diameter of an FAE cloud that is formed from 22.7 kg (50 lb) of propylene oxide. Two perpendicular rows of pressure gauges were used in the series of experiments and are shown on the diagram of Figure 8. The short leg, S, has four gauges at 3.0, 9.1, 12.2 and 18.3 m (10, 30, 40 and 60 ft) from the nozzle head. The long leg, L, has four gauges located at 6.1, 12.2, 24.4 and 48.8 m (20, 40, 80 and 160 ft). So as to be consistent with previously established terminology, these gauge locations are denoted by S10, S30, S40 and S60 on the short leg and L20, L40, L80 and L160

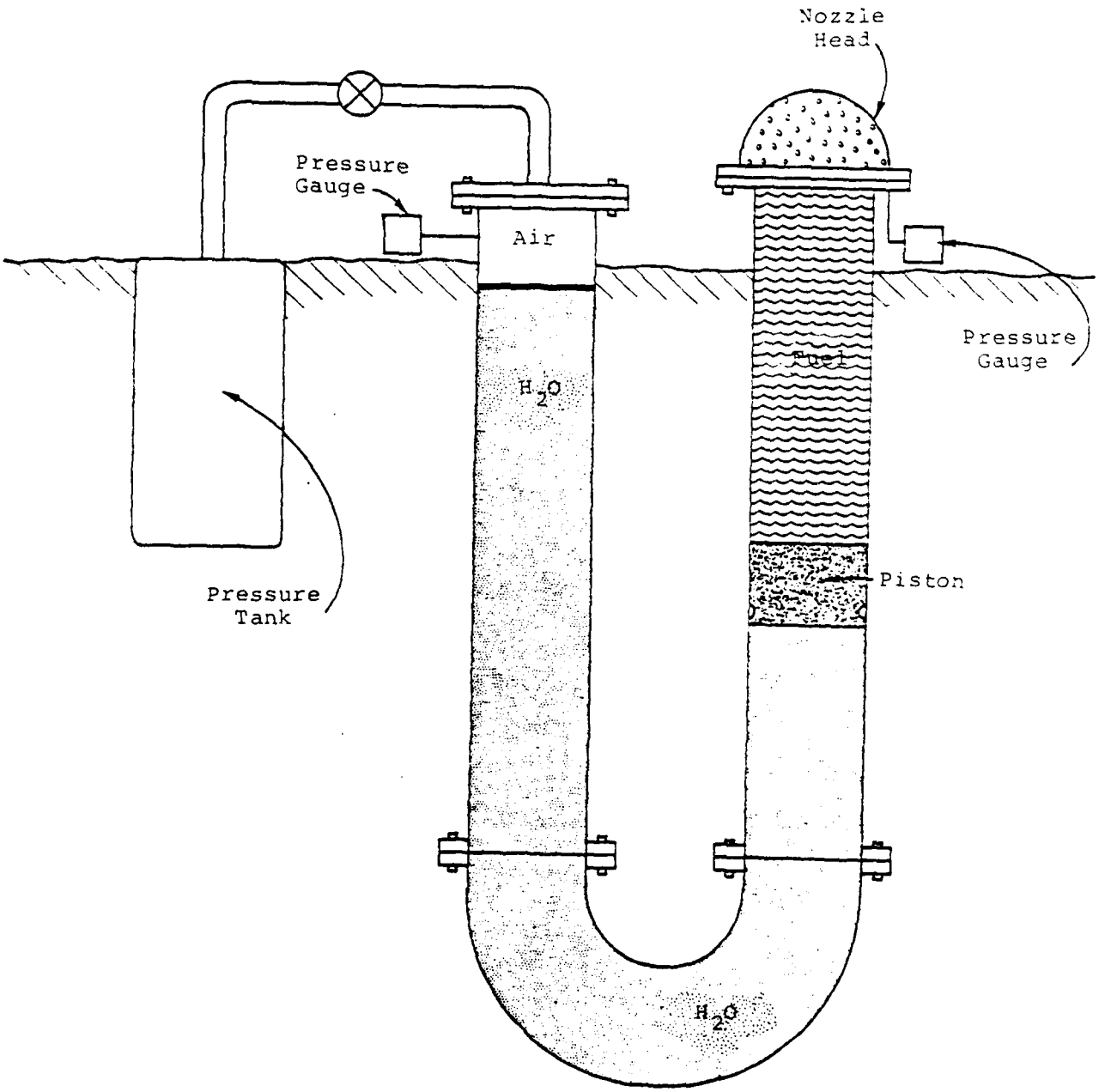

Figure 6. Schematic diagram showing the U-tube used in the experimental investigation for disseminating hemispherical fuel-air explosive clouds. One leg of the U-tube was pressurized in order to force the fuel through a nozzle head attached to the other leg of the U-tube.

Figure 7. Photograph of the U-tube showing the nozzle head used for disseminating hemispherical FAE clouds.

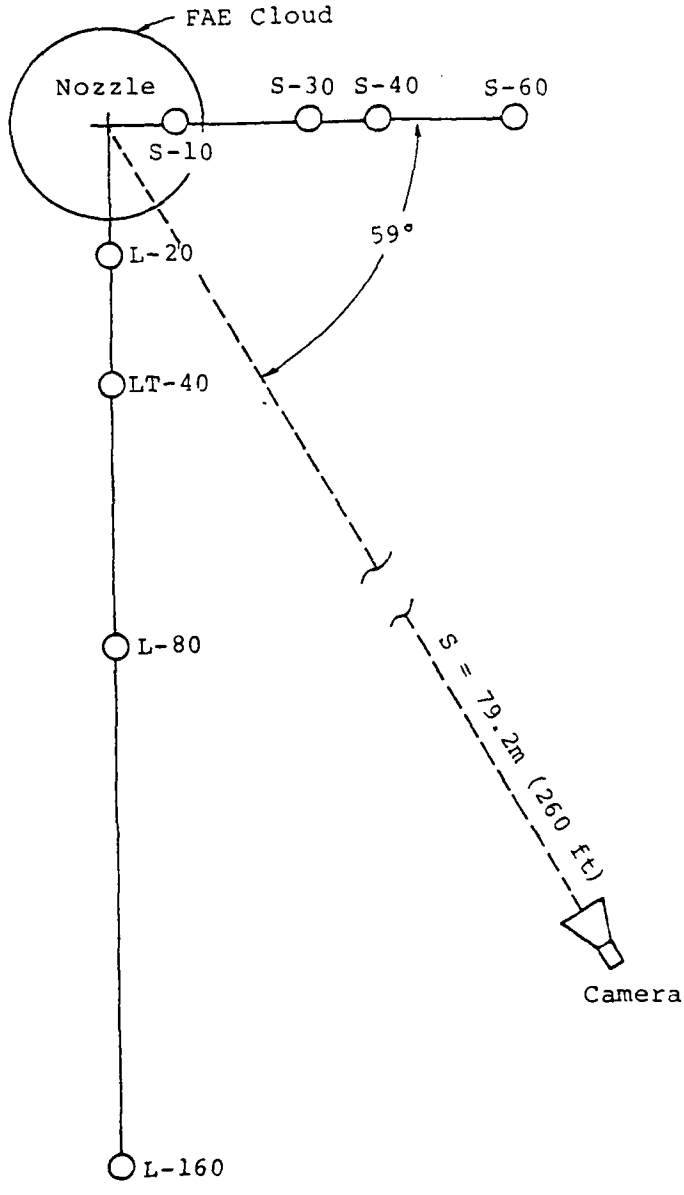

Figure 8. Plan View of the test pad showing the two perpendicular pressure gauge arrays and the line of sight of the Fastax camera.

on the long leg. The two gauges located at equal ranges in the two legs, S-40 and L-40, were included for the purpose of determining the degree of blastwave symmetry achievable with the present system. The side-on pressure, as a function of time, was measured at all gauge locations. In some of the experiments, additional gauges were included for measuring the stagnation pressure. The dynamic pressure can be determined if both the side-on pressure and the stagnation pressure at a given range are known. The Fastax camera is located in the quadrant between the two perpendicular gauge lines at an angle of 59° from the short-gauge leg and is at a range of 79.2 m (260 ft) from the nozzle head.

The photograph of Figure 9, which was taken from an area near the Fastax camera station, shows the elevation view of the test pad. The U-tube, most of which is buried underground, is shown at the center of the photo. The nozzle head is clearly visible. The two uprights are located 4.6 m (15 ft) from the center of the nozzle head. The graduation marks on the uprights are 1.5-m (5-ft) apart and the uprights themselves are 4.6-m (15-ft) high. The sign in the foreground indicates the date and number of the test and the rectangular sheet in the background provides a means for determining the relative transparency of the detonated products, which is an indication of the efficiency of the detonation process. The actual vantage point of the Fastax camera was such that the sign, the nozzle head, and the rectangular sheet were in line with the camera.

Figure 10 is a still photograph showing the configuration of a cloud formed when water is disseminated through the nozzle head at a pressure of about 0.68 MPa (100 psi). It is seen that a very nearly hemispherical cloud is formed with approximately a 4.6-m (15-ft) radius. For comparison, Figure 11 is a single frame enlargement taken from a Fastax movie and shows the early time configuration of a propylene oxide/air cloud formed in a manner similar to the water cloud. The different physical properties caused the cloud formation process to be somewhat different from that for water

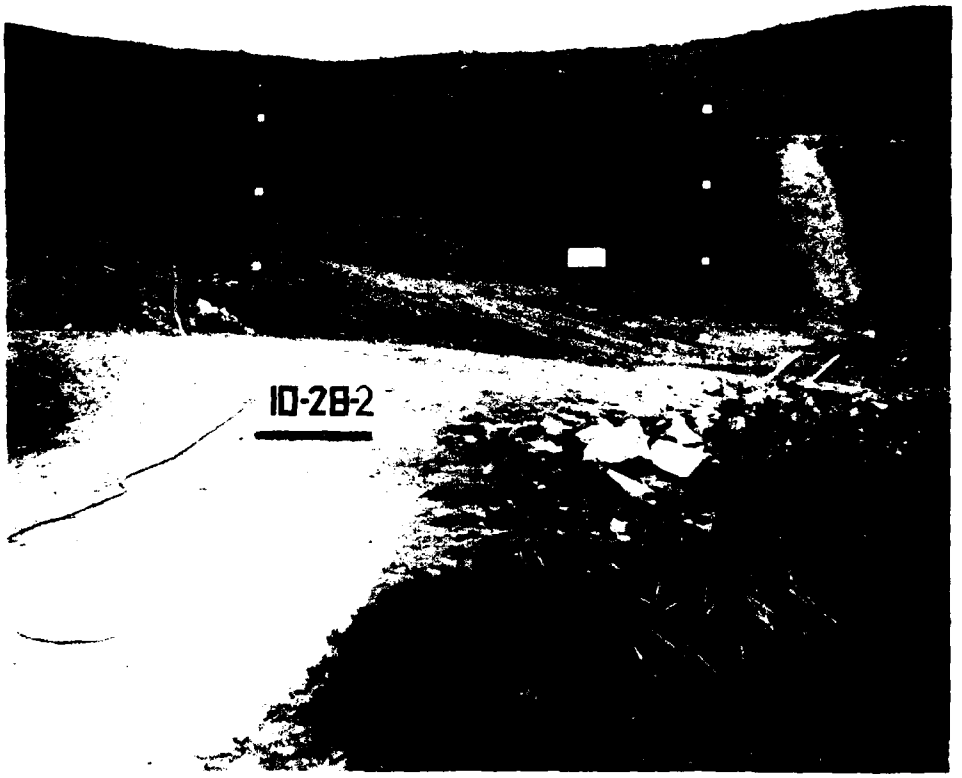

Figure 9. Photograph showing the elevation view of the test pad. The nozzle head can be seen in the center of the photograph and the graduated uprights are positioned a distance of 4.57 m (15 ft) on either side of the nozzle head. The separation between the graduation marks on the uprights is 1.52 m (5.0 ft). The numbered sign in the foreground identifies the particular shot. A Cellotex sheet was placed in the background for the purpose of determining the relative transparency of the detonated products, a measure of the detonation efficiency.

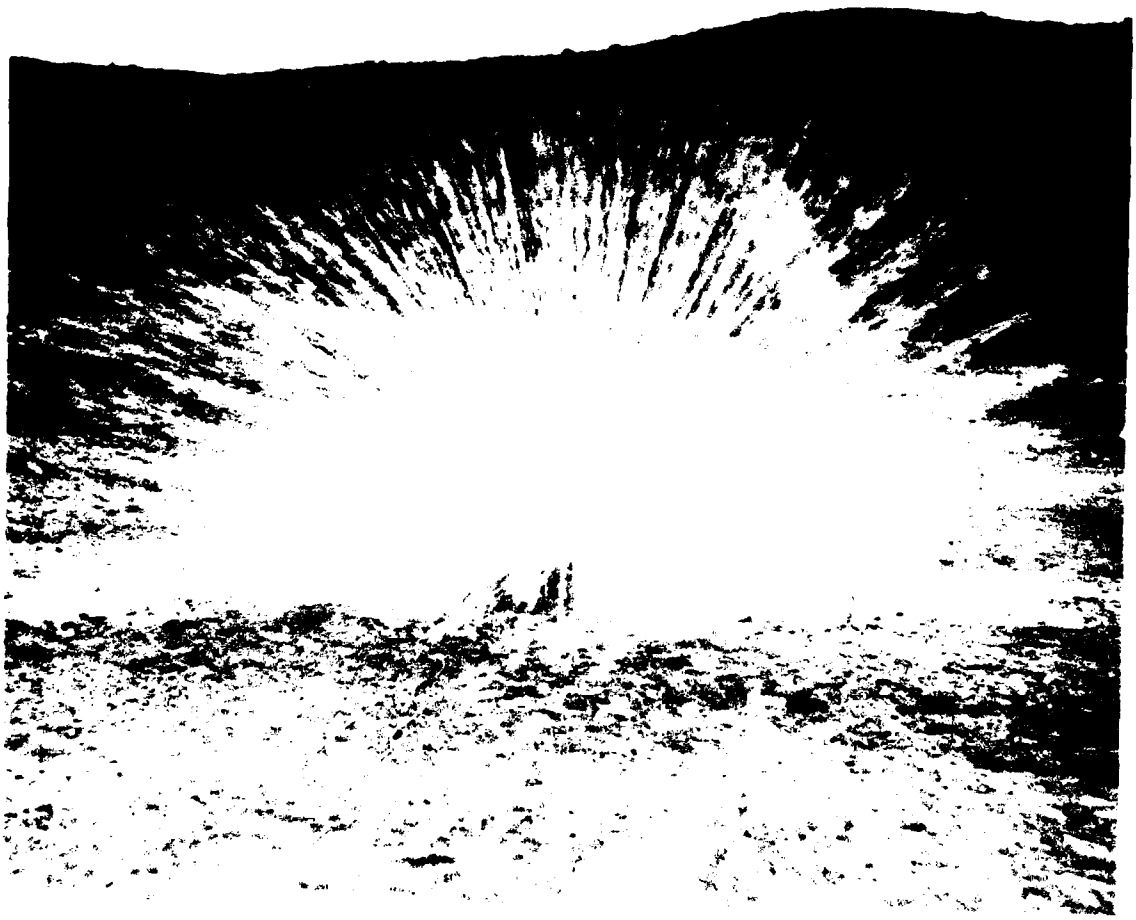

Figure 10. A still photograph showing water being disseminated through the hemispherical nozzle head.

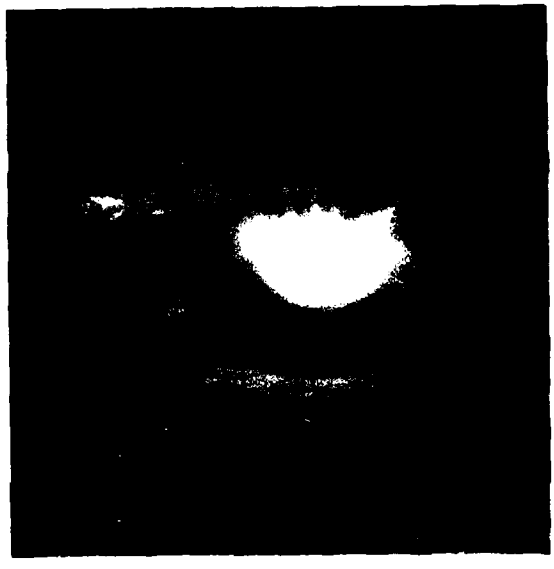

Figure 11. Photograph taken from Fastax movie of propylene oxide being disseminated from the hemispherical nozzle head. The shape of the cloud being formed led to a decision to design the nozzle head with larger diameter holes near the axis of symmetry and smaller diameter holes near the nozzle head periphery. Such a design gave a more hemispherically shaped cloud.

dissemination. It is believed that the vapor pressure of the propylene oxide is such that vaporization takes place at an early stage in the dissemination process, thus causing the visible cloud shape to be somewhat non-hemispherical. The apparent cloud-flattening was enhanced by fuel evaporation near the top of the cloud. Fastax movies indicated that the detonable cloud had an elliptical shape. In an effort to offset the cloud-flattening effect, the distribution of holes in the nozzle head was changed by plugging up selected holes in the bottom rows to enrich the central, more nearly vertical section of the cloud. The results indicated that the effective number of holes and their size distribution as a function of polar angle had a pronounced effect on the resulting cloud shape. By redrilling the dome with a better hole location and size distribution (larger diameter holes near the top), satisfactory (nearly hemispherical) spray patterns were achieved. In the final configuration, the holes were 3.302 mm (0.13 in) in diameter at the center of the nozzle head and their density and diameter decreased smoothly to 2.70-mm (0.106-in) diameter at the periphery. Figure 12 is a series of four frames from a Fastax movie showing cloud growth for a typical propylene oxide dissemination experiment using the final nozzle design. Figure 13, which shows two Fastax movie frames near the end of the detonation of the cloud shown in Figure 12, indicates that the detonable cloud is very nearly hemispherical.

5.2 FAE TEST PROGRAM

The test program was divided into three parts. The first series of tests were oriented toward the design of the U-tube test facility. The second series involved the use of the U-tube facility to disseminate FAE into hemispherical clouds which were subsequently detonated. In this series of tests, static and stagnation pressures were measured at various ranges and Fastax cameras were used to record detonation velocity.

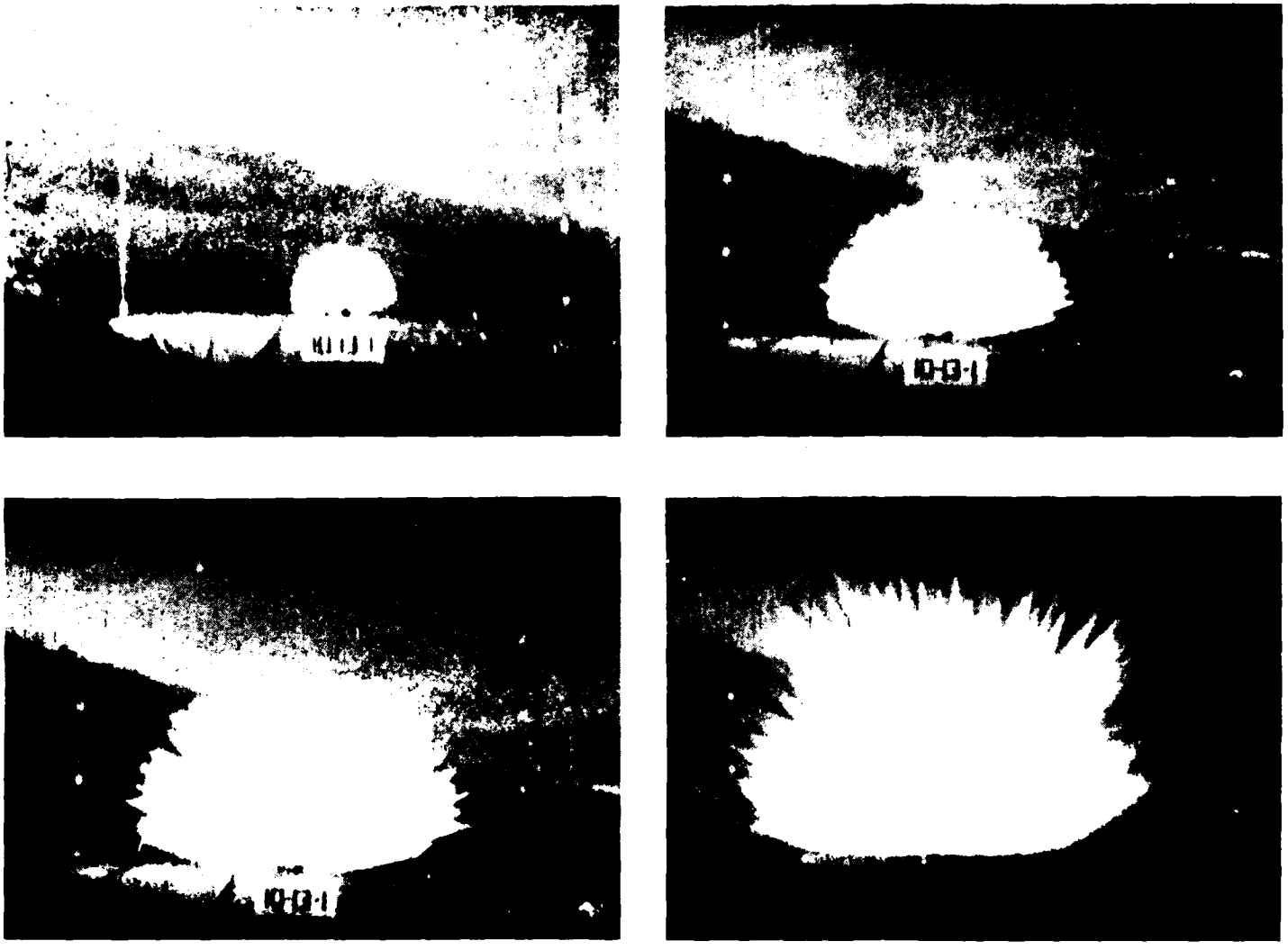

Figure 12. Four frames from a Fastax movie of the dissemination process for the case of propylene oxide being disseminated from the nozzle head of the U-tube facility.

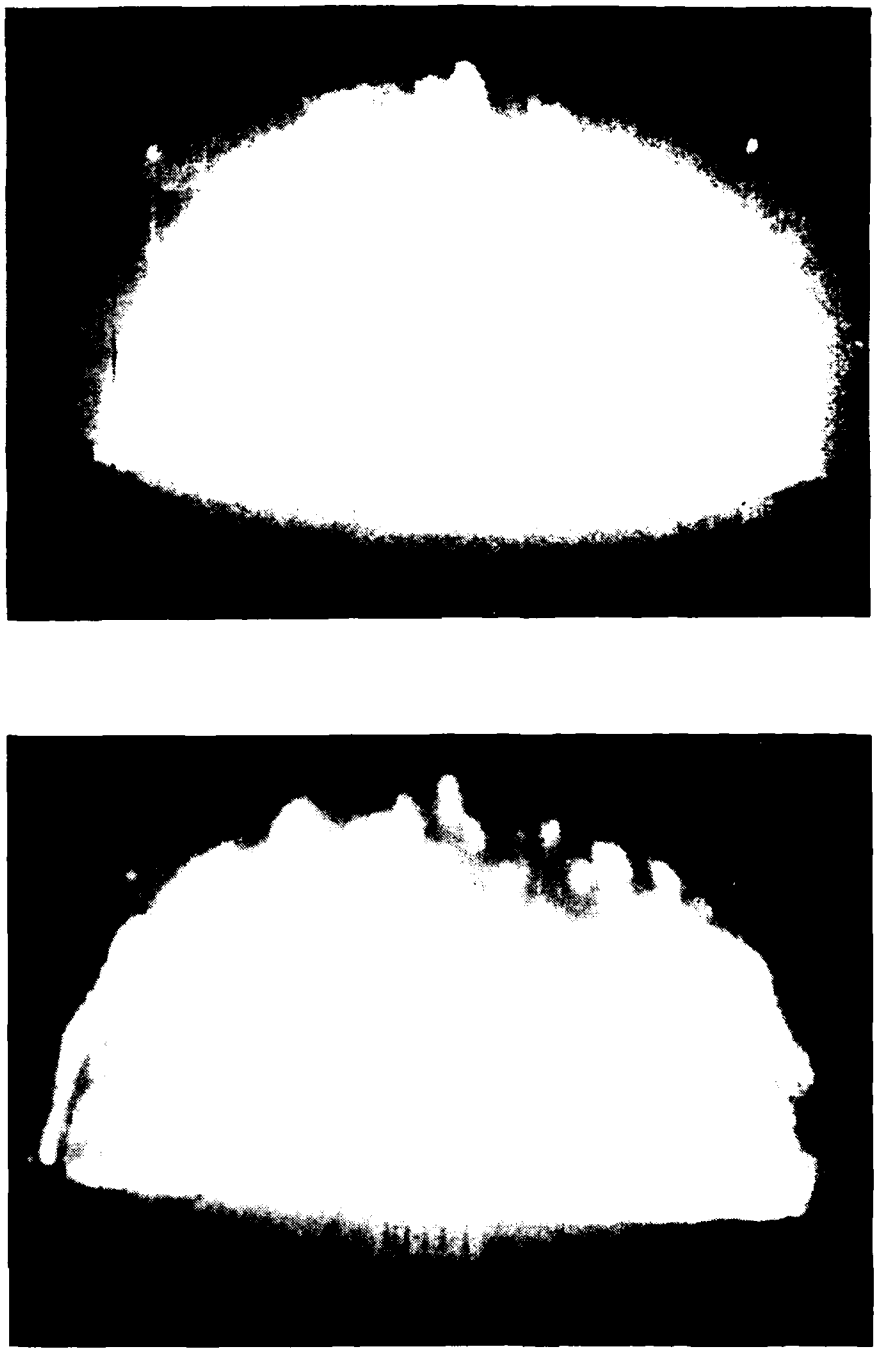

Figure 13. Two frames from a Fastax movie of the final stages of detonation of a hemispherical FAE cloud. The extent of the detonable portion of the cloud is easily identifiable and is seen to be hemispherical in nature.

The final series of tests involved the dissemination of water and fuel from single nozzles in an attempt to determine the feasibility of scaling to the full-sized test facility.

5.2.1 U-Tube Design Tests

The details of the U-tube design tests will not be presented here since the object of these tests was simply to develop a U-tube facility that would adequately disseminate 22.7 kg (50 lb) of propylene oxide into hemispherical, detonable FAE clouds. The series of design tests that were performed resulted in the achievement of that objective. The various parameters that were investigated during the design test series along with the ranges of those parameters are provided in the following list:

- Driving pressure, 0.27 - 2.04 MPa (40 - 300 psi)
- Fuel weight, 0.91 - 2.27 kg (2 - 50 lb)
- Spray angles, 6° - 180°
- Total nozzle area in head, 1.3 - 45 cm^2 (0.2 - 7.0 in^2)
- Nozzle, L/D (length to diameter) 1 - 5
- Number of nozzles in array, 63 - 1,200
- Delay time, 300 - 1,500 ms
- Detonator mass, 25 - 100 g
- Height of detonator, 0.46 - 4.6 m (1.5 - 15 ft)
- Ambient temperature, 7 - 32°C (45 - 90°F)
- Wind velocity, 0 - 5.1 m/s (0 - 10 knots)

These tests led to the following design decisions. The required U-tube driving pressure for forming a 9.1-m (30-ft) diameter hemispherical propylene oxide cloud was of the order of 0.68 MPa (100 psi). The amount of propylene oxide required

to fill this volume in the proper fuel-air mixture is 22.2 kg (49 lb) and the nozzle heads used for fuel dissemination consisted of 20.32-cm (8.0-in) diameter aluminum domes made from either 1.5-mm (0.06-in) or 7.9-mm (0.31-in) thick aluminum with approximately 600 3.2-mm (1/8-in) or 2.9-mm (0.114-in) diameter holes. In one of the designed nozzle heads, the hole size varied from 3.3 mm (0.13 in) in diameter at the center of the nozzle to 2.7 mm (0.106 in) in diameter at the periphery.

5.2.2 FAE Blast Wave Measurements

After the U-tube facility design tests were completed, the facility was used to perform a series of dissemination and detonation tests in which pressure-time histories at various locations were measured. Gauges were installed on the facility to record both side-on and stagnation pressures at various ranges. Figure 14 shows a series of overpressure versus time waveforms that were direct readouts from the eight-channel recorder. The numbers on the left side of the chart are the gauge location designations. As indicated earlier, the letter S denotes the short-gauge leg and the letter L the long-gauge leg. In addition, the notation, LT, indicates stagnation or total pressure for the long-gauge leg. The location of these gauges is shown in Figure 8 which gives a plan view of the FAE test pad facility.

In Figure 14, the time (abscissa) has a constant calibration factor: 1.0 cm (0.394 in.)(vertical line) equals 10 ms. Each overpressure (ordinate) on this recording has its own calibration factor as shown in Table I. It should be noted that, whereas the recorder operates at a constant speed and therefore the cm-to-time conversion does not change, the cm-to-pressure conversion factors occasionally change between shots as gauges are recalibrated or replaced. The gauge readings shown in Figure 14 are from shot number 1, 0800, Tuesday, 18 October 1977,

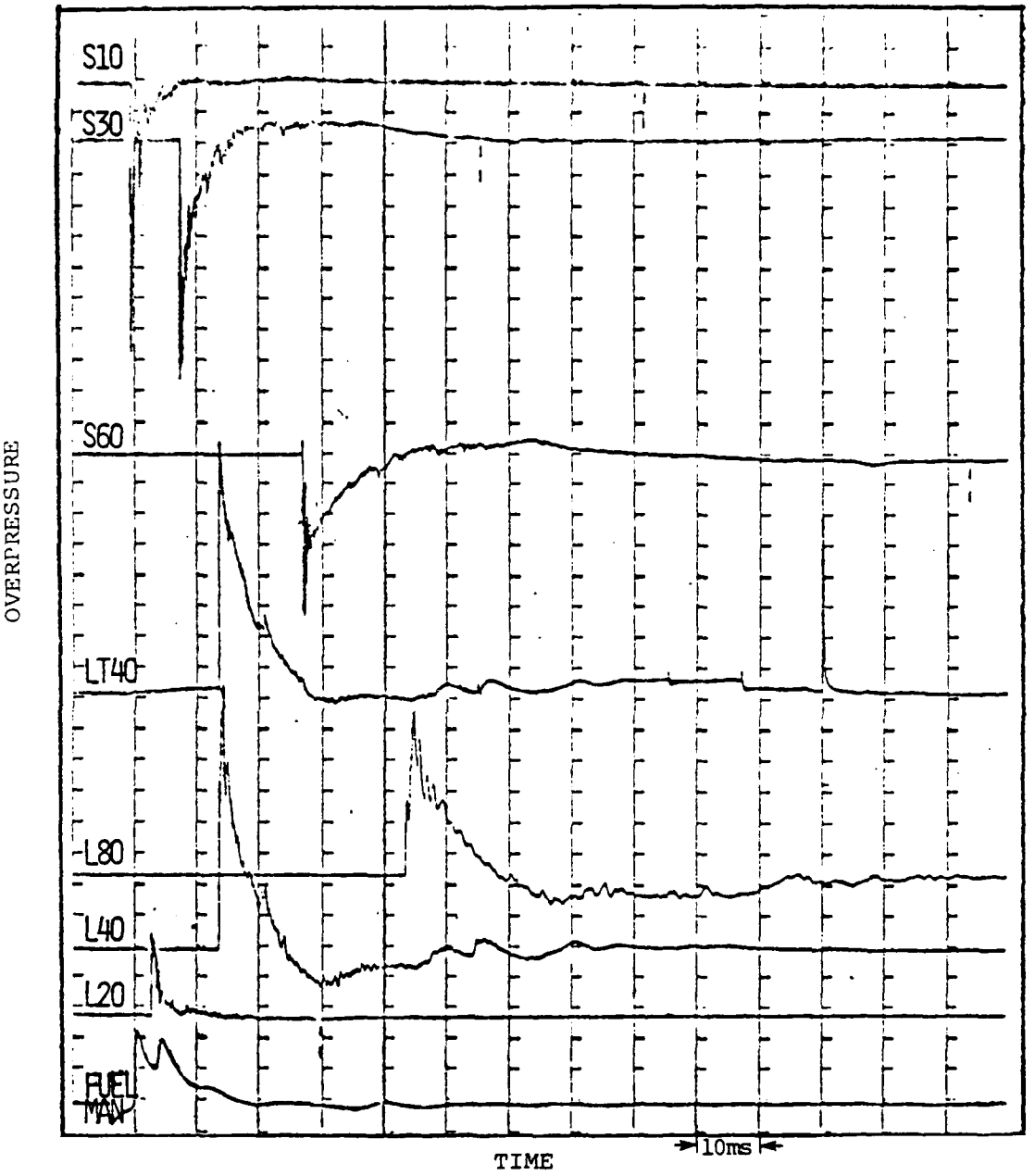

Figure 14. Typical pressure gauge readings from an FAE detonation experiment. The letters S and L refer to the short and long gauge leg respectively. The numbers identify the location in distance of the gauge with respect to the nozzle head. The gauge calibration factors are shown in Table I. The short leg gauge records are inverted in order to plot all gauge readings on a single chart.

Table I. Gauge Calibration Factors for Shot No. 1, 0800 Tuesday, 18 October 1977

Gauge	Calibration Factors	
	MPa/cm	psi/in
S10	0.3348	125.00
S30	0.0670	25.00
S60	0.0339	12.67
LT40	0.0497	18.57
L80	0.0160	5.97
L40	0.0287	10.72
L20	0.3501	130.72

which involved 22.2 kg (49 lb) of propylene oxide disseminated through a hemispherical nozzle head. The blast waveforms from the gauges in the short leg are shown inverted on the chart.

The overpressure time data in several of the tests were digitized and stored on computer tape so that the data could easily be scaled and plotted for comparison with nuclear blast wave data. Such comparisons are shown in the next section.

It was important in this series of tests to also demonstrate that the blast wave data generated by the facility were both repeatable and symmetric. Figure 15 is a plot of peak static overpressure as a function of range involving measurements from three separate experiments. The letters S and L in the figure represent the short and long gauge legs, respectively. The gauge legs were positioned 90° apart so that cloud symmetry could also be investigated. It is seen that with the exception of one gauge (L20) there is very little scatter in the peak pressures between shots indicating good repeatability in those quantities. Figure 16 is a plot showing total static impulse at each gauge location plotted as a function of range. Again, it is seen that there is very little scatter between shots. Also, since the peak static overpressures and total impulses obtained at the perpendicular gauge locations lie very close to a single curve (with the exception of L20), indications are that good cloud symmetry has been obtained. The following two subsections are devoted to a detailed investigation of the degree of blast wave repeatability and symmetry attainable with the U-tube facility.

5.2.2.1 Blastwave Repeatability

The curves in Figure 17 through 20 are shown to demonstrate the degree of blast wave repeatability attainable with the U-tube facility. In Figure 17, the measured static over-

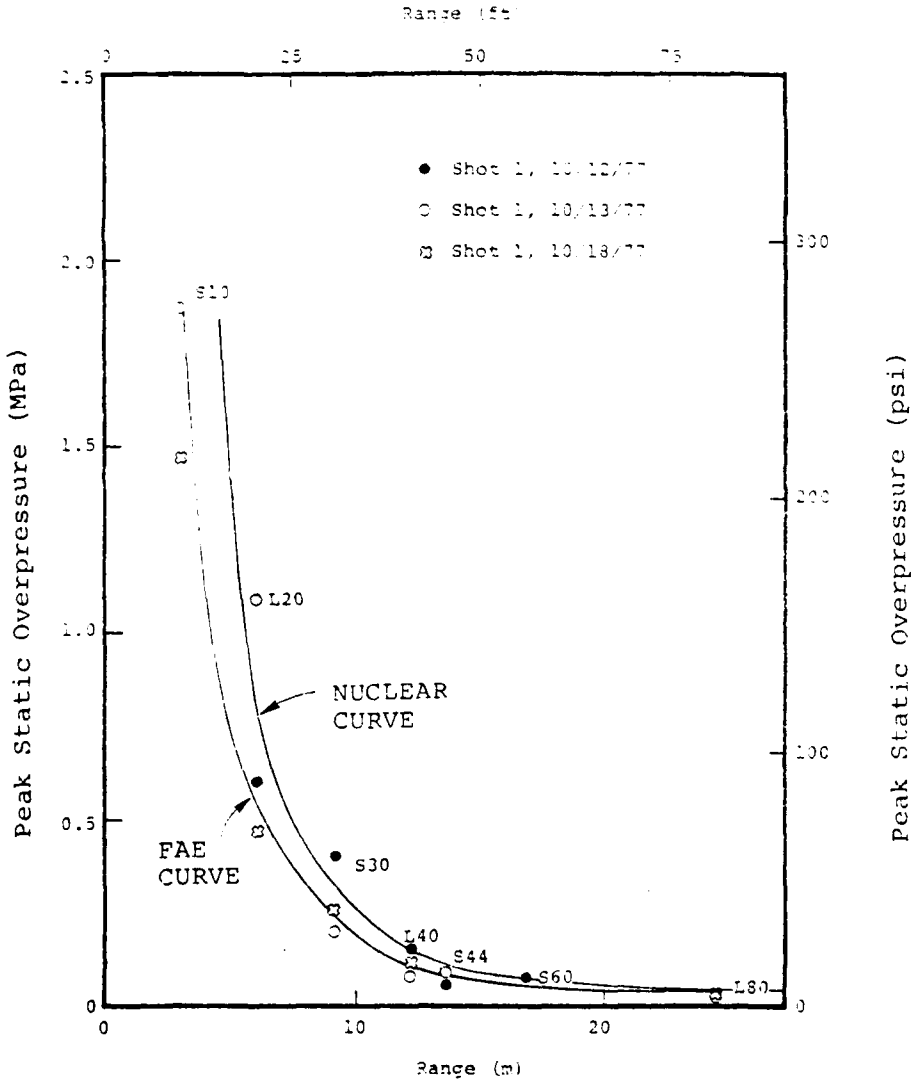

Figure 15. Plot of measured peak static overpressure versus range for three different experiments. The fact that most of the pressures lie very close to a smooth curve indicates that repeatability between experiments is good. In addition, since the gauges labeled L and S were separated by 90 degrees the curve indicates that a high degree of symmetry was attained. An additional gauge, S-44, at a range of 13.4 m (44 ft) was included in two of the experiments

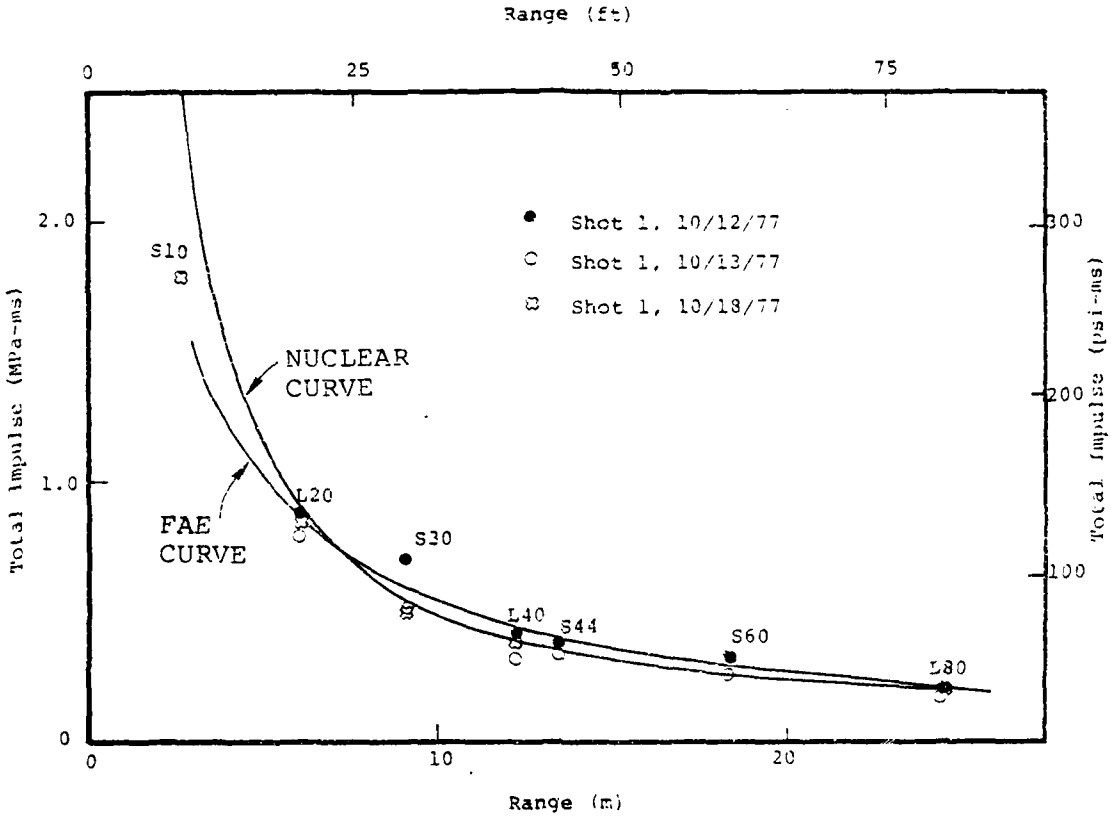

Figure 16. Plot of maximum positive phase impulse versus range for three different experiments. Again it is seen that the points are close to a single curve indicating good repeatability and since the L and S gauge locations were separated by 90 degrees, good cloud symmetry is implied.

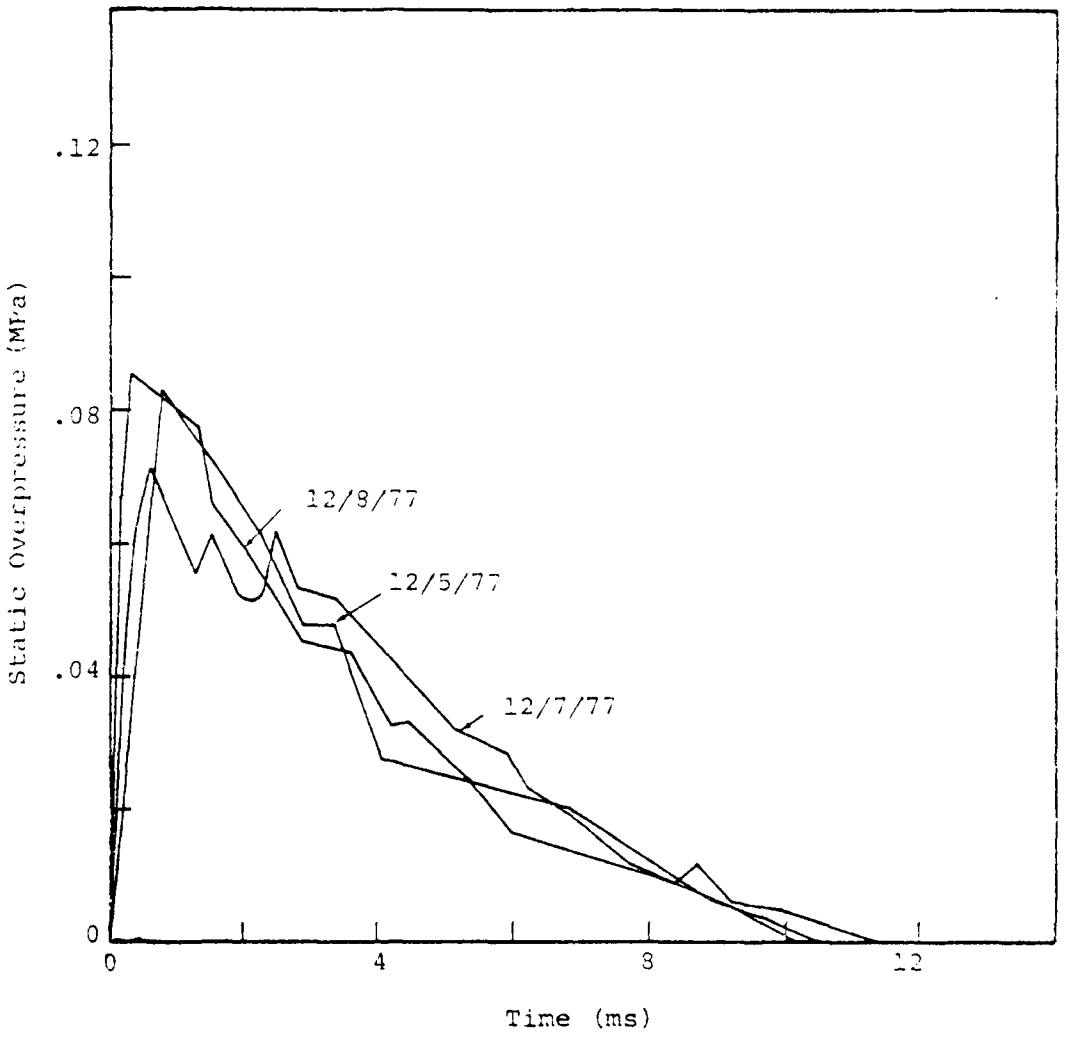

Figure 17. Plot of measured static overpressure as a function of time at the 12.2-m (L40 ft) station from three separate experiments.

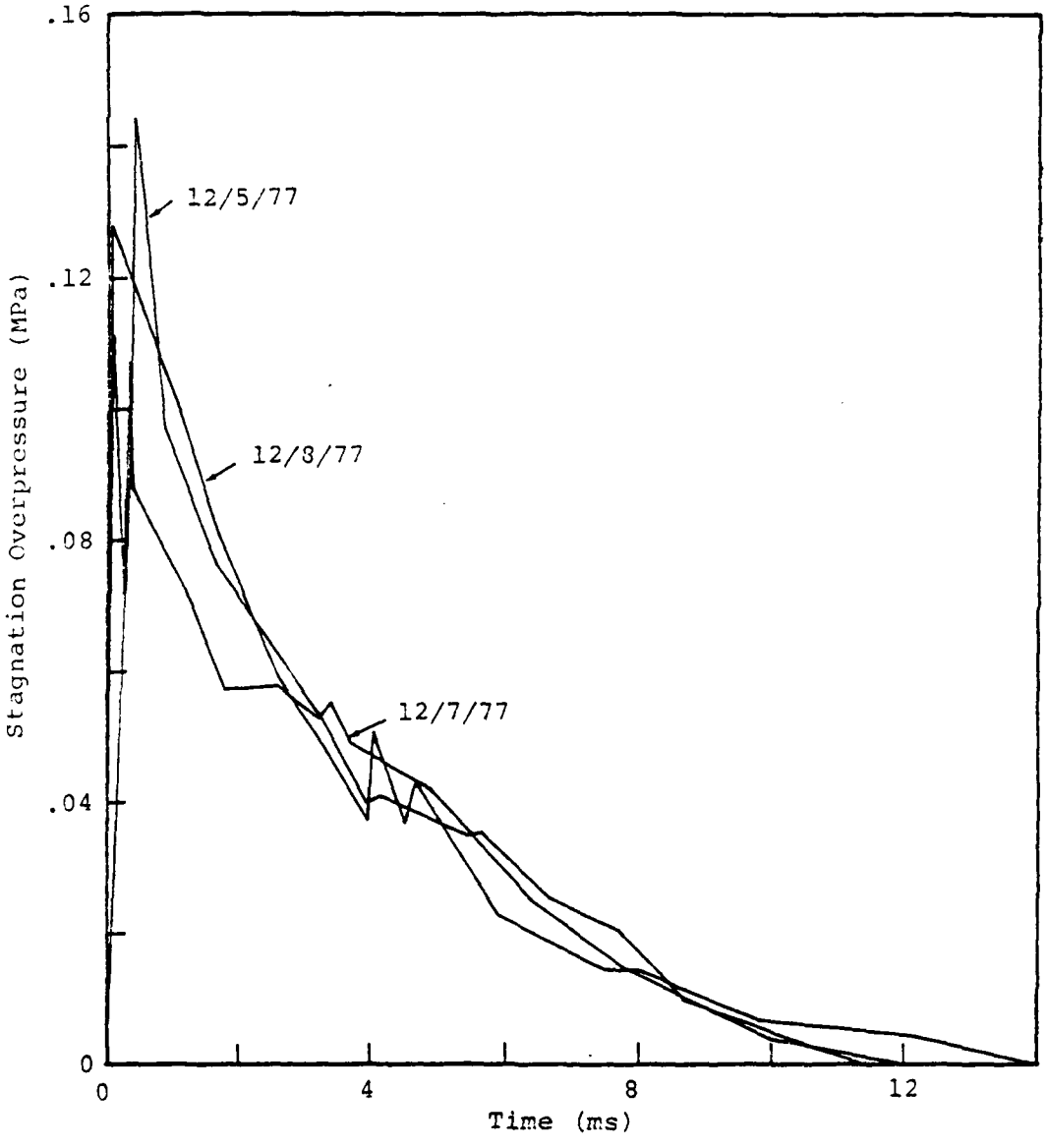

Figure 18. Plot of measured stagnation overpressure as a function of time at the 12.2-m (L-40 ft) station from three separate experiments.

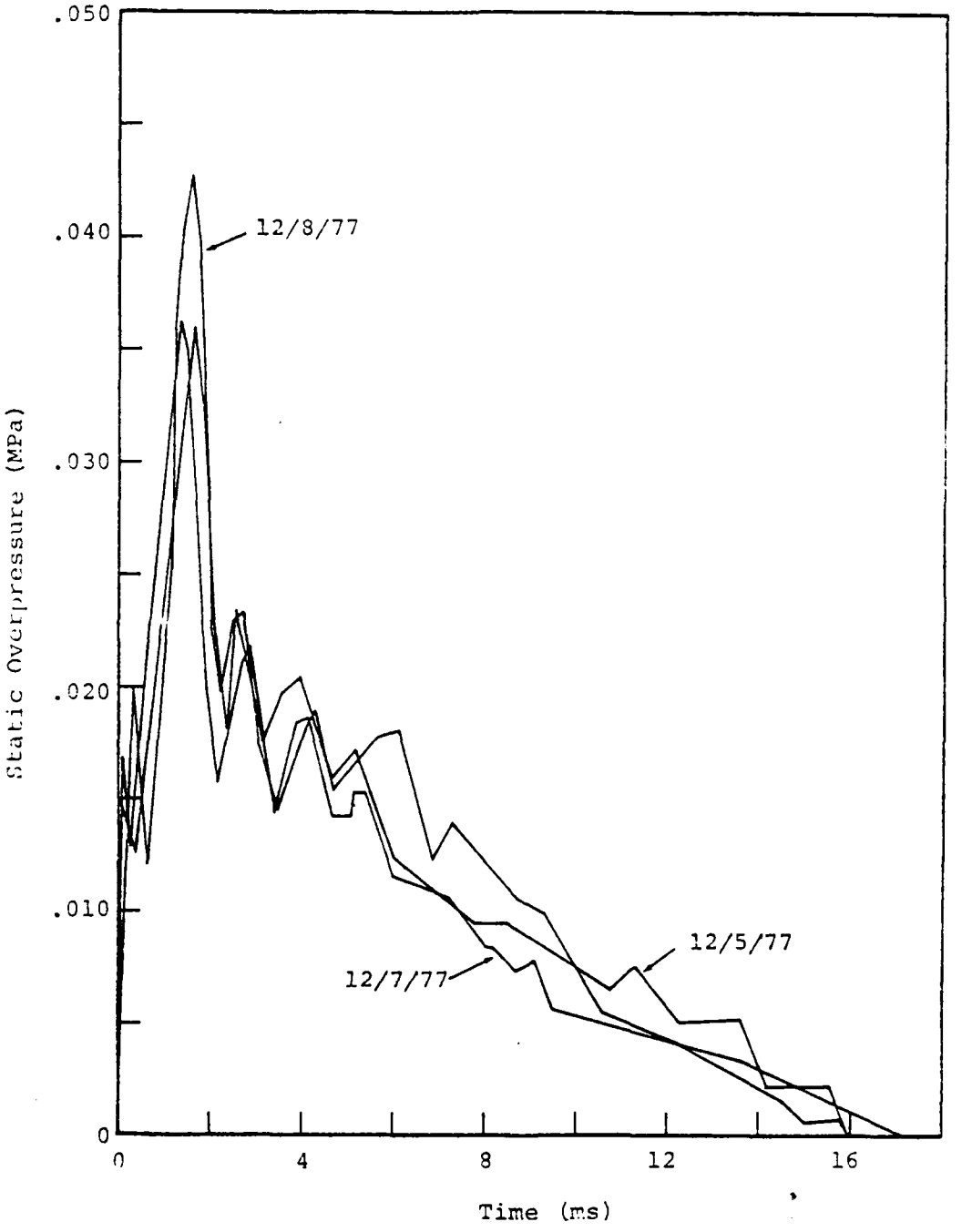

Figure 19. Plot of measured static overpressure as a function of time at the 24.4-m (80-ft) station from three separate experiments.

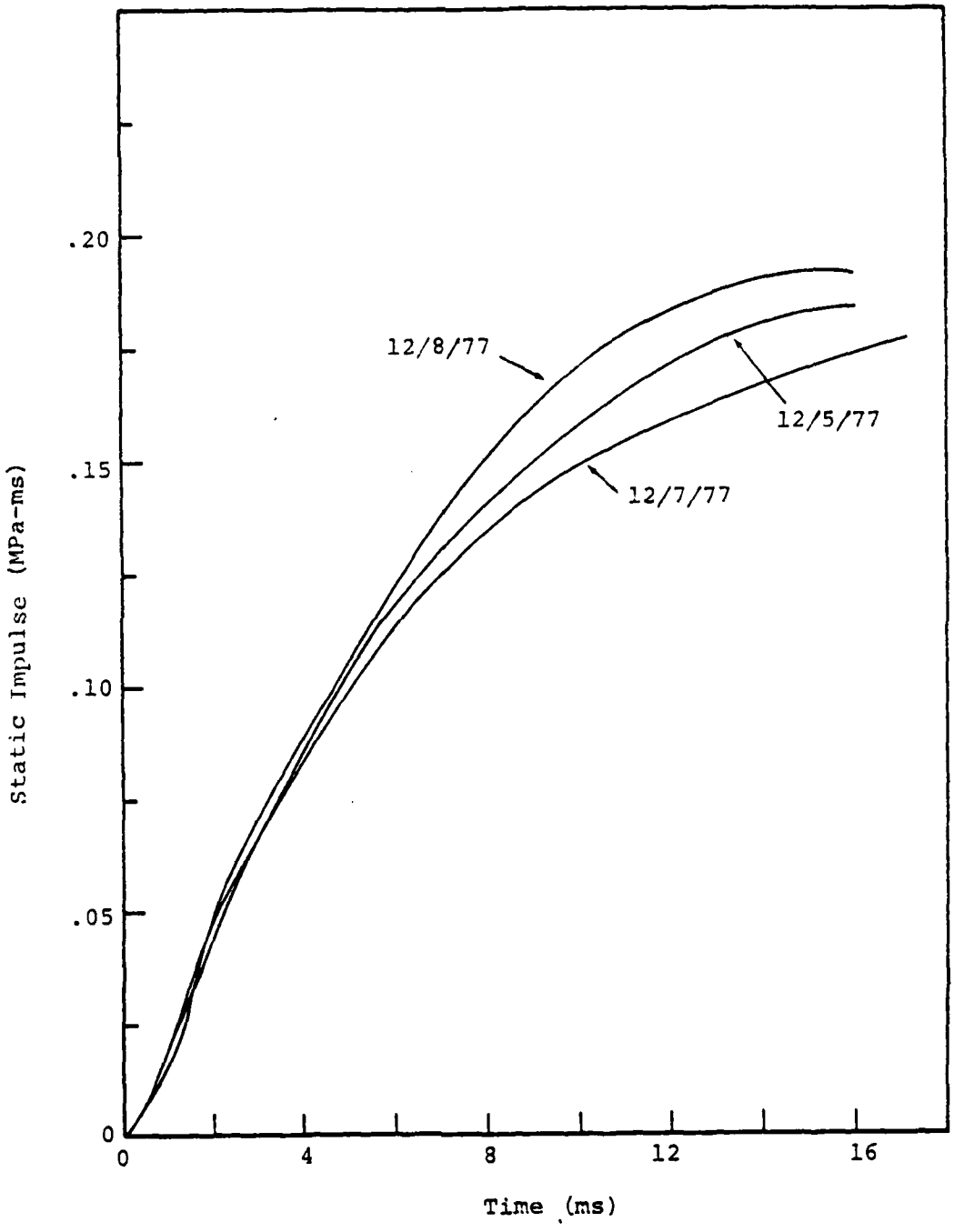

Figure 20. Measured positive phase static impulse as a function of time at the 24.4-m (80-ft) station from three separate experiments.

pressure, as a function of time at the 12.2-m (L-40 ft) station, is shown for three different experiments. Figure 18 is a similar comparison for the measured stagnation overpressure at that range. Figure 19 is a comparison of the measured static overpressure as a function of time at the 24.4-m (80-ft) station from the same three experiments. Figure 20 is a plot of the static impulse as a function of time at the 24.4-m (80-ft) station, again for the same three experiments.

It is seen from the data plotted in Figures 17 through 20 that the degree of repeatability attainable with the U-tube facility is well within acceptable limits.

5.2.2.2 Blast Wave Symmetry

Figures 21 through 23 are provided to demonstrate the degree of symmetry attainable with the U-tube facility. In Figure 21, the measured static overpressure, as a function of time at the 12.2-m (40-ft) station, is plotted for the two stations located 90° apart in a given experiment. Figure 22 provides a similar comparison taken from a different experiment. In Figure 23, static impulse is plotted as a function of time at the same range for two gauges located 90° apart.

It is seen from Figures 21 through 23 that the symmetry attainable with the small-scale U-tube facility is well within acceptable limits.

5.2.3 Single Nozzle Tests

The purpose of the single nozzle tests was to determine if the method of disseminating fuel into hemispherical clouds used in the small-scale test facility could be scaled up to a size that would be practical for the large-scale blast simulator. In the large-scale blast simulator, each nozzle must attain a reach of 80 m (262 ft) in order

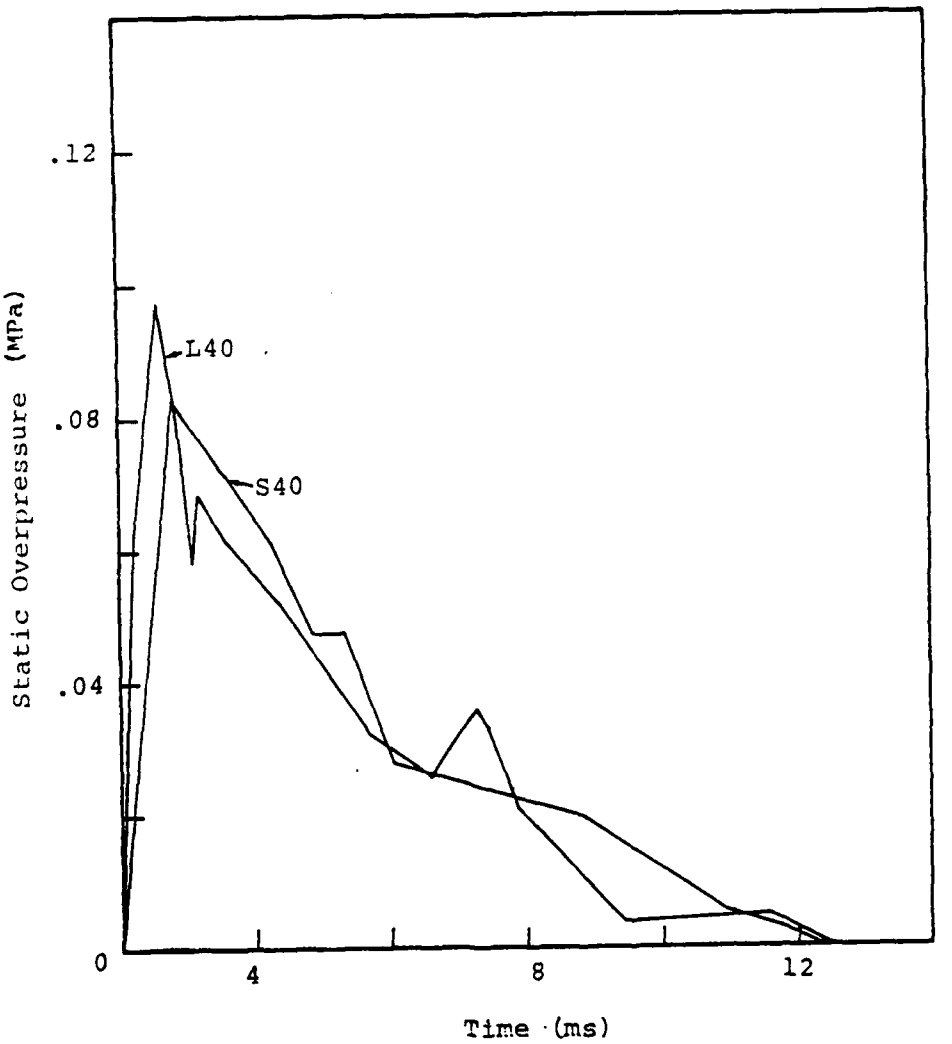

Figure 21. Plot of measured static overpressure as a function of time from a single experiment. The gauges were both located at a range of 12.2 m (40 ft) but were separated by 90 degrees. The experimental data were taken from Shot No. 1, 5 December 1977.

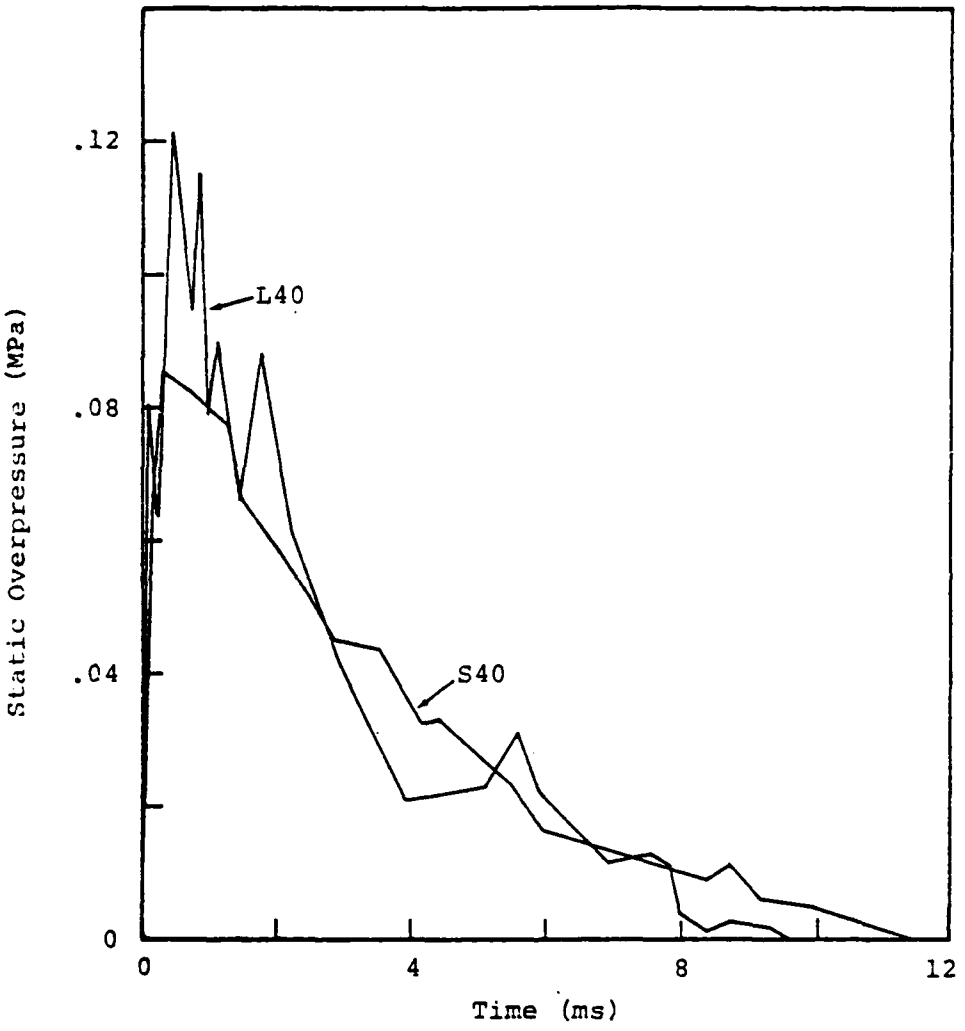

Figure 22. Plot of measured static overpressure as a function of time taken from a single experiment. Both gauges were located at a range of 12.2 m (40 ft) but separated by 90 degrees. The comparison is similar to that shown in Figure 21 except that the data plotted are from Shot No. 1, 8 December 1977.

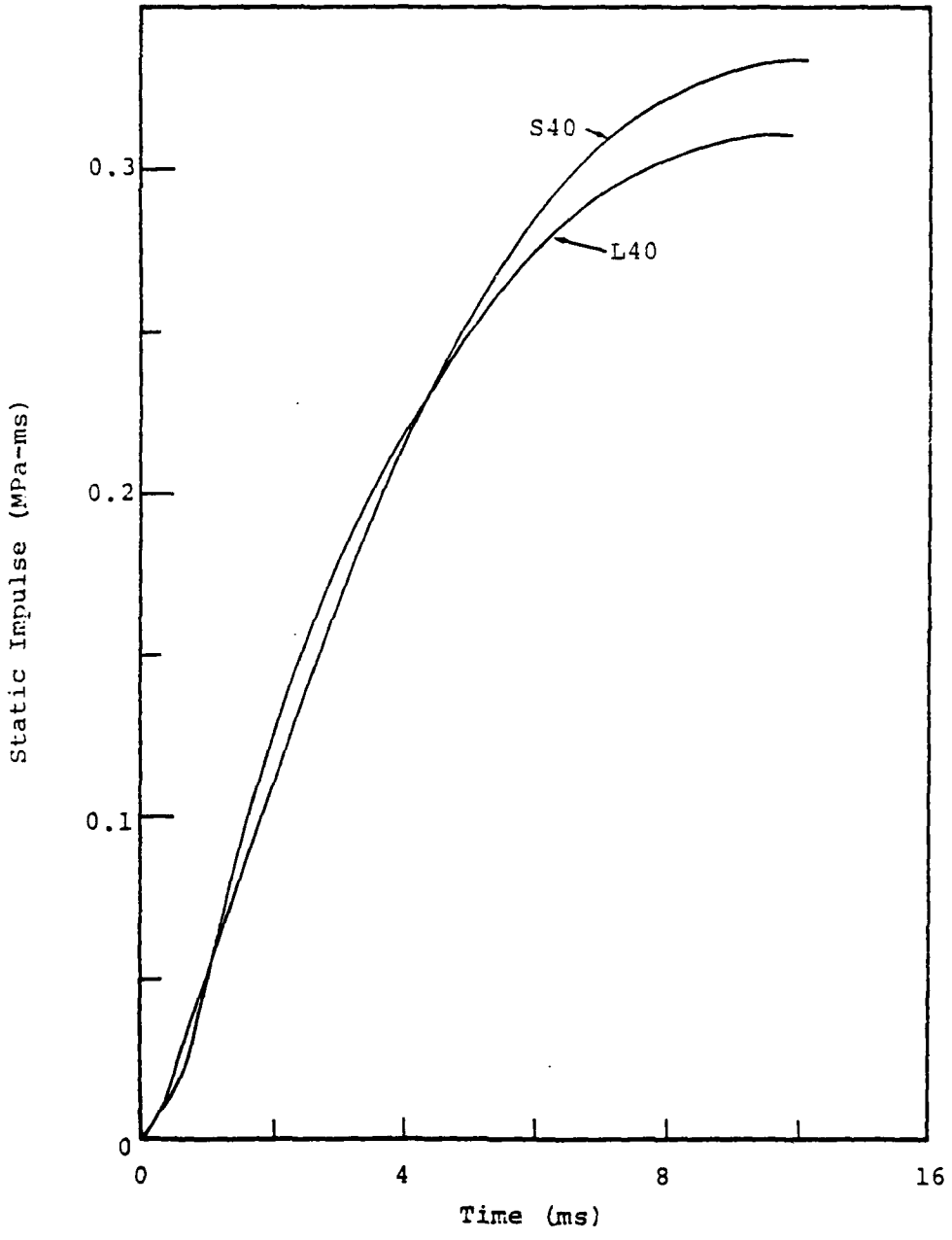

Figure 23. Positive phase static impulse as a function of time from a single experiment. Both gauges were located at a range of 12.2 m (40 ft) but were separated by 90 degrees. The experimental data were taken from Shot No. 1, 8 December 1977.

to form a cloud 160 m (524 ft) in diameter in order to simulate a 1-KT nuclear surface burst. Such a capability can be investigated by using single nozzles and determining reach as a function of driving pressure and nozzle diameter.

A series of single-nozzle reach experiments has been performed for the purpose of determining the parameters required to project fuel to heights that will be necessary in the full-scale blast simulator. Figure 24 shows various stages of a water stream being projected from a 6.35-cm (2.5-in) diameter nozzle. The small upright near the base of the nozzle has markers spaced two meters apart. The perpendicular distance from the nozzle to the horizon is about 55 m (180 ft). The height of the water stream shown in the last photograph of Figure 24 is approximately 61 m (200 ft); however, the contrast against the sky is not good enough for the top of the stream to be seen in the figure. The width of the stream near the top is approximately 5 m (16.4 ft).

The four photographs in Figure 25 show the progress of a propylene oxide stream being projected from a 6.35-cm (2.5-in) diameter nozzle. The final stream height is about 55 m (180 ft). Additional experiments are planned using nozzles of larger diameter in order to obtain streams up to 80 m (262 ft) in height.

The single-nozzle reach experiments performed to date are described in Table II. The initial results have been analyzed in an attempt to determine stream height or reach as a function of nozzle diameter and exit velocity, which is related to driving pressure. Results presented later indicate that physical properties of the liquid being projected also affect stream height; however, since only water and propylene oxide have been projected thus far, it is not certain which of the physical properties are important in determining stream characteristics.

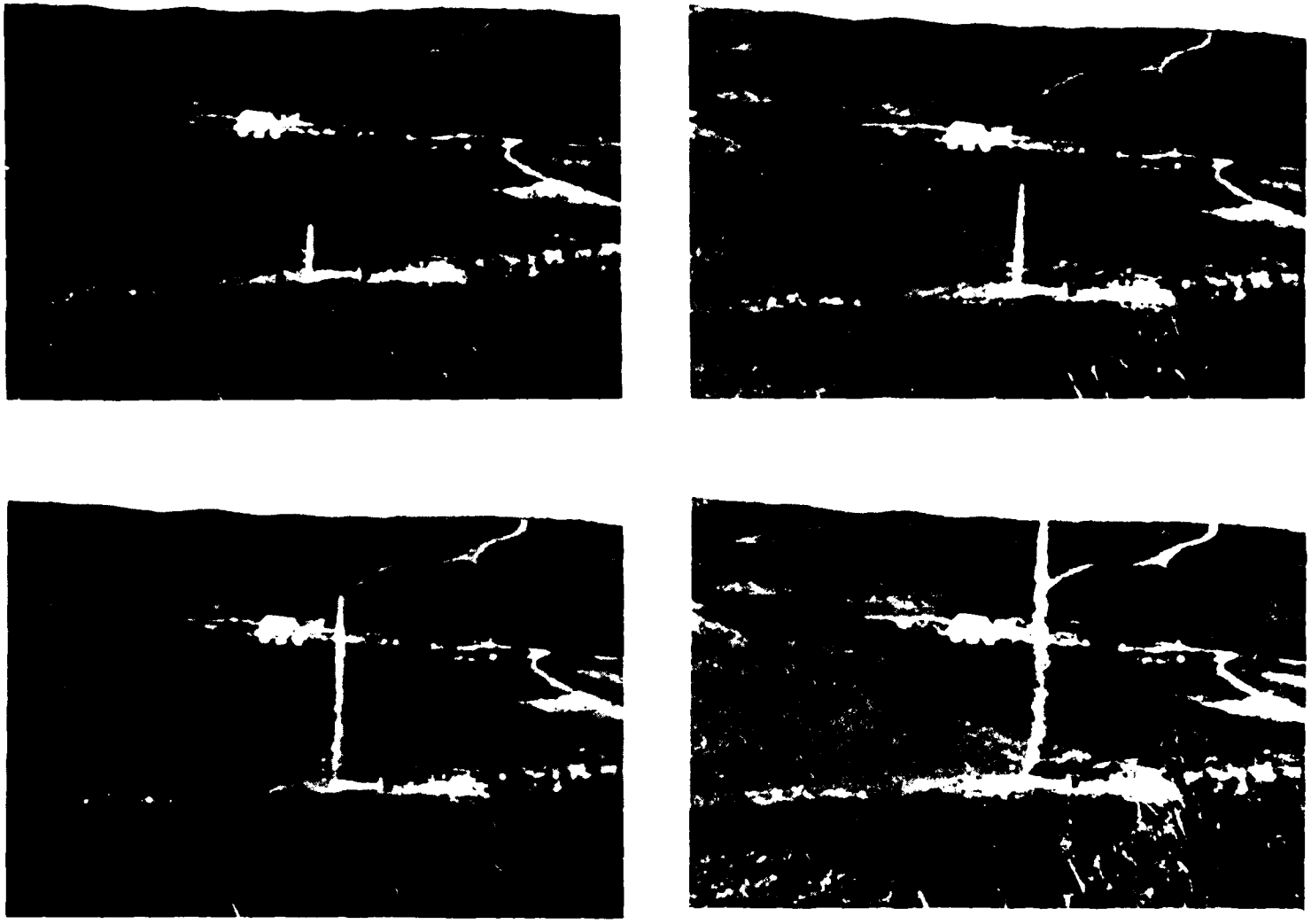

Figure 24. Photographs taken with the Fastax camera showing various stages of a water stream being projected from a 6.35 cm (2.5 in) diameter nozzle.

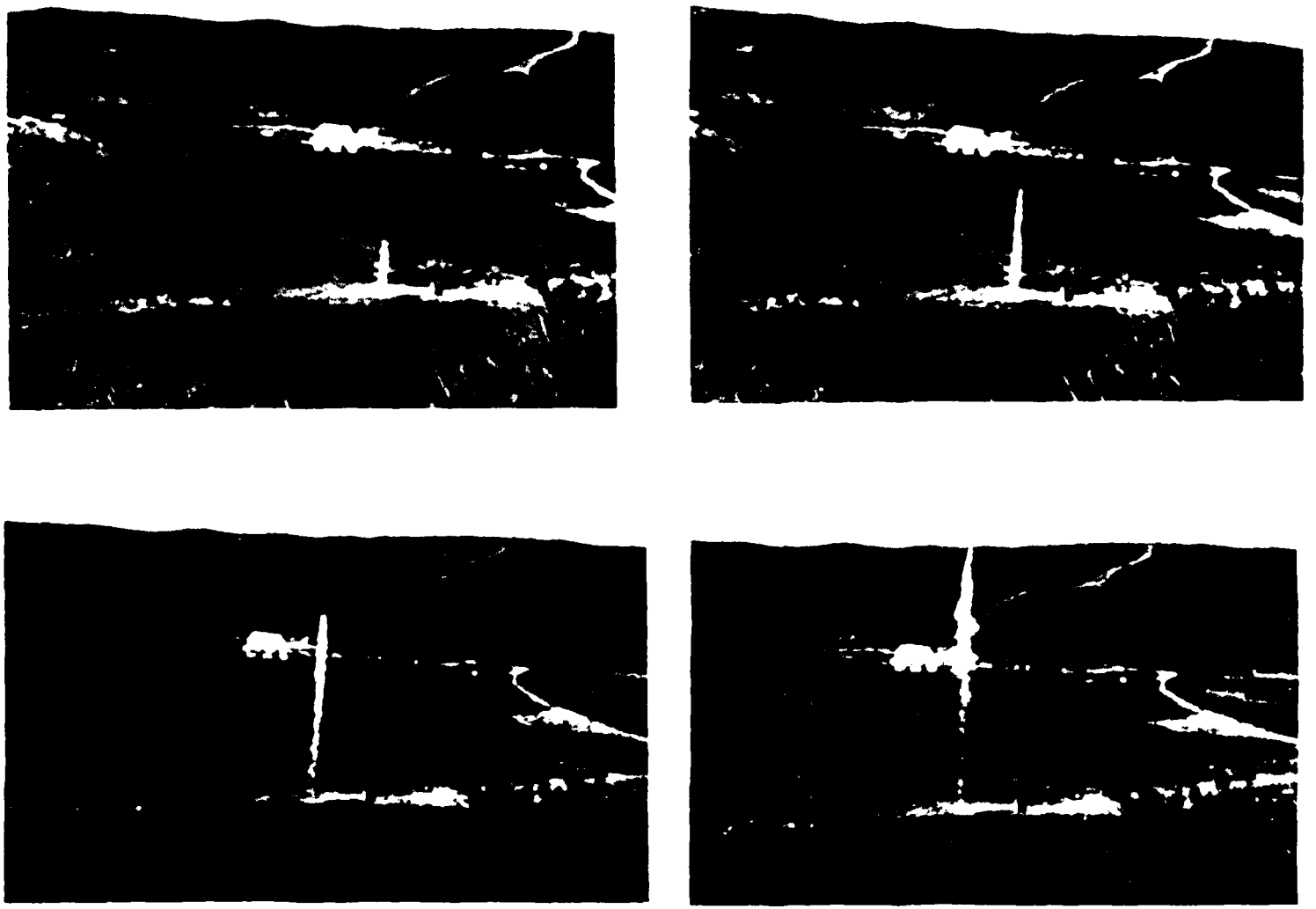

Figure 25. Photographs taken with the Fastax camera showing various stages of propylene oxide stream being projected from a 6.35 cm (2.5 in) diameter nozzle.

Table II. Single Nozzle Reach Experiments					
Experiment Number	Liquid	Nozzle Diameter		Nozzle Exit Velocity	
		(cm)	(in)	(m/s)	(ft/s)
1	H_2O	3.81	1.5	50.5	165
2	H_2O	3.81	1.5	72.0	236
3	PO	3.81	1.5	51.5	169
4	PO	3.81	1.5	72.0	236
5	H_2O	6.35	2.5	42.0	138
6	PO	6.35	2.5	44.5	146

If it is assumed that the deceleration of a stream is a result of gravitational forces and drag forces that are proportional to the square of the velocity, the equation of motion of a vertical stream can be written as

$$\ddot{y} = - g - k(\dot{y})^2 \qquad (1)$$

where y is vertical distance above the nozzle, g is acceleration due to gravity and k is a drag coefficient. Equation (1) can be solved for stream height to obtain

$$y = \frac{1}{k} \ell n \cos (c_1 - \sqrt{kg} \cdot t) + c_2$$

where $$c_1 = \tan^{-1}\left(\sqrt{\frac{k}{g}} \cdot \dot{y}_0\right)$$

$$c_2 = - \frac{1}{k} \ell n \cos c_1$$

and $\dot{y}_0$ is the initial velocity of the jet as it emerges from the nozzle.

To determine how well Equation (1) models the stream dynamics, the observed stream height from two different experiments in which water was projected from a 3.81-cm (1.5-in) diameter nozzle are plotted as a function of time in Figure 26, along with the solution of this equation. The initial velocities of the streams were different for the two experiments. It is seen that at early times stream height is modeled well by the equation of motion involving only gravitational forces and drag forces proportional to the square of the velocity [Equation (1)]. However, as the initial velocity is increased, the stream at some point in time decelerates much faster than predicted by the model. A coefficient, k, equal to 8×10^{-5} m^{-1}, gives the best agreement between experiment and theory for this particular case of water being projected from this size nozzle.

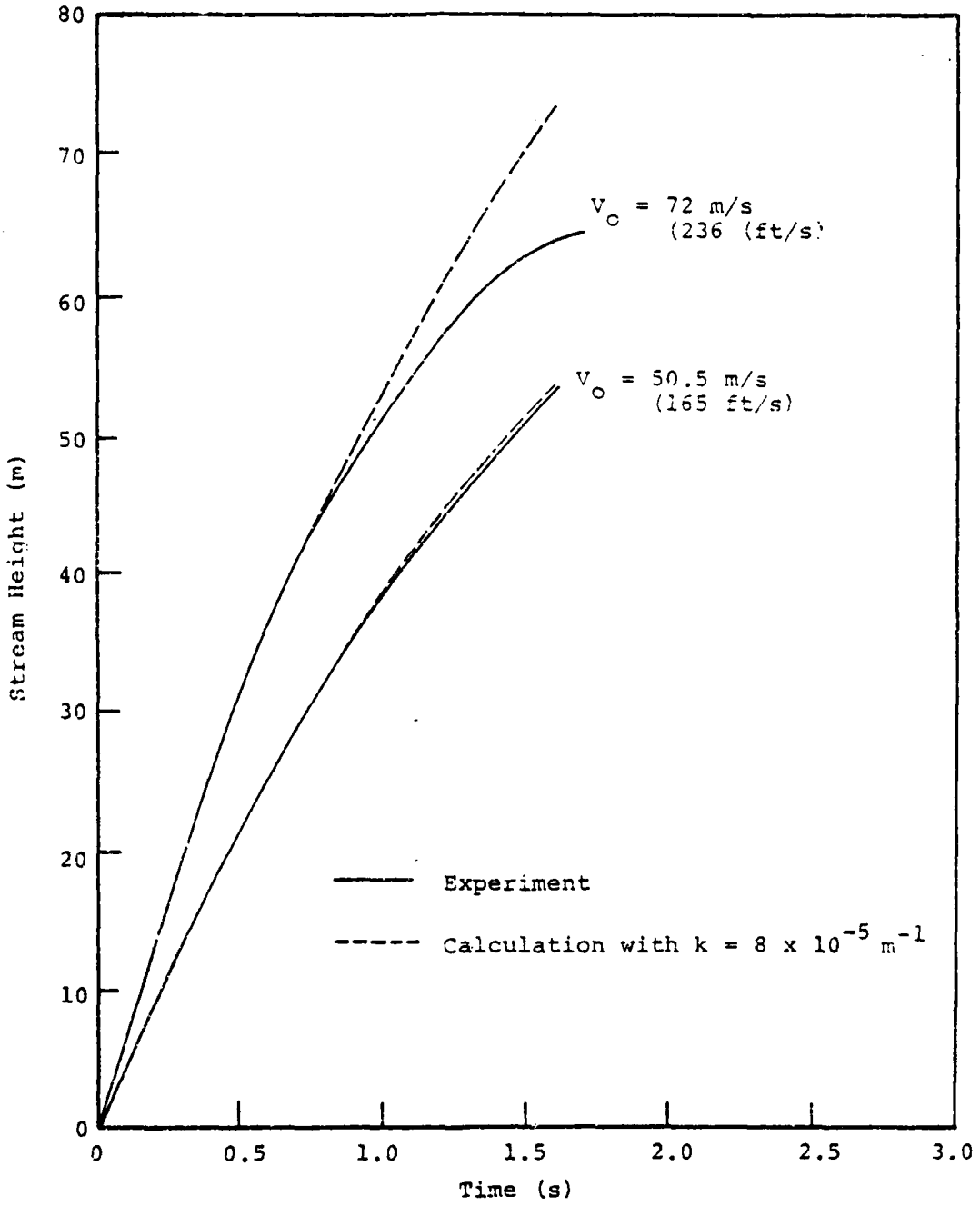

Figure 26. Comparison of stream height as a function of time for two experiments involving the projection of water from a 3.80-cm (1.5-in) diameter nozzle with Equation 1. The value of the coefficient k used in Equation 1 was 8 x 10^{-5} m^{-1}.

In Figure 27, stream height is plotted versus time for two experiments involving the projection of propylene oxide from the same diameter nozzle at two different initial velocities. It is seen that the effect of increasing the initial velocity seems to cause the increase in deceleration to occur at an earlier time. It is also noted from Figure 27 that increasing the initial velocity does not significantly increase the reach.

In Figure 28, water and propylene oxide stream heights are compared for the case of both fluids being projected from the same 3.81-cm (1.5-in) diameter nozzle at initial velocities of 72 m (236 ft) per second. It is seen that the water attained a much greater height and that the propylene oxide began to decelerate faster than that predicted by the model at an earlier time than did the water. This difference in the behavior of the water and propylene oxide streams projected at identical initial velocities from equal diameter nozzles is due to differences in physical properties such as mass density, viscosity, surface tension and vapor pressure. Since only two different fluids have been projected, the dependency of stream height on any of these physical properties cannot be determined here. It can be speculated, however, that the propylene oxide stream decelerates at a greater rate and at an earlier time than does the water stream as a result of increased droplet breakup and stream spreading. Just how droplet breakup and stream spreading are affected by liquid physical properties under the dynamic conditions associated with the high-velocity projection of fuel through a nozzle is not well known at this time.

Stream height is plotted versus time in Figure 29 for the case of water being projected from a 6.35-cm (2.5-in) diameter nozzle. The change in nozzle diameter from 3.81 cm to 6.35 cm required a change in the coefficient, k, of Equation (1) from 8×10^{-5} m^{-1} to 1×10^{-5} m^{-1} in order to

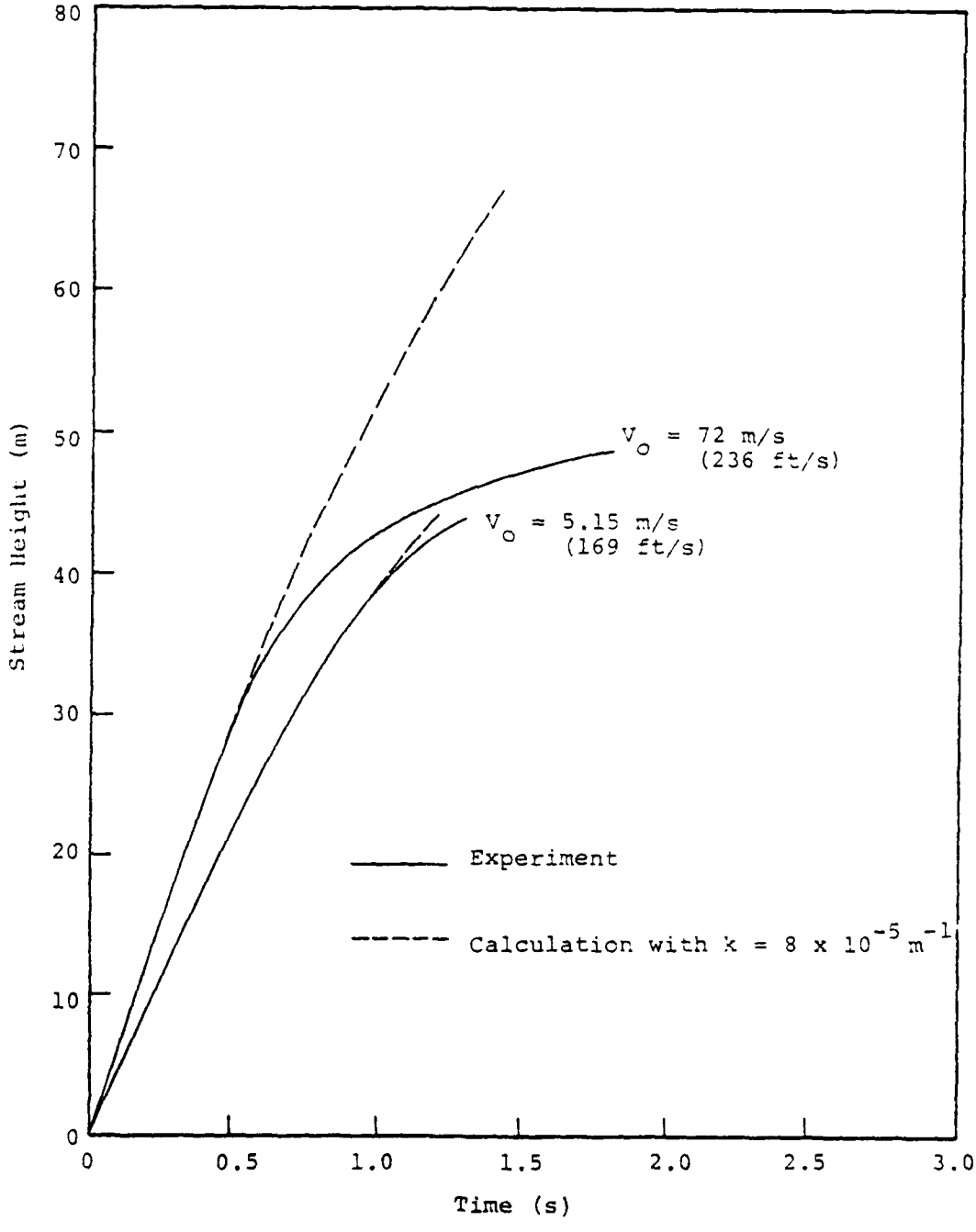

Figure 27. Comparison of stream height as a function of time for two experiments involving the projection of propylene oxide from a 3.81-cm (1.5-in) diameter nozzle with Equation 1. The value of the coefficient k used in Equation 1 was 8 x 10^{-5} m^{-1}.

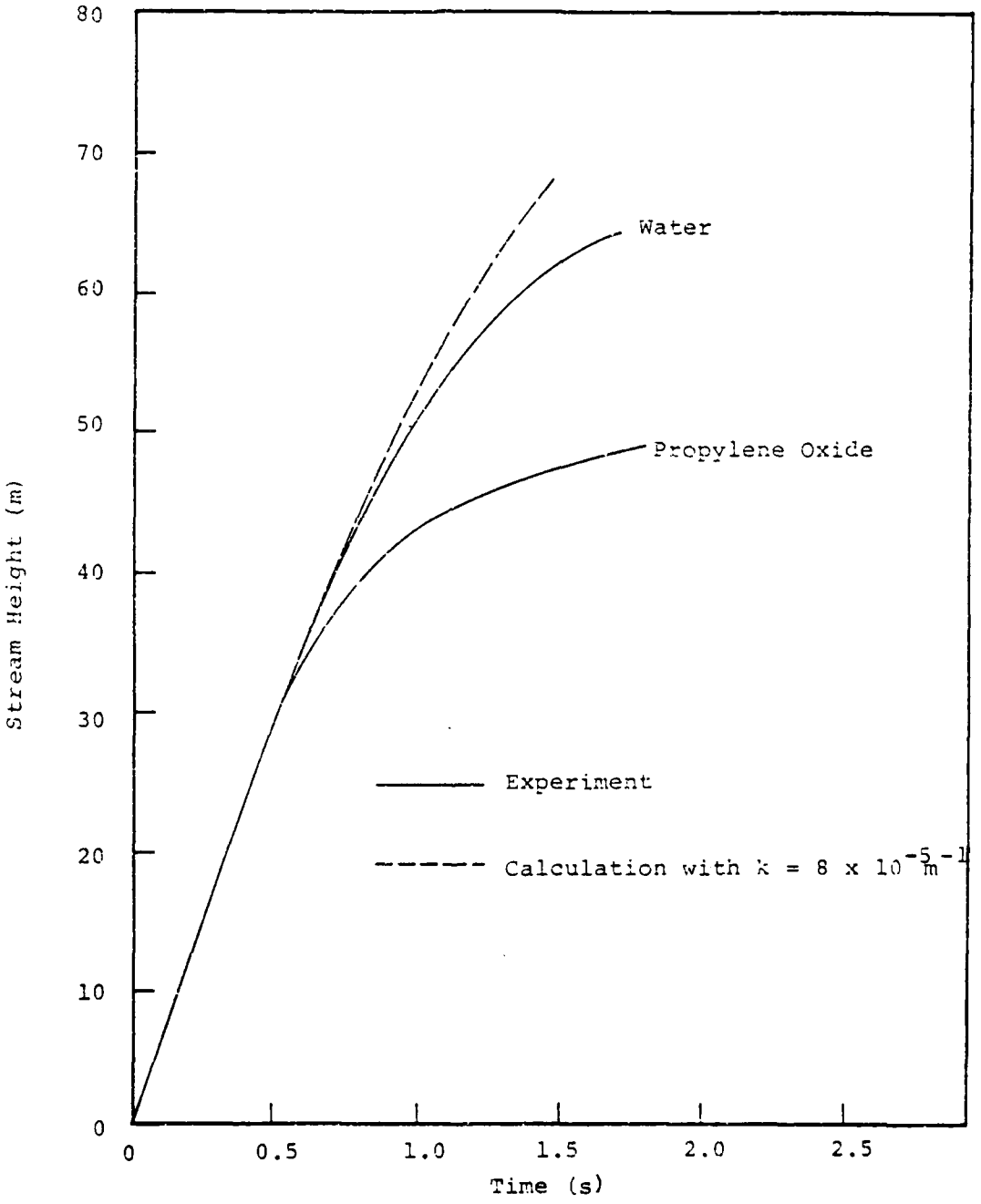

Figure 28. Comparison of water and propylene oxide stream height from two experiments involving projection from a 3.81-cm (1.5-in) diameter nozzle at initial velocities of 72 m/s (236 ft/s).

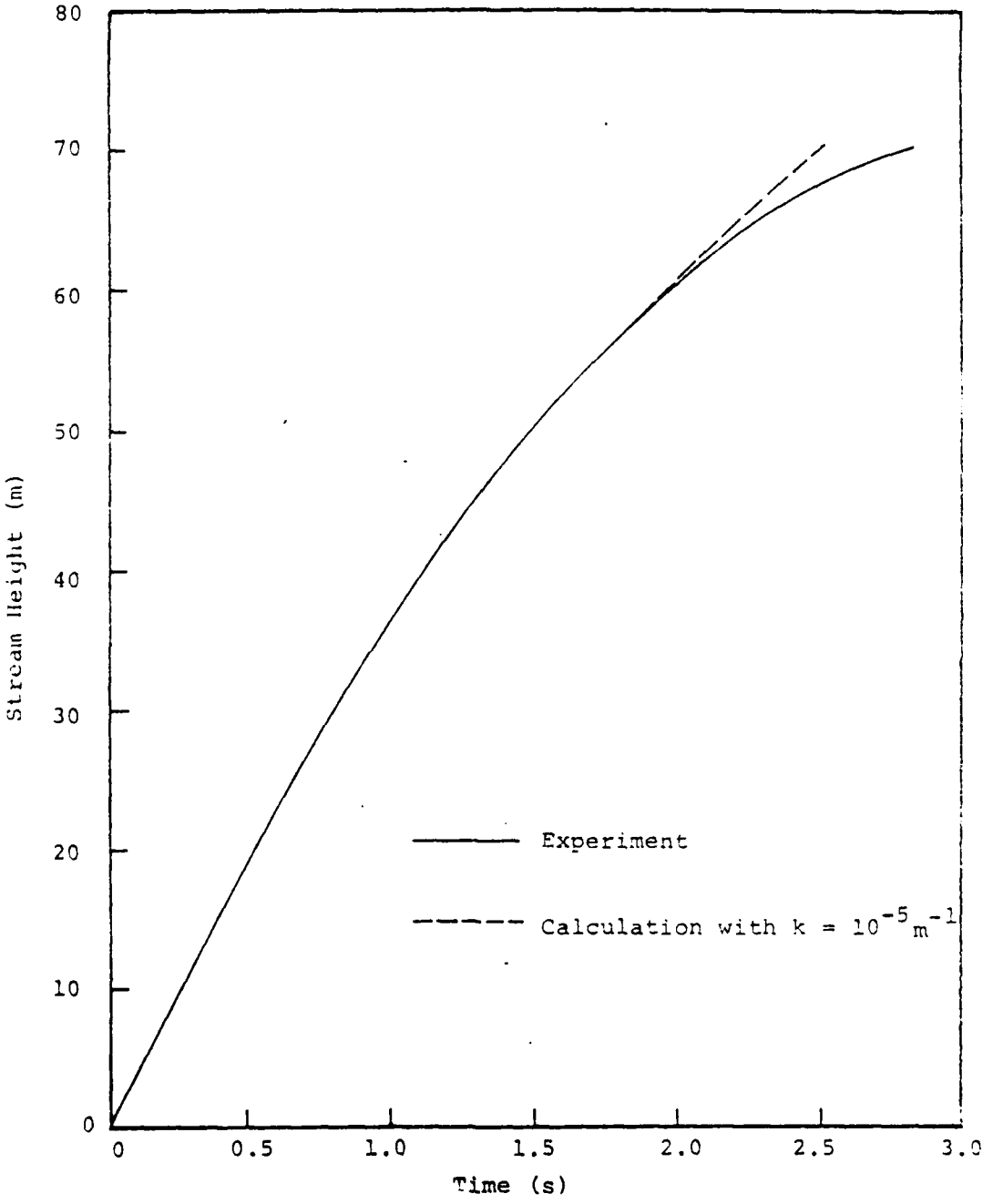

Figure 29. Comparison of stream height as a function of time for the case of water being projected from a 6.35-cm (2.5-in) diameter nozzle with predictions from Equation 1. The coefficient k used in Equation 1 was 1 x 10^{-5} m^{-1} and the initial velocity was 42 m/s (138 ft/s).

obtain the best theoretical-experimental fit. It is interesting to note that this coefficient changes with nozzle diameter but is not a function of the physical properties of the fluid being projected. It should be mentioned here that the 3.81-cm and 6.35-cm diameter nozzles employed in the two experiments were not similar, i.e., their length-to-diameter ratios were different. For this reason, no conclusions can be drawn at this time regarding the relationship between the drag coefficient and nozzle diameter.

Figure 30 is a plot of stream height versus time for the case of propylene oxide being projected through a 6.35-cm (2.5-in) diameter nozzle at an initial velocity of 44.5 m/s (146 ft/s). Again, up to the point of rapid increase in deceleration, it appears that the coefficient, k, is more sensitive to changes in nozzle diameter than to changes in fluid properties. The final stream height of the propylene oxide was about 54 m (177 ft), which is about 70 percent of the height required for the full-scale blast simulator. In order to obtain greater stream heights, it probably will be necessary to use nozzles having diameters greater than 6.35 cm (2.5 in).

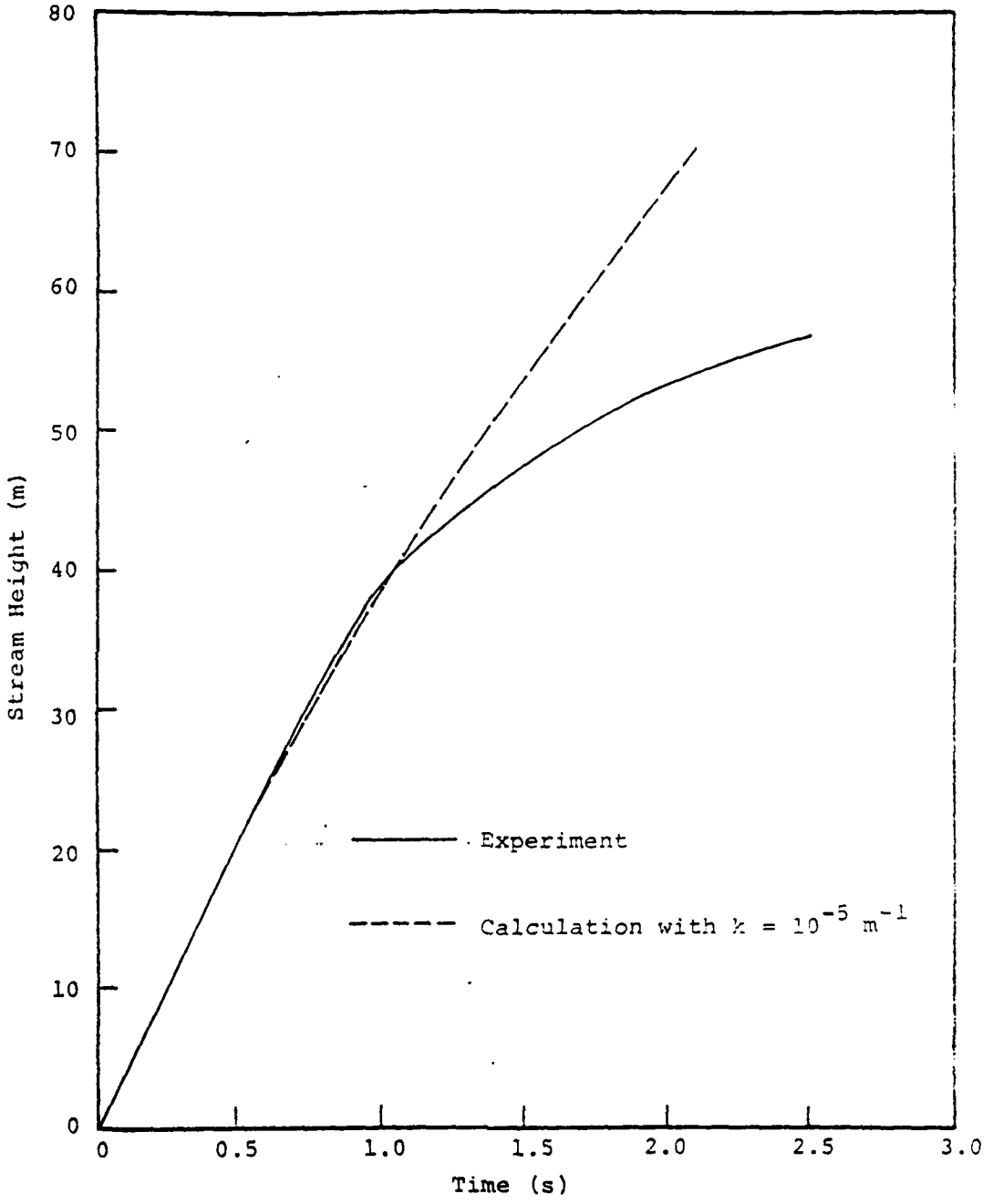

Figure 30. Comparison of stream height as a function of time for the case of propylene oxide being projected from a 6.35-cm (2.5-in) diameter nozzle with predictions from Equation 1. The initial velocity of the stream was 44.5 m/s (146 ft/s).

VI. SCALING LAWS AND EQUIVALENCES

In order to scale the experimental FAE blast wave data for comparison with 1-KT nuclear blast wave data, the governing scaling laws as well as the fuel-air-explosive energy equivalence of a given nuclear yield must be known. In scaling either nuclear or FAE blast wave data to different yields, simple cube root scaling holds, i.e., range, time and impulse scale as the cube root of the ratio of the yields. However, if it is required to scale blast wave data from a given yield of FAE for comparison with blast wave data from a nuclear source of a different yield, the equivalent FAE energy for representing the nuclear yield must be known. In the current effort the blast wave data generated by an FAE cloud formed from 22.2 kg (49 lbs.) of propylene oxide was to be scaled for comparison with 1-KT nuclear blast wave data. To accomplish this it was first necessary to determine the yield of FAE equivalent to a 1-KT nuclear yield. A fuel-air-explosive cloud formed from 136,000 kg (300,000 lbs.) of propylene oxide has a theoretical energy equivalent to 1 KT. Thus if the FAE-Nuclear energy equivalence factor were unity, the scale factor would be 18.3 since that is the cube root of the ratio of 136,000 kg (300,000 lbs.) to 22.2 kg (49 lbs.). An analysis of the data generated to date, however, has indicated that the FAE-Nuclear energy equivalence factor is 0.67 rather than unity and that the scale factor is 16 rather than 18.3. The procedure used to determine both the FAE-nuclear energy equivalence factor and the scale factor is outlined in the following paragraphs.

In order to establish the scale factor and the FAE-nuclear equivalence factor, reference was made to the following equation from Brode[1] which relates the positive phase static impulse (psi-s) at a range, R (kft), to the yield, Y (MT):

$$I_p^+ = 1.83\ (\Delta P_s)^{1/2}\ Y^{1/3}[1.0 + 0.00385\ (\Delta P_s)^{1/2}] \quad (2)$$

where ΔP_s, the peak static pressure, is given by

$$\Delta P_s = 3300 \left(\frac{Y}{R^3}\right) + 192 \left(\frac{Y}{R^3}\right)^{1/2} .$$

The positive phase impulse determined from measured FAE blast wave data at various ranges and averaged over several experiments allowed Eq. (2) to be solved for the yield, Y, which is the equivalent nuclear energy yield required to generate the measured blast wave data. The scale factor for scaling the experimental data for comparison with 1-KT nuclear data is therefore simply $(1/Y)^{1/3}$. Table III tabulates the data used to obtain the scale factor including the positive phase impulses determined at five gauge locations, the values of Y as determined by Eq. (2) at each gauge location and finally the values of $(1/Y)^{1/3}$ at each gauge location. The average scale factor over all five gauge locations was 15.84 which was rounded to 16.0.

Thus the nuclear/fuel-air-explosive equivalence factor and the scale factor used in the next section are 1.5 and 16 respectively.

This simply means that 9.08×10^4 kg (200,000 lb.) of fuel rather than 1.36×10^5 kg (300,000 lb.) will be required in the full scale simulator for simulating the blast wave from a 1-KT nuclear event. In addition, range, time and positive phase impulse associated with the small scale experimental data involving 22.2 kg (49 lbs.) of dispersed fuel must be scaled by a factor of 16 for comparison with 1-KT nuclear blast wave data.

Another type of scaling that must be understood before a large-scale blast simulator can be constructed is related to the dissemination process itself. More specifically, it must be determined how cloud radius or stream reach and dissemination time scale with such parameters as nozzle diameter,

Table III. Summary of Positive Phase Static Impulses, FAE Yield Equivalences and FAE/Nuclear Equivalence Factors for Five Selected Ranges Using Shots of 12 October, 13 October and 18 October 1977.

		Gauge				
		L20	S30	L40	S44	L80
Positive Phase Static Impulse MPa-ms and (psi-s)	Shot No. 1, 12 Oct	0.887 (0.130)	0.713 (0.105)	0.420 (0.062)	0.392 (0.057)	0.217 (0.032)
	Shot No. 1, 13 Oct	0.800 (0.118)	0.495 (0.073)	0.327 (0.048)	0.346 (0.051)	0.184 (0.027)
	Shot No. 1, 18 Oct	0.825 (0.121)	0.509 (0.075)	0.392 (0.058)	0.347 (0.051)	0.218 (0.032)
	Average	0.837 (0.123)	0.572 (0.084)	0.380 (0.056)	0.361 (0.053)	0.206 (0.030)
FAE Yield (KT)		2.06×10^{-4}	2.50×10^{-4}	2.30×10^{-4}	3.17×10^{-4}	2.74×10^{-4}
FAE Nuclear Scale Factors		16.9	15.9	16.3	14.7	15.4
Average Scale Factor		15.84				

nozzle length-to-diameter ratio, and driving pressure. Such scaling laws remain to be determined; however, it can be noted from the data presented in Section V that dissemination time does not scale linearly with cloud diameter and that maximum reach increases with nozzle diameters.

VII. SCALED FAE-NUCLEAR BLAST WAVE DATA COMPARISON

The measured overpressure blast waveforms from several of the FAE experiments were digitized and stored in the computer for facilitating both scaling and plotting. Figures 31 through 38 are computer plots of scaled digitized data for several gauge locations for FAE Shot No. 1, 1220 Tuesday, 18 October 1977. Both the experimental ranges and time were scaled linearly, using the previously determined scale factor of 16. As described in Section VI, the scale factor was determined by fitting the measured impulses at various ranges to a 1-KT nuclear impulse versus range curve. Peak impulse rather than peak static pressure was used for determining the scale factor, since the measured peak static overpressures were, in general, low due to finite gauge response times. The solid lines in the plots (Figures 31 through 34) are the scaled experimental blast waveforms and the dashed lines are nuclear blast wave data from a 1-KT yield nuclear event. It is seen that agreement between the scaled FAE data and the nuclear data is acceptable.

Figures 35 through 38 are plots of the positive phase impulse. The data plotted in these figures are from the same gauge locations as those used in the plots of pressure as a function of time. Again, the scaled experimental FAE data are represented by the solid lines and the 1-KT nuclear blast data are represented by the dashed lines. It is seen that agreement is good and in general within 20 percent. In Appendices A through D a similar series of scaled overpressure and positive phase impulse plots from four different tests are presented.

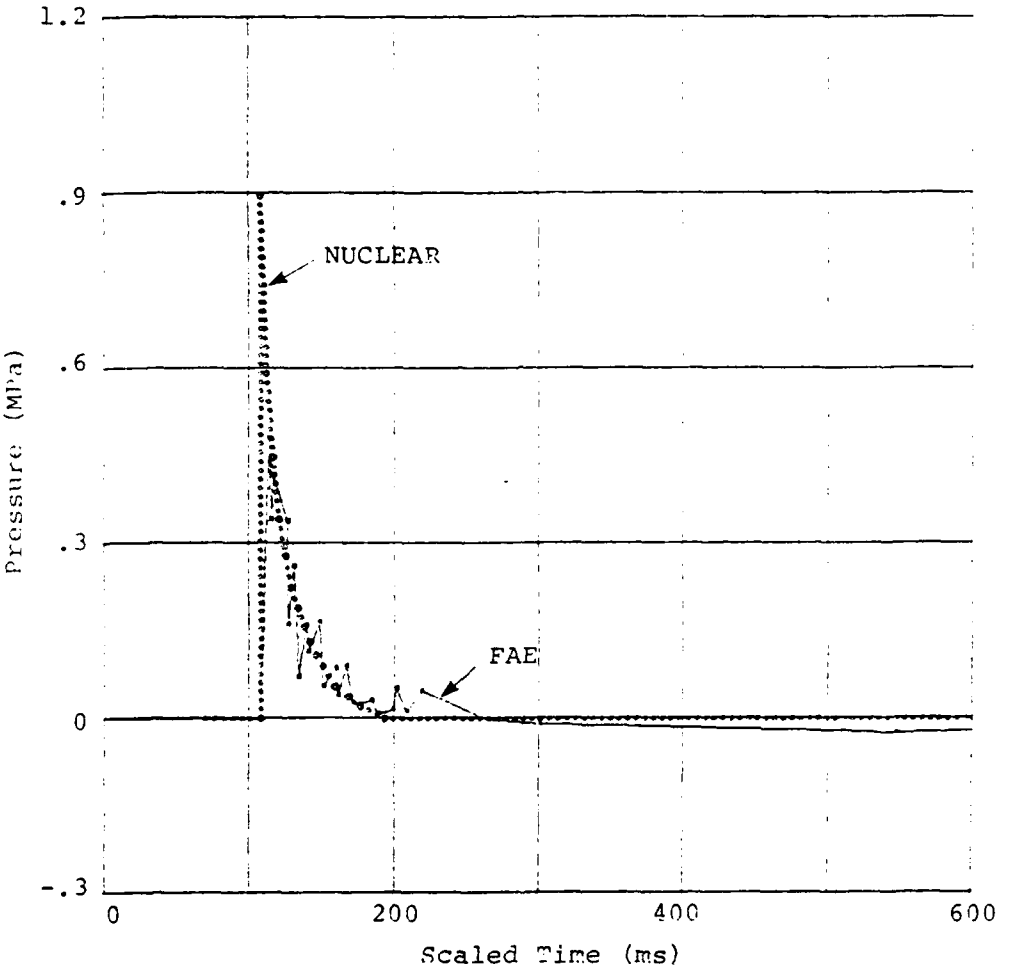

Figure 31. Comparison of scaled measured overpressure as a function of time with a 1-KT nuclear blast waveform. The scaling factor used was 16 and the scaled range was 98 m (320 ft). The experimental data were taken from Shot No. 1, 18 October 1977.

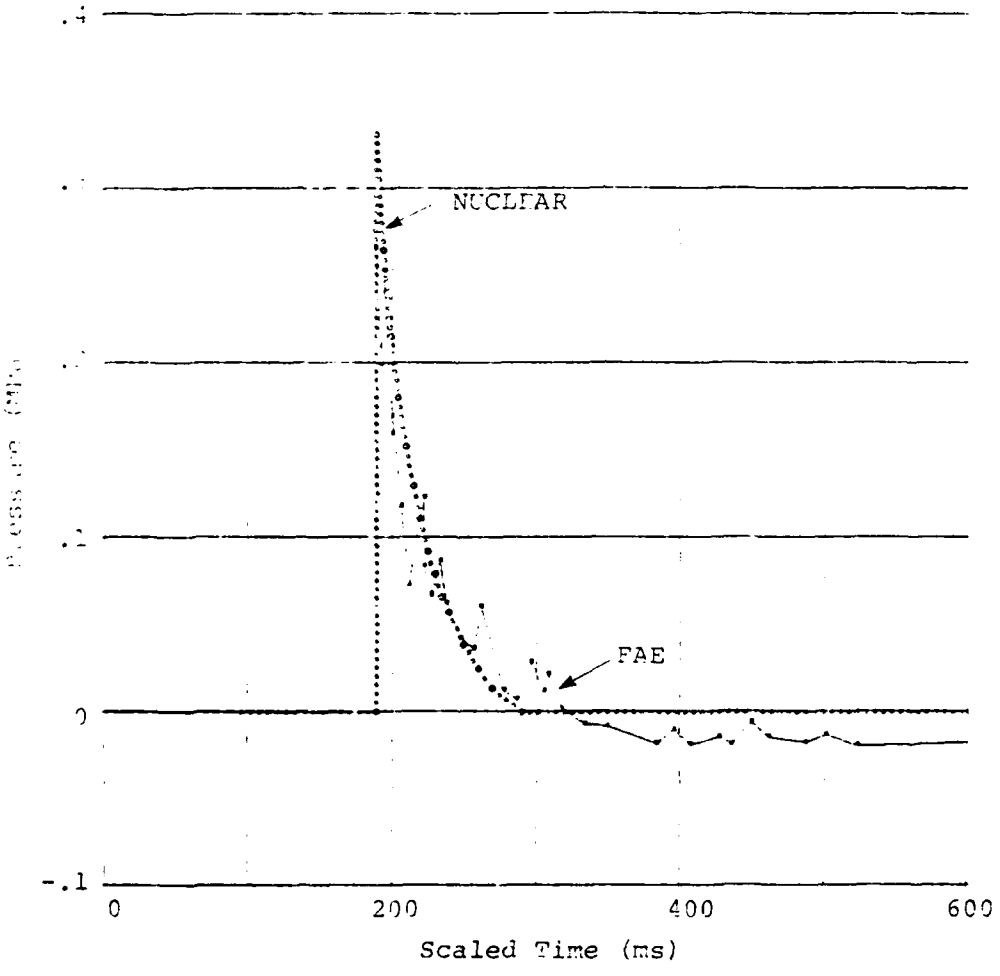

Figure 32. Comparison of scaled measured overpressure as a function of time with a 1-KT nuclear blast waveform. The scaling factor used was 16 and the scaled range was 146 m (479 ft). The experimental data were taken from Shot No. 1, 18 October 1977.

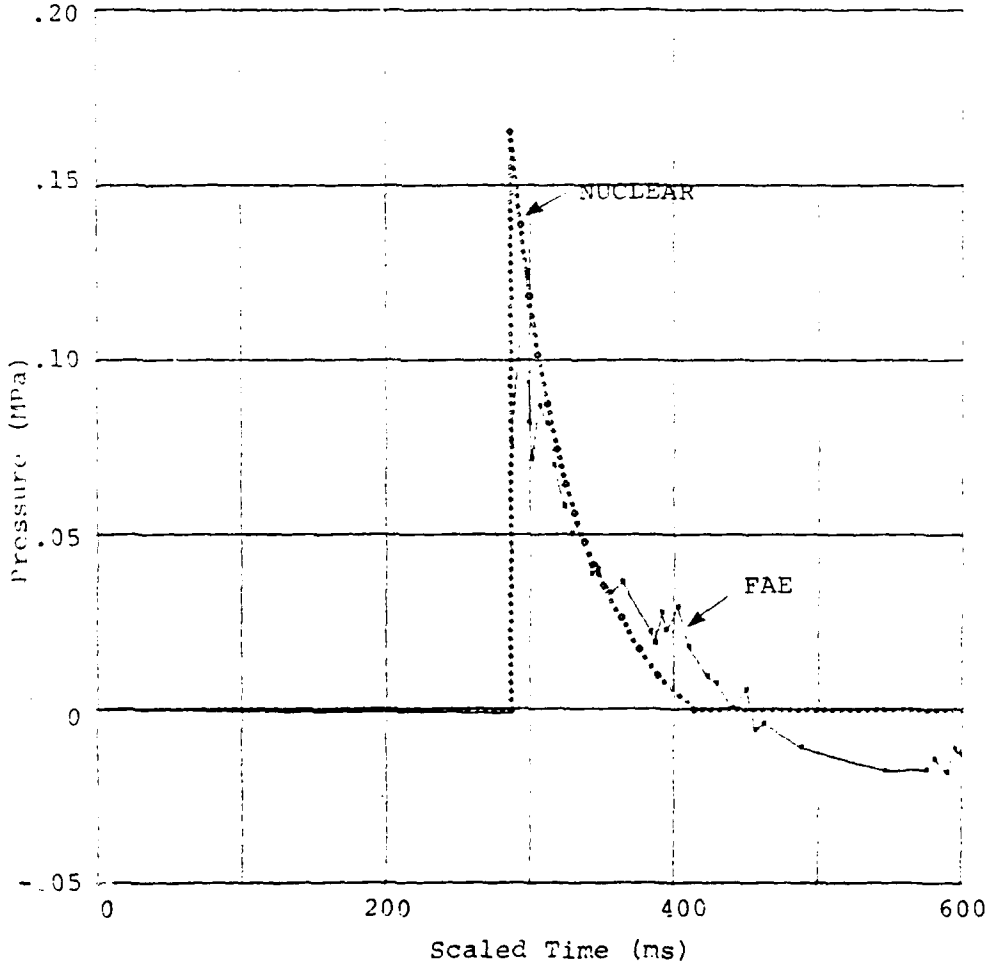

Figure 33. Comparison of scaled measured overpressure as a function of time with a 1-KT nuclear blast waveform. The scaling factor used was 16 and the scaled range was 195 m (640 ft). The experimental data were taken from Shot No. 1, 18 October 1977.

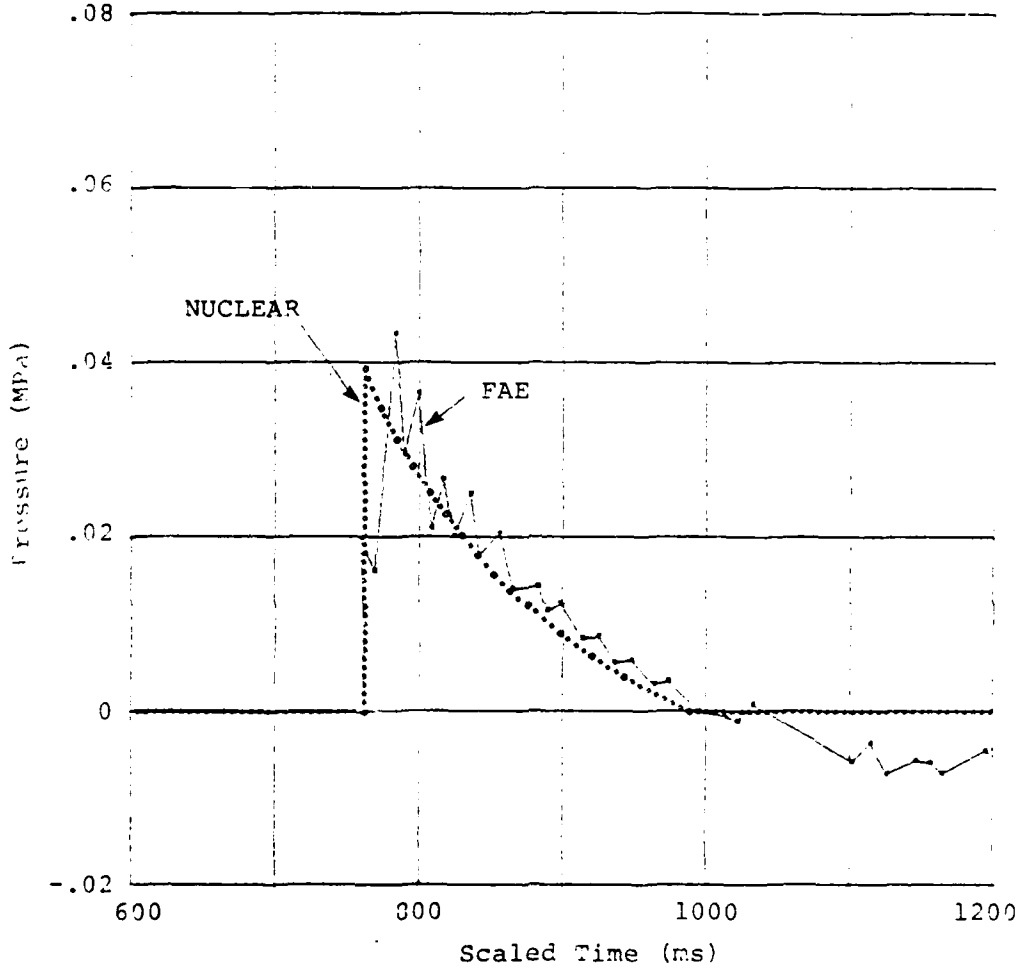

Figure 34. Comparison of scaled measured overpressure as a function of time with a 1-KT nuclear blast waveform. The scaling factor used was 16 and the scaled range was 390 m (1280 ft). The experimental data were taken from Shot No. 1, 18 October 1977.

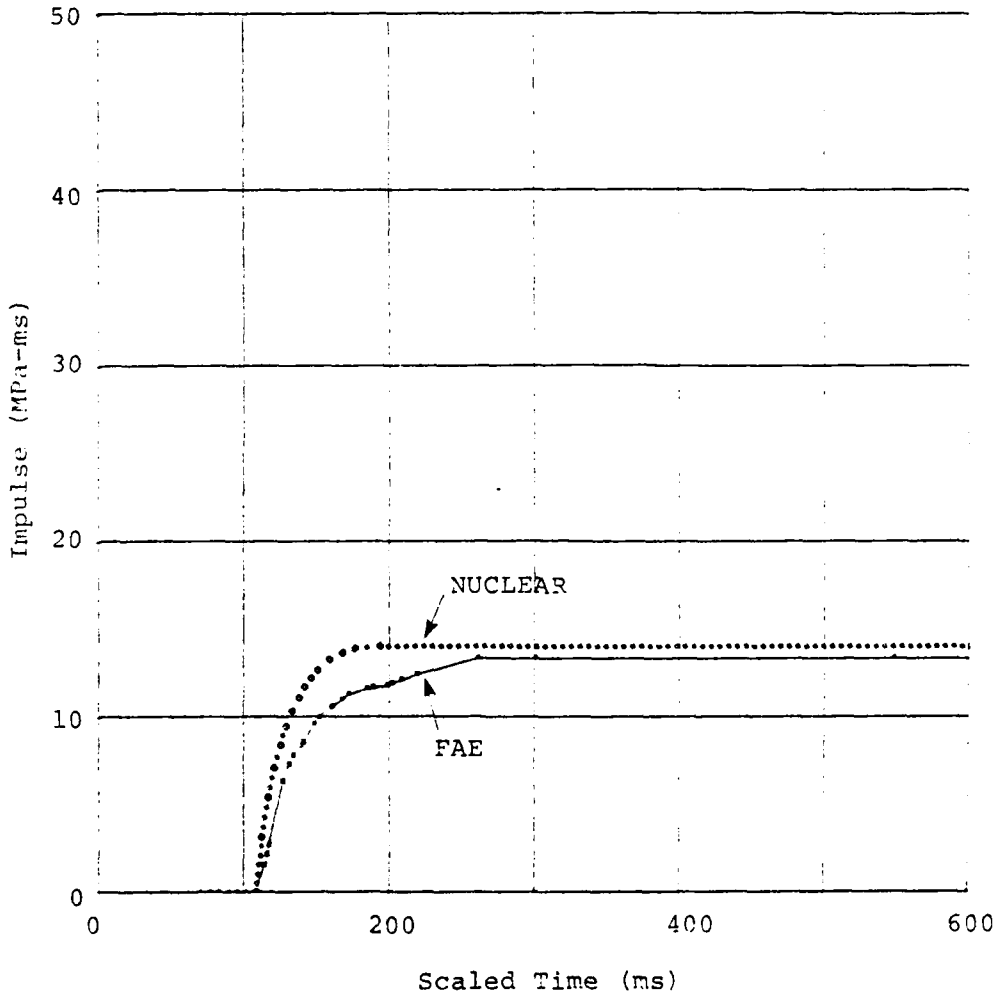

Figure 35. Comparison of scaled measured positive phase impulse with 1-KT nuclear data. The scale factor used was 16 and the scaled range was 98 m (320 ft). The experimental data were taken from Shot No. 1, 18 October 1977.

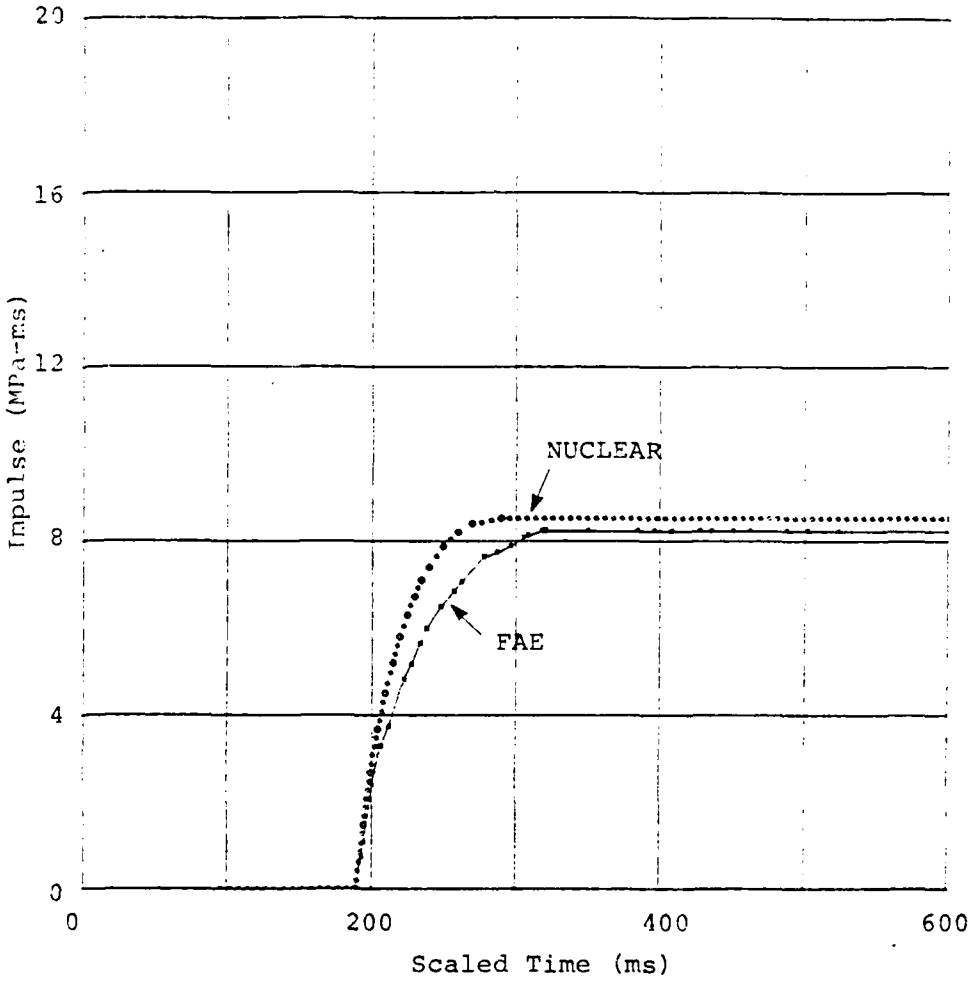

Figure 36. Comparison of scaled measured positive phase impulse with 1-KT nuclear data. The scale factor used was 16 and the scaled range was 146 m (479 ft). The experimental data were taken from Shot No. 1, 18 October 1977.

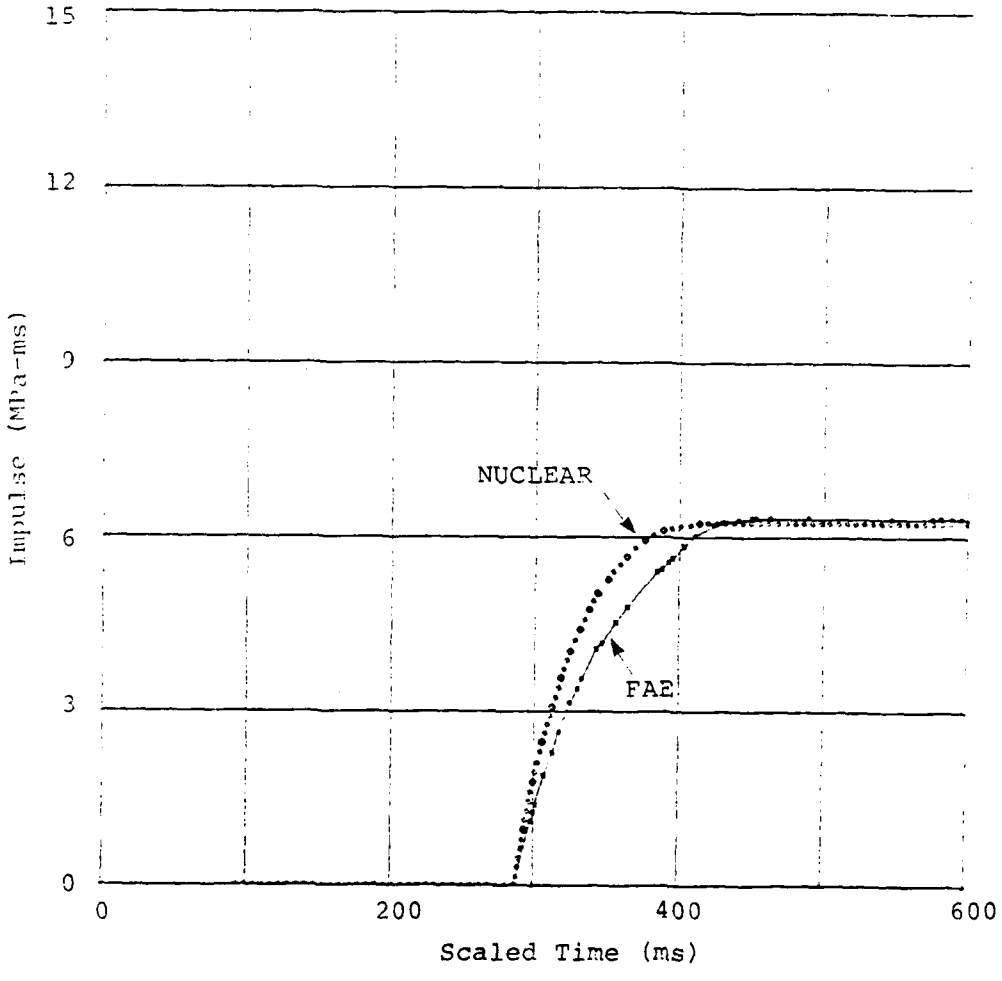

Figure 37. Comparison of scaled measured positive phase impulse with 1-KT nuclear data. The scale factor used was 16 and the scaled range was 195 m (640 ft). The experimental data were taken from Shot No. 1, 18 October 1977.

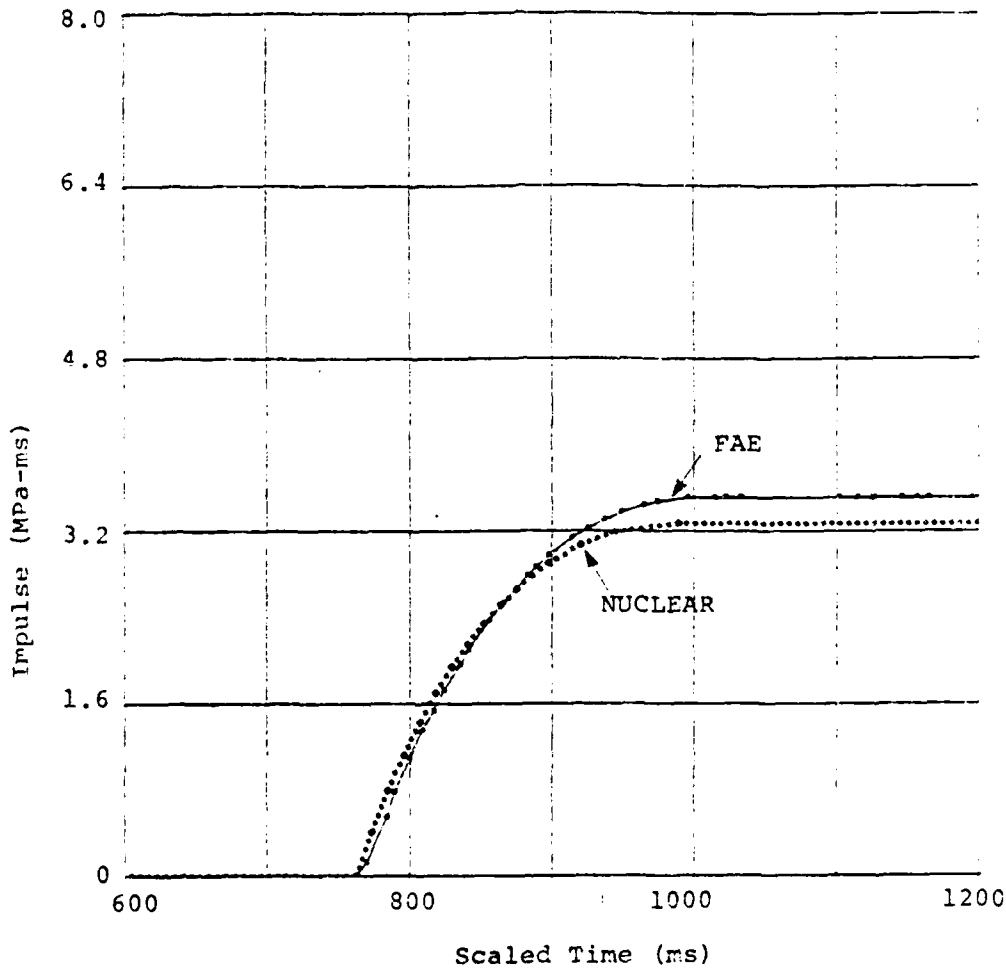

Figure 38. Comparison of scaled measured positive phase impulse with 1-KT nuclear data. The scale factor used was 16 and the scaled range was 390 m (1280 ft). The experimental data were taken from Shot No. 1, 18 October 1977.

VIII. FULL-SCALE SIMULATOR

It was shown in Section VI that the simulation of airblast from a 1-KT nuclear device requires a 160-m (524-ft) diameter hemispherical FAE cloud formed from 91,000 kg (200,000 lb) of propylene oxide. A full-scale FAE blast simulator of the type investigated here will require dispersal of that amount of fuel into a hemispherical cloud which can be detonated at a point on the axis of symmetry near its center. To be effective, the technique for dispersing the fuel should have the following characteristics:

- The dispersal of the entire mass of fuel should be accomplished in a time of the order of several seconds in order to minimize disturbing effects of wind.
- The fuel must be distributed as uniformly as possible throughout the hemispherical cloud and form a detonable fuel-air mixture.
- The cloud shape, size and fuel distribution must be accurately repeatable.
- The dispersal facility must be reusable.
- The dispersal technique should be as simple as possible.

The dispersal method proposed for the full-scale blast simulator under investigation here is one that has all the above-listed characteristics and, in addition, can be incorporated into a full-scale facility design at relatively low cost.

8.1 DESCRIPTION OF DISPERSAL HARDWARE

The proposed method of dispersing the fuel into a hemispherical cloud is illustrated in a general way in Figure 39. The fuel is dispersed from an array of dispensers, perhaps 0.6 m (2.0 ft) in diameter and 18 m (60 ft) long,

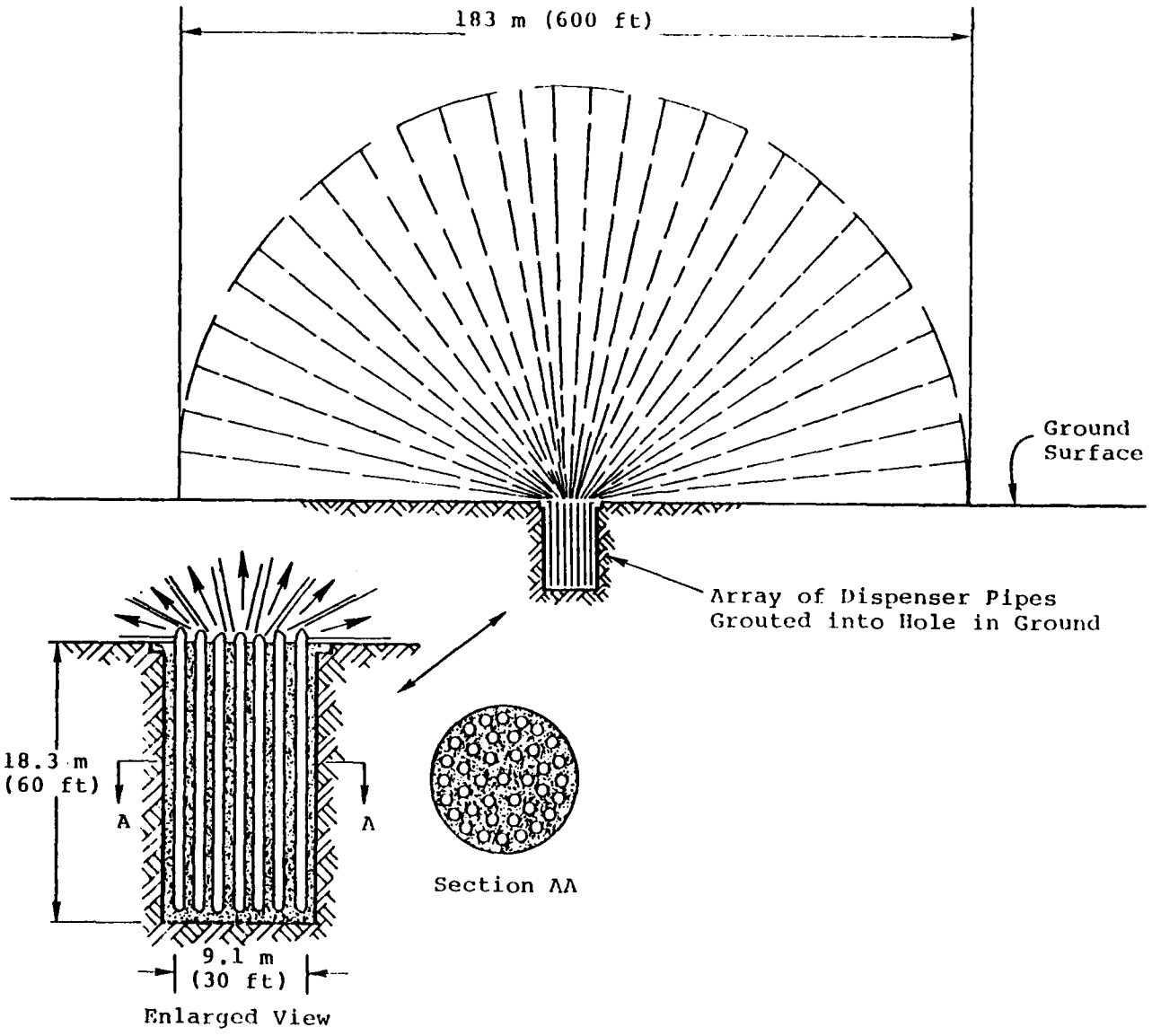

Figure 39. General arrangement of fuel dispenser.

embedded vertically in the ground near the center of the hemispherical cloud that is to be formed. The tops of the dispensers are at ground level and are capped with heads containing arrays of nozzles. Fuel is forced through the nozzles at high velocity by pressure produced by a gas generator. The arrays of nozzles in the dispensers heads are arranged so as to produce a uniform distribution of fuel streams throughout a hemispherical volume. The reach to which the fuel is projected decreases continuously as the propellant pressure in the dispenser decreases. Later in this discussion it will be shown that, in principle, the decreasing pressure can be tailored to produce a uniform distribution of fuel throughout the hemispherical volume. After the fuel is completely dispersed and allowed to mix with air, the resulting FAE cloud will be detonated by a high-explosive charge (or multiple charges to ensure reliability) mounted near the center of the hemisphere. Past experience has shown that the clouds can be detonated with 0.1-kg (0.2-lb) HE charges.

Figure 40 shows a conceptual design of an individual dispenser. The dispenser actually consists of two concentric pipes as shown, the inner pipe having a solid head and the head of the outer pipe containing the nozzle array. The pipes are filled with fuel to the appropriate level (it will be shown later that the appropriate level may be about two-thirds the length of the pipe). The solid propellant is located in the volume of the inner pipe between the top of the fuel and the top of the pipe. Pressure produced upon ignition of the propellant forces fuel down the inner pipe, up the annular space between the inner and outer pipes and out the nozzles. Only a few pounds of solid propellant are required to produce the necessary 3.4-MPa (500-psi) pressure to expel the fuel from the dispensers with sufficient velocity to fill a 160-m (520-ft) diameter hemisphere.

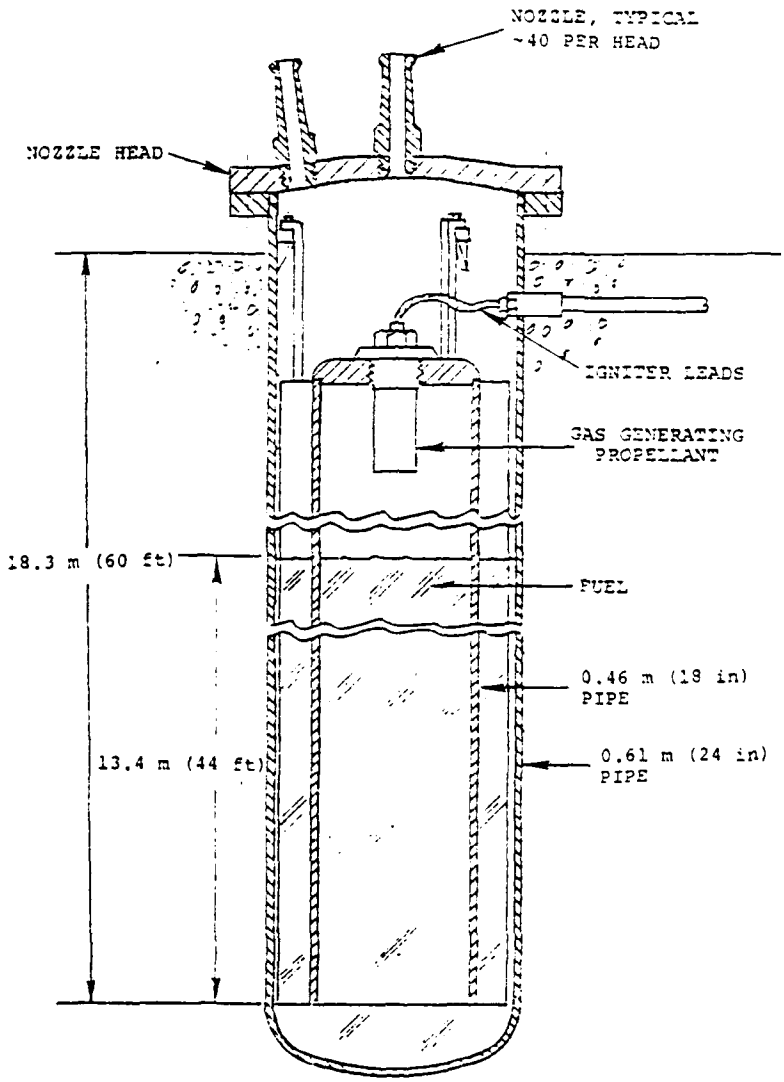

Figure 40. Conceptual design of a single dispenser assembly

The fuel could initially be at the same level in both the inner and outer pipes, as shown in Figure 40, or if this arrangement produces undesirable "water hammer" effects when the fuel first impacts the nozzle head, the inner pipe could be pressurized (perhaps with nitrogen) to raise the top of the fuel in the outer pipe to the level of the nozzle head. The nozzles will probably have smooth round holes of constant diameter, with entrances rounded as shown in Figure 40. They can be made as machined parts (much as fire hose nozzles) that screw into threaded holes in the nozzle head. The nozzle head on each of the dispensers will be oriented in the proper direction and at the proper angle to direct the streams from that particular dispenser into their appropriate volume element of the hemisphere. Figure 41 shows two such head arrangements, one for nozzles directed nearly vertically and the other for nozzles directed nearly horizontally. Other heads would have nozzles directed at other angles.

8.2 FUEL DISPERSAL TECHNIQUES

The dispersal method is based upon the properties of liquid streams that are produced by flow through nozzles of the proposed design. The available information on such streams is largely from measurements that have been made on the characteristics of streams from nozzles used on fire hoses. A characteristic of such streams is that they remain solid streams for about 80 percent of their total length, after which they break up and disperse over a region much larger than that of the solid stream. In measuring the height of vertical fire hose streams, the height that is measured is that of a "good stream," which is defined as a stream in which 90 percent of its volume falls within a circle of 38.1 cm (15 in) diameter. In a "good stream," 61 m (200 ft) in height, for example, at least 90 percent of the water reaches a height of 61 m and breaks up and

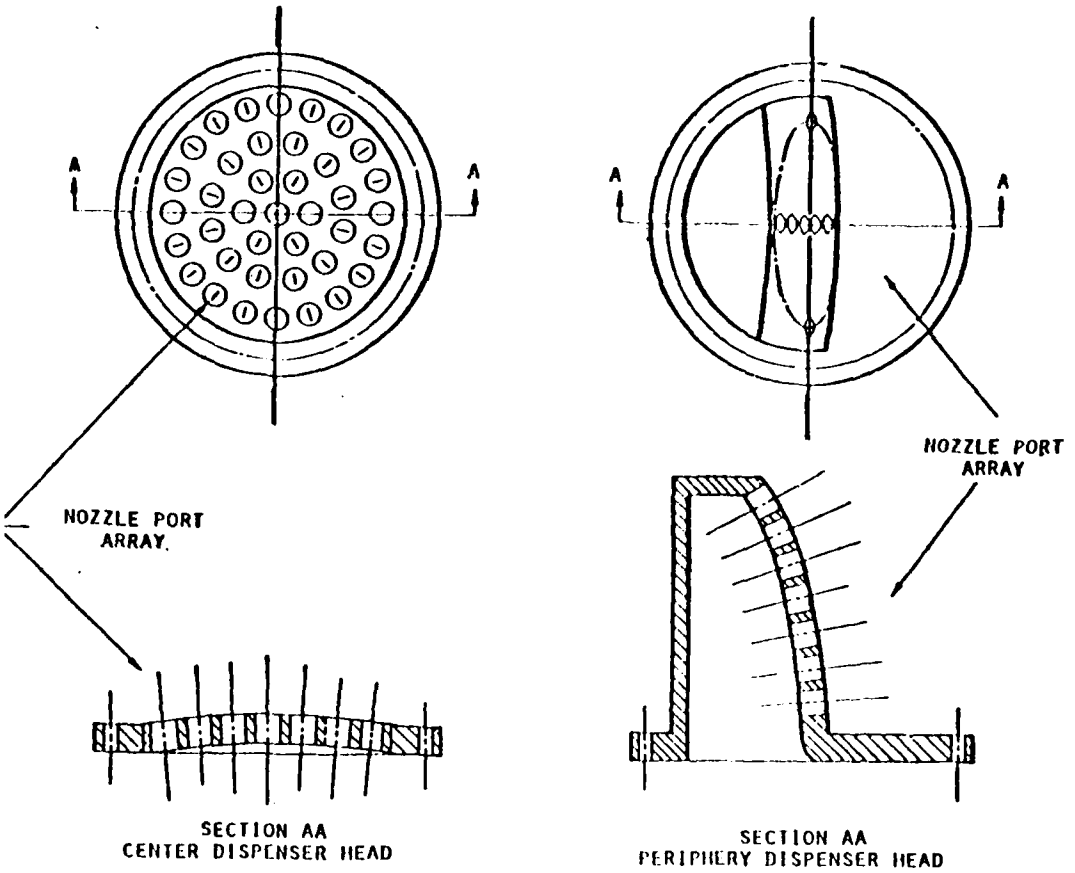

Figure 41. Typical dispenser heads for directing fuel streams at different angles.

disperses within a short distance above this height. The fact that most of the liquid is dispersed near the end of the stream is, as discussed below, the basis for producing a uniform distribution of the fuel throughout the hemispherical cloud.

Data on the height of fire hose streams are from tests by the Chicago Fire Department [2] on the height of streams from smooth nozzles of the type proposed here. The height measured was that for a "good stream" as previously defined. The data on stream height versus nozzle pressure for a 5.1-cm (2.0-in) diameter nozzle are presented in Figure 42.

The following equation was found to be a good fit to the data of Figure 42:

$$P = 2.08 \times 10^{-5} R^{2.72} \quad (1)$$

where

P = nozzle pressure (MPa).

R = stream height (m).

Equation (1) indicates that a nozzle pressure of 3.12 MPa (460 psi) is required to produce a stream height of 80 m (262 ft) which is that of the hemispherical cloud in the FAE blast simulator. These data are for the flow of water; the flow of FAE fuel can be expected to be somewhat different because of differences in viscosity (which affects flow velocity) and in surface tension (which affects stream breakup). However, data on the flow of water appears to be the only data available and is the data upon which the following discussion is based. Similar data for use in designing the FAE blast simulator is currently being generated for various FAE fuels. The equations governing the flow of FAE fuels are expected to be of the same form as

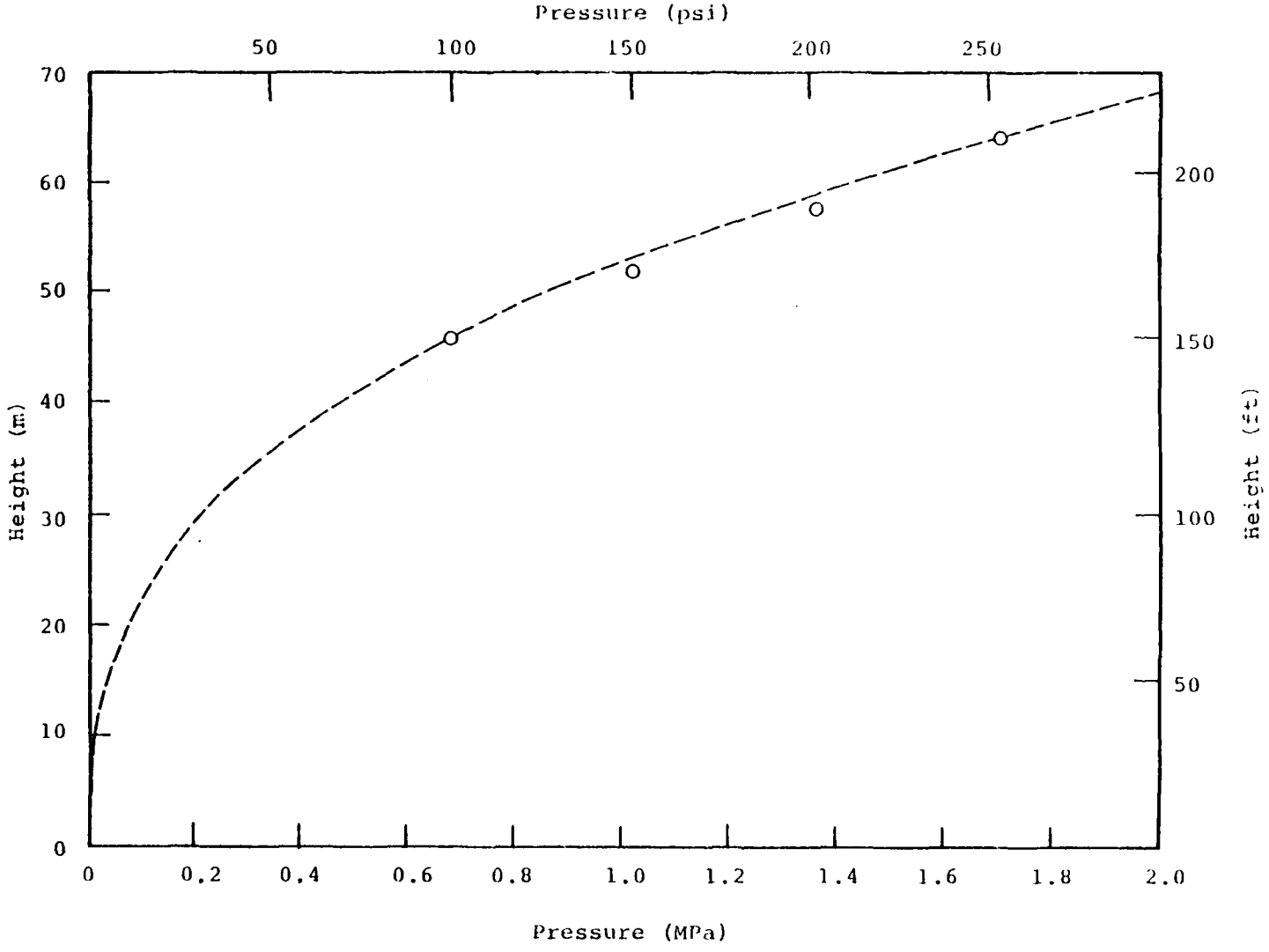

Figure 42. Plot of stream height versus driving pressure for a vertical stream of water. The data were taken from Reference 2 and are for a 5.08-cm (2.0 in) diameter nozzle.

those for water. Therefore, the method for calculating dispersal that is presented below using equations for water should also apply to FAE fuels, but with different constants.

Streams that are directed at angles other than vertical have a somewhat greater range than vertical streams, thus requiring that the amount of propellant in the dispensers be adjusted so that the initial range of the streams will be 80 m (262 ft) at all angles from vertical to horizontal.

In the following, we develop an equation for the nozzle pressure versus time that would be required to uniformly fill a hemispherical volume with fuel which is dispersed by individual streams that break up at the ends of their range. We then compare this equation with the pressure versus time of the expanding propellant gases, assuming an isentropic expansion for these gases. It will be seen that the pressure versus time of the expanding propellant gases is a close approximation to that required to uniformly disperse the fuel throughout the hemispherical volume.

We assign to each fuel stream a solid angle which is its "fair share" of the total solid angle of the hemisphere. In order to uniformly disperse the fuel throughout the cloud, each fuel stream must uniformly disperse its fuel within a prescribed solid angular region and out to the final radius R_o of the FAE cloud. The solid angle ω, expressed in steradians, assigned to each stream is given by

$$\omega = \frac{2\pi}{N}$$

where N is the number of fuel streams. The area, A, subtended by ω at a radius R is simply ωR^2. In an ideal dispersal system, the fuel stream would uniformly spread over the area, A, at the end of its range as the range decreased from $R = R_o$ to $R = 0$ as the propellant pressure decreased from $P = P_o$ to $P = 0$, where P_o is the initial pressure of the propellant.

The volume within the solid angle ω swept through by area A is given by

$$U = \int_{R}^{R_o} AdR = -\int_{R_o}^{R} AdR = -\int_{o}^{t} A\left(\frac{dR}{dt}\right) dt$$

which upon differentiation gives

$$\frac{dU}{dt} = -A\frac{dR}{dt}$$

But since A is proportional to R^2, we have

$$\frac{dU}{dt} \propto -R^2\frac{dR}{dt} \tag{2}$$

In the ideal dispersal system we want

$$Q \propto \frac{dU}{dt} \tag{3}$$

where Q is the fuel flow rate through the nozzle. The flow rate is given by

$$Q = \frac{\pi d^2}{4} \cdot v \tag{4}$$

where d is the nozzle diameter and v is the velocity of the fluid through the nozzle. The velocity as determined from Bernoulli's equation can be expressed as

$$v = \left[\frac{2P}{\rho}\right]^{1/2} \tag{5}$$

and substituted into Equation (4) to obtain

$$Q = 1.11\ d^2P^{1/2} \tag{6}$$

since, for water, the density is 1×10^3 kg/m^3. If d is expressed in m and pressure in MPa, the units associated with the flow rate, Q, are m^3/s.

From Equation (1), which is for the case of a 5.1-cm (2.0-in) diameter nozzle,

$$R = 52.64\ P^{0.368}$$

and

$$\frac{dR}{dt} \propto P^{-0.632}\ \frac{dP}{dt} \tag{7}$$

Substituting (3), (5), (6) and (7) into (2) and solving for $\frac{dP}{dt}$ gives

$$-\frac{dP}{dt} \propto d^2 P^{0.396} \tag{8}$$

Equation (8) can be integrated to obtain

$$P = P_o\left[1 - \left(\frac{t}{t_D}\right)\right]^{1.65} \tag{9}$$

where t_D is the total time to dispense the water.

Equation (9) thus gives the nozzle pressure as a function of time that would be required to uniformly distribute water throughout the solid angle assigned to each nozzle.

We are not likely to be so fortunate as to have the pressure of the propellant gases decrease with time in agreement with Equation (9). However, the pressure of the propellant gases is likely to decrease according to

$$(P + P_A) = (P_o + P_A)\left(\frac{V_o}{V}\right)^{\gamma} \tag{10}$$

where

V_o = initial volume of propellant gases.

V = volume of propellant gases at time, t.

P_A = atmospheric pressure.

Equation (10) can be solved stepwise to determine P as a function of t for various values of V_o and the results compared with Equation (9) to determine how closely the decrease in propellant pressure can be expected to follow the desired decrease. To do this, V is determined for each step in the calculation from

$$V = V_o + \sum_{o}^{t} Q \cdot \Delta t = V_o + 1.11\, d^2 \sum_{o}^{t} \left(\frac{P}{\rho}\right)^{1/2} \cdot \Delta t \qquad (11)$$

where the expression for Q is obtained from Equation (4). Curves of P versus t with P_o = 3.12 MPa and V_o = 2 m^3 as determined from Equations (10) and (11) are compared in Figure 43. These calculations are for a 5.08-cm diameter nozzle and γ = 1.27, a value that fits the expansion of HE detonation gases.

The comparison in Figure 43 shows that for this particular case (i.e., for water and a 5.08-cm diameter nozzle), the expansion of the propellant gases results in a pressure versus time curve that is within 23 percent of that required for uniform dispersal for pressures above 1 MPa. At pressures below 1 MPa, the propellant gases produce a pressure higher than required, resulting in streams longer than would be required to fill the volume near the center of the hemisphere. It is likely that this portion of the cloud would be filled by the fuel that is stripped from the streams during their passage through the air. If, however, this were not sufficient

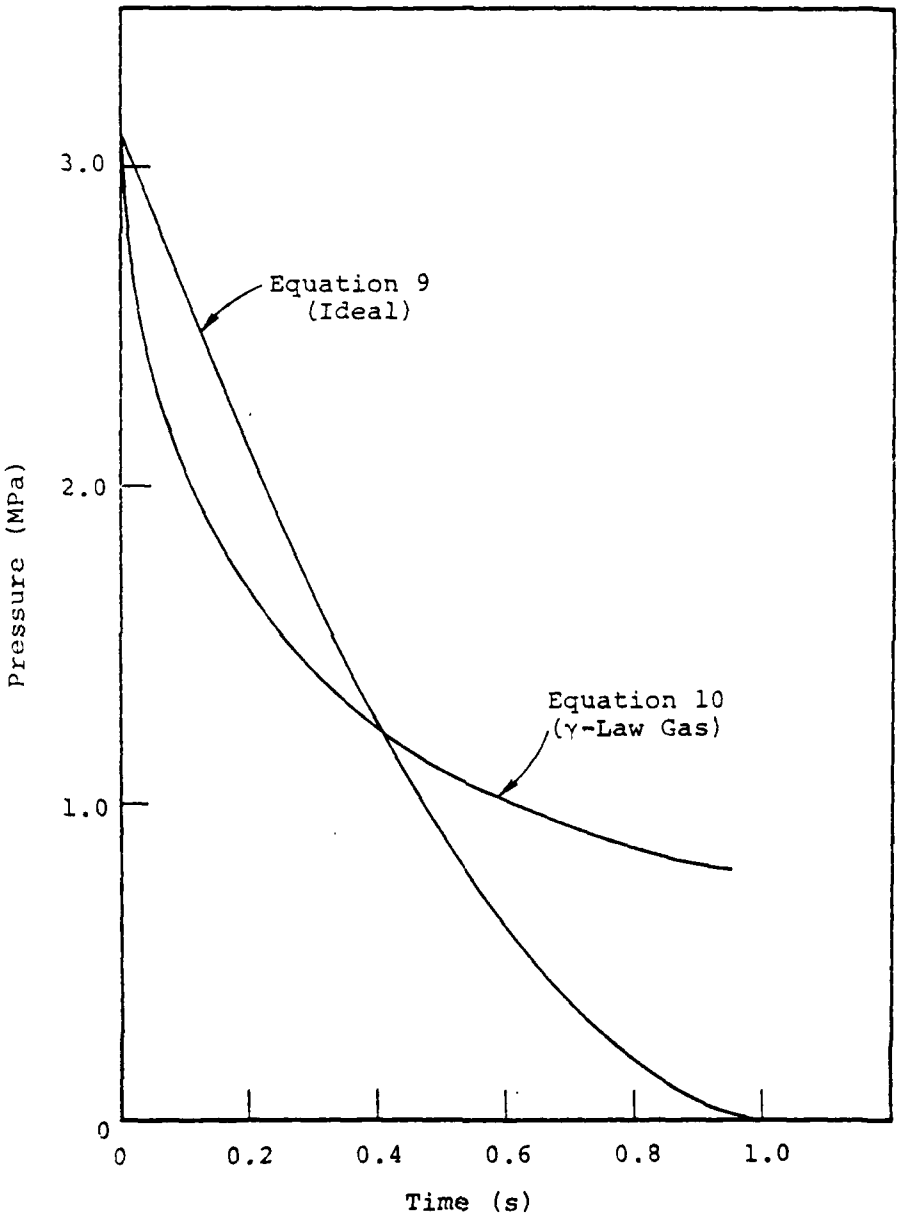

Figure 43. Propellant pressure versus time curves for a uniform dispersal of fuel into a hemispherical cloud and for a γ-law gas (γ = 1.27).

to fill the inner volume of the cloud with fuel, additional nozzles of small diameter could be used to fill that volume. Streams from nozzles of small diameter have a shorter range at the same pressure than those from larger nozzles. The curve in Figure 43 for a γ-law gas is for a particular P_o and V_o. Also, $\gamma = 1.27$ may not be the appropriate value for propellant gases; however, the shape of the P versus t curve is not very sensitive to the value of γ. It should also be pointed out that the fact that the pressure of the propellant gases does not approach zero at the end of the dispersing process is beneficial since that would result in very large droplets in the vicinity of the nozzles.

As an example, using the above calculations for the dispersal of 136,000 kg (300,000 lbs) of propylene oxide into a hemispherical cloud 160 m (524 ft) in diameter with 0.051-m (2-in.) diameter nozzles, we would have:

- Initial propellant pressure = 3.13 MPa (460 psi)
- Flow per nozzle = 68 L (18 gallons)
- Total number of nozzles required = 1,600
- Fraction of dispenser filled with fuel = 0.68
- Fuel per dispenser = 2702 L (714 gallons)
- Number of dispensers required = 40
- Size of dispenser (for example) = 0.61 m (2 ft) diameter x 18.3 m (60 ft) long. (This is only an example and should not be construed as a proposed design.)

There are several variables at our disposal in determining the actual design for an FAE blast simulator. For example, since the flow through a nozzle varies as the square of the nozzle diameter, with 7.6-cm (3-in.) diameter nozzles, only 764 nozzles would be required. The same number of

dispensers would be required unless the dispensers were made larger. However, the dimensions of the dispensers could be varied, i.e., they could be made larger in diameter and shorter. The size and number of nozzles will be determined by how the fuel streams break up and disperse at the ends of their range. This will be determined from measurements with full-size nozzles. Other variables at our disposal are the initial volume of the propellant gases relative to the volume of fuel and the initial pressure of the propellant gases.

8.3 DISPENSER DESIGN CONSIDERATIONS

Once the initial pressure of the propellant is chosen, the wall thickness of the dispensers is determined by their diameter. As an example, for an initial pressure of 3.4 MPa (500 psi) and a dispenser diameter of 0.61 m (24 in), the required wall thickness would be less than 1.27 cm (0.5 in). The dispensers would probably be emplaced in a concrete matrix. Filling a dispenser with fuel could be through the top by opening its head, or it could be with a system of underground pipes from a central storage facility. Filling through the tops of the dispensers from fuel trucks, much as jet airplanes are fueled, seems to offer advantages in simplicity of design and low cost of installation. Provision will also have to be made for placement of propellant in the inner tubes of the dispensers and for detonator leads to the propellant as indicated in Figure 40.

The design of the nozzles will be critical to the performance of the entire simulator. To minimize pressure losses, the bore of the nozzles must be as smooth as possible and the nozzle entrances must be well-rounded and also as smooth as possible. With a well-rounded entrance, the entrance loss in a 5.08-cm (2-in) nozzle should be less than 0.14 MPa (20 psi). As noted earlier, the nozzles would be machined as

separate units and screwed into threaded holes in the heads. The length of the nozzles will have to be several times their bore diameter.

There is a potential problem concerning the flow of the fuel in the annular channel between the inner and outer pipes of the dispenser. Once the fuel has been expelled from the inner pipe, the propellant gases will be forcing the fuel up the channel between the pipes by applying pressure to the bottom of the fuel in this channel. This is an unstable situation and there may be a tendency for bubbles of propellant gas to rise in the fuel. Because of the very high flow velocity in this channel (several hundred ft/s). it is deemed unlikely that such bubbles would actually form in the fuel. However, if they do form they could probably be eliminated by a series of vertical baffles extending radially between the inner and outer pipe to form a series of parallel narrow channels within the annular space between the pipes. Such baffles are shown in the design of Figure 40.

IX. CONCLUSIONS AND RECOMMENDATIONS

It can be concluded that the small-scale U-tube facility can be used to disseminate hemispherical FAE clouds, that the clouds can be detonated and that the scaled blast waveforms are in good agreement with 1-KT nuclear waveforms at the scaled ranges. It has also been demonstrated that blast waves generated by the facility are symmetric and repeatable.

Initial data from single nozzle reach experiments indicate that cloud formation time does not scale linearly with cloud diameter. Above a critical nozzle pressure, propylene oxide stream heights are significantly less than those for water. This indicates that nozzles of larger diameter will be required to obtain the heights necessary for the full-scale blast simulator.

Table IV lists the remaining problem areas that must be addressed before a full-scale blast simulator can be designed, as well as proposed methods of solution. These problem areas include alternate fuel detonability, fuel property effects, single nozzle stream characteristics, driving pressure requirements, contact surface effects, dispenser design, safety requirements, and construction and life-cycle costs.

Table IV. Recommendations for Further Investigations	
Remaining Problem Areas	Proposed Methods of Solution
Alternate Fuel Detonability	Hemispherical Cloud Detonation Studies
Fuel Property Effects - Viscosity - Vapor Pressure - Surface Tension	Single Nozzle Experiments Using Various Fuels
Single Nozzle Stream Characteristics - Total Height - Breakaway Height - Stripping - Fuel Distribution - Fuel-Air Mixing	Single Nozzle Experiments
Safety Requirements - Test Procedures - Fuel and Propellant Handling	Hazards Analysis and Required Tests
Construction and Life-Cycle Costs - Hardware Configuration and Costs - Fuel Costs - Test Setup Time - Turn-Around Time - Instrumentation - Personnel Requirements	Cost Analysis
Driving Pressure Requirements - Maximum Pressure - Pressure History	Single Nozzle Experiments
Contact Surface Effects - Density Discontinuities - Effect on Close-In Gauge Readings	Hemispherical Cloud Detonation Studies - Drag Measurements - Finely Resolved 1-D Calculation
Dispenser Design Requirements - Test Design Concept - Dispenser Unit Requirements - Nozzle Requirements	Dispenser Tests and Analysis

X. REFERENCES

1. Brode, Harold L., "Review of Nuclear Weapons Effects," Annual Review of Nuclear Science, Vol. 18, pp. 153-202, 1968

2. "Fire Protection Handbook," 14th Edition, National Fire Protection Association, 1976.

APPENDIX A

COMPARISON OF SCALED EXPERIMENTAL FAE BLAST WAVEFORMS AND POSITIVE PHASE IMPULSES FOR SHOT NO. 1, 0810 WEDNESDAY, 12 OCTOBER 1977 WITH NUCLEAR DATA.

The five plots immediately following compare the experimental pressure histories at different gauge locations (solid lines) with the theoretical waveforms for nuclear surface bursts given by Brode [1].

The plotted experimental pressures were obtained by digitizing a pressure recording similar to that shown in Figure 14 and scaling the time and (implicitly) the range by a factor of 16. The dashed lines indicate the theoretical positive phase pressures at the same scaled range for a 1-KT surface blast. The annotation in the upper right corner of each plot indicates the gauge location; e.g., "L20" denotes the 20-foot gauge on the "long" leg. The theoretical arrival times are not indicated; rather, the indicated arrival times for both curves are that of the scaled experimental data.

The pressure curves were numerically integrated over their positive phases to generate the impulses shown on the remaining five plots.

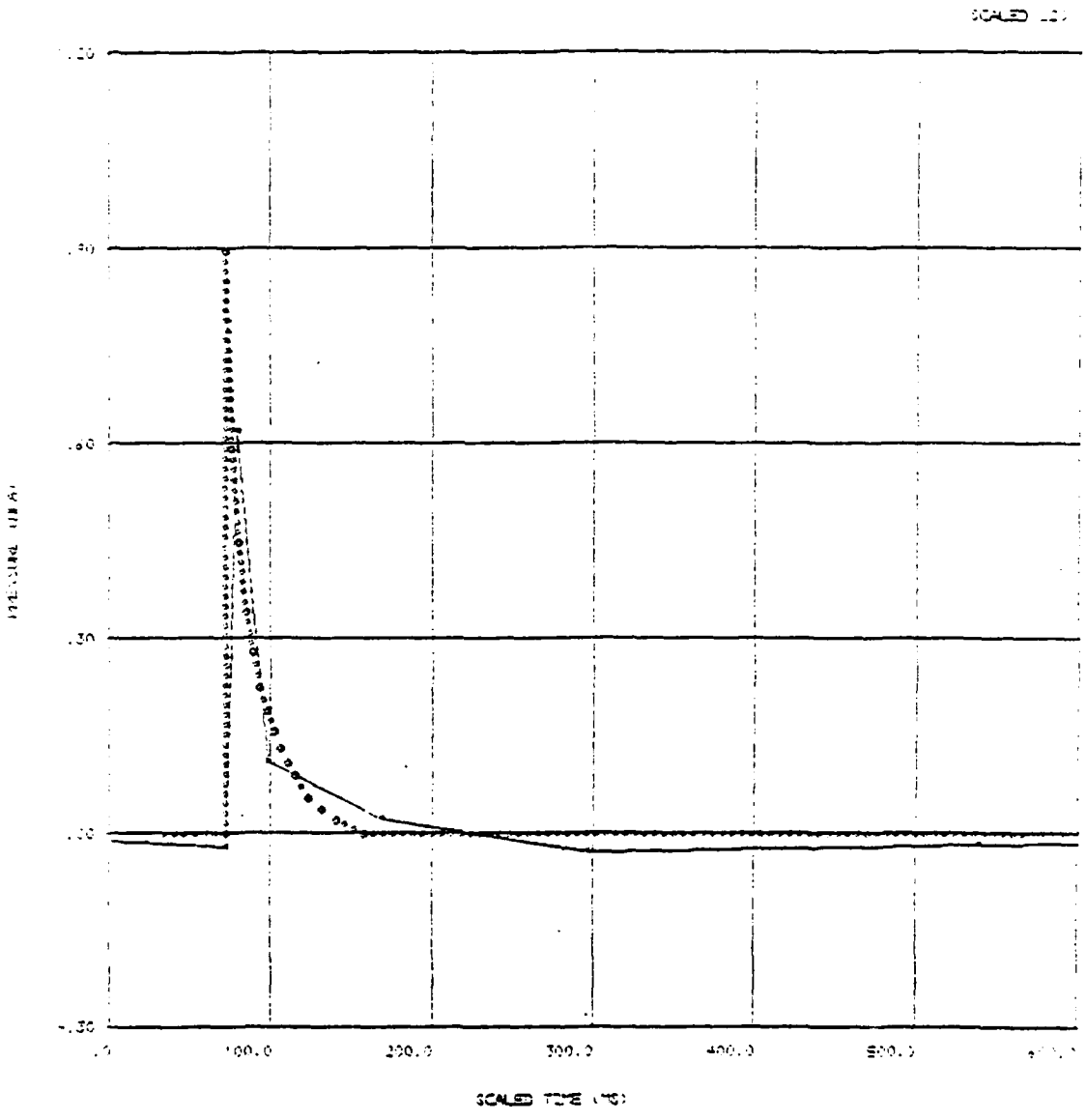
SHOT NO 1 0810 WED 12 OCT 77
SCALED TIME (MS)
100.0
200.0
300.0
400.0

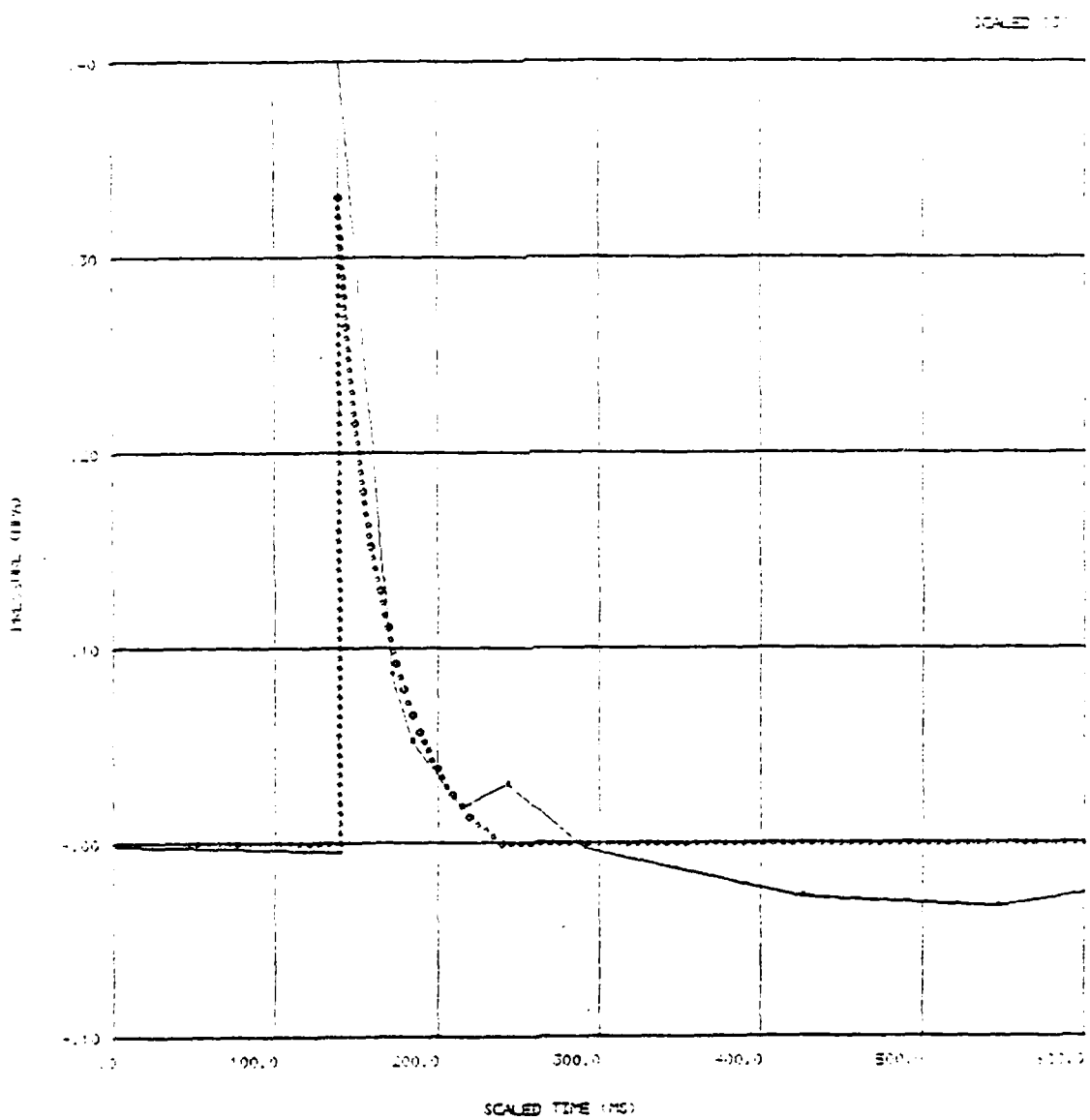
SHOT NO 1
0810 WED 12 OCT 77
100.0
200.0
300.0
SCALED TIME (MS)

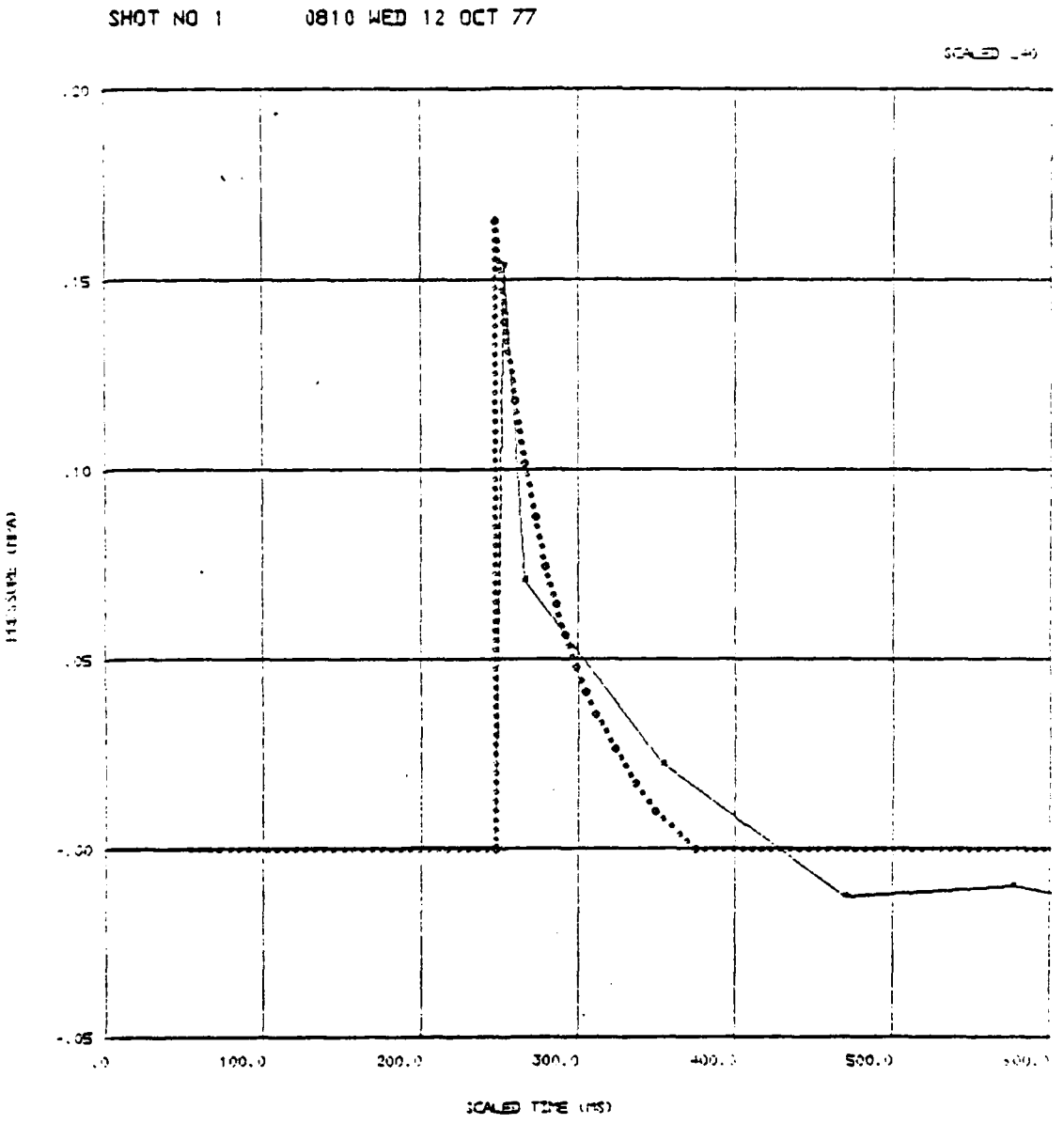
SHOT NO 1
0810 WED 12 OCT 77
.20
.15
.10
.05
-.05
100.0
200.0
300.0
500.0
SCALED TIME (MS)

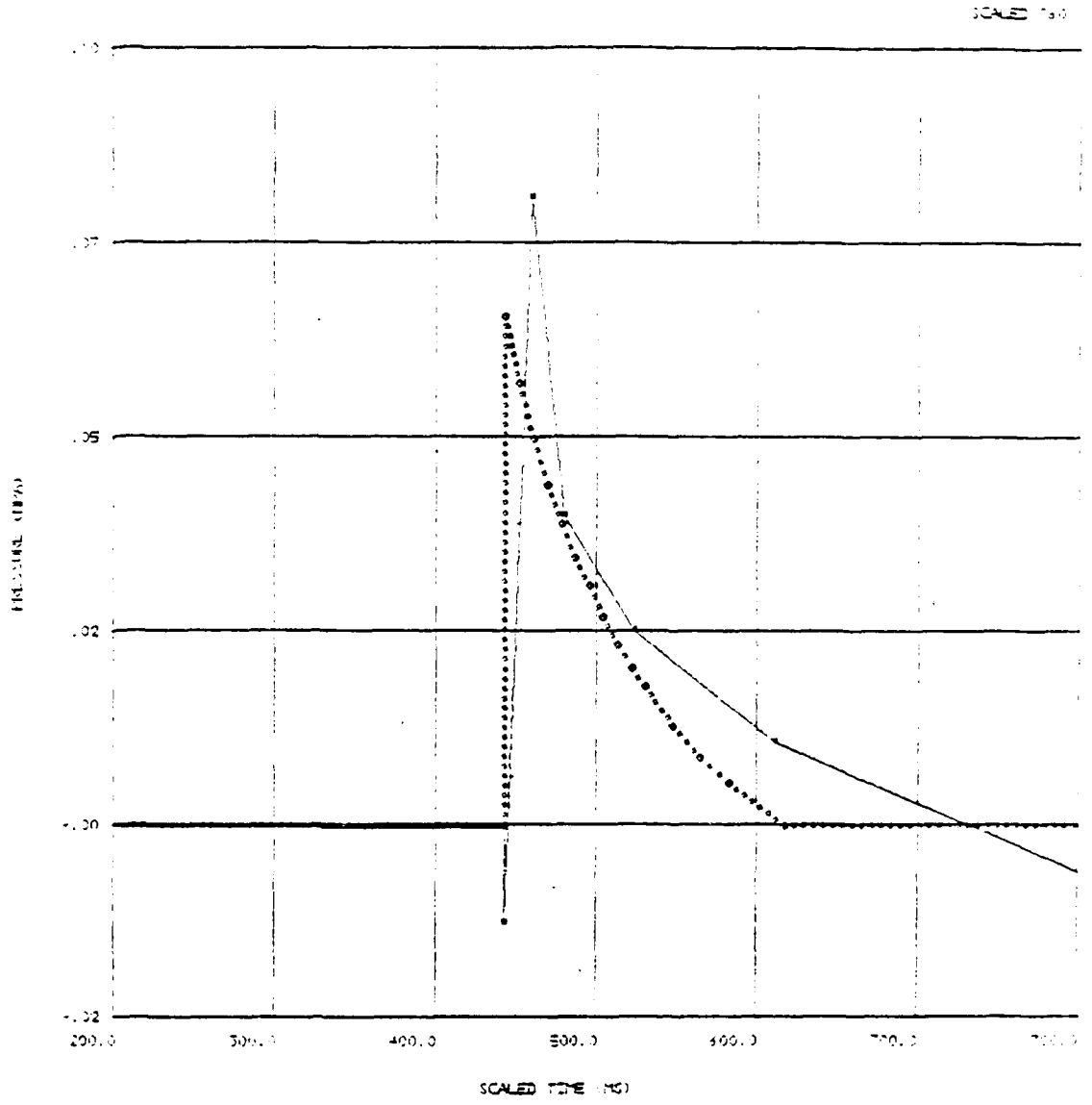
SHOT NO 1
0810 WED 12 OCT 77
.05
.02
-.02
400.0
500.0
600.0

AD-A086 219 SYSTEMS SCIENCE AND SOFTWARE LA JOLLA CA F/G 14/2
FEASIBILITY INVESTIGATION OF A PERMANENT FUEL-AIR EXPLOSIVE BLA--ETC(U)
AUG 78 R T SEDGWICK, H B KRATZ, R G HERRMANN DNA001-77-C-0251
UNCLASSIFIED SSS-R-78-3737 DNA-5059T NL

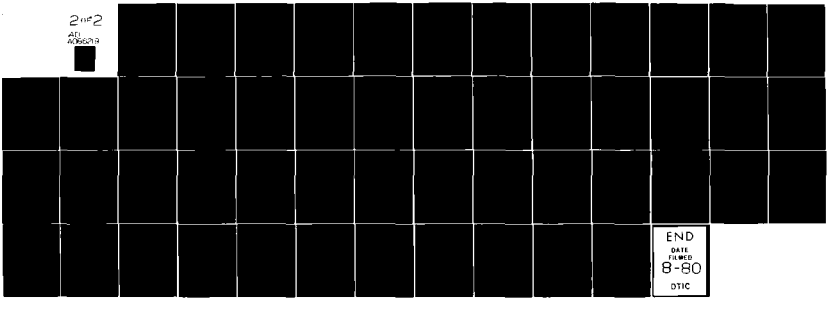

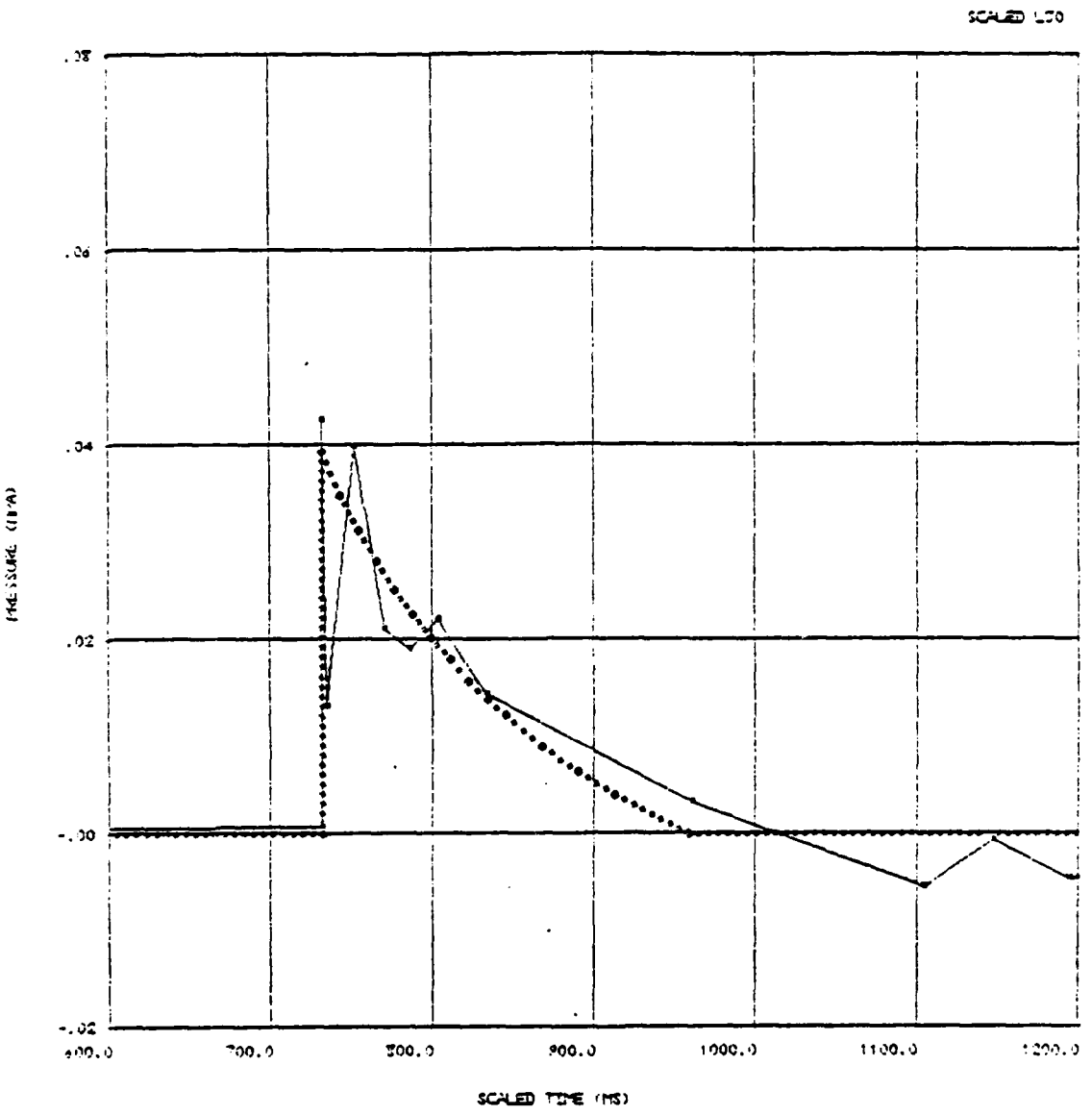
SHOT NO 1 0810 WED 12 OCT 77
SCALED LOG
.08
.06
.04
.02
-.00
-.02
700.0
900.0
1000.0
1100.0
SCALED TIME (MS)

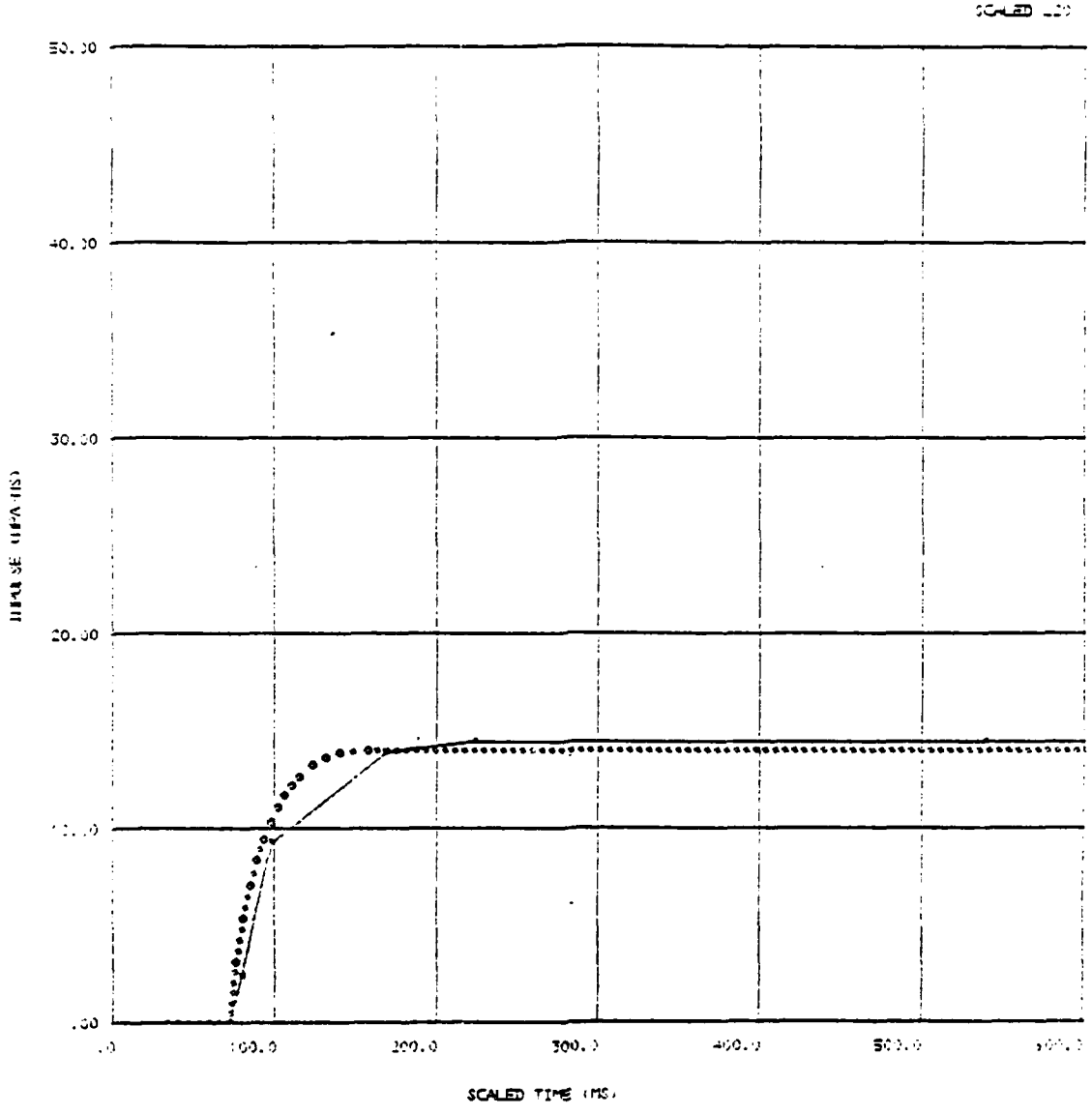
SHOT NO 1 0810 WED 12 OCT 77
50.00
40.00
30.00
20.00
.00
SCALED TIME (MS)

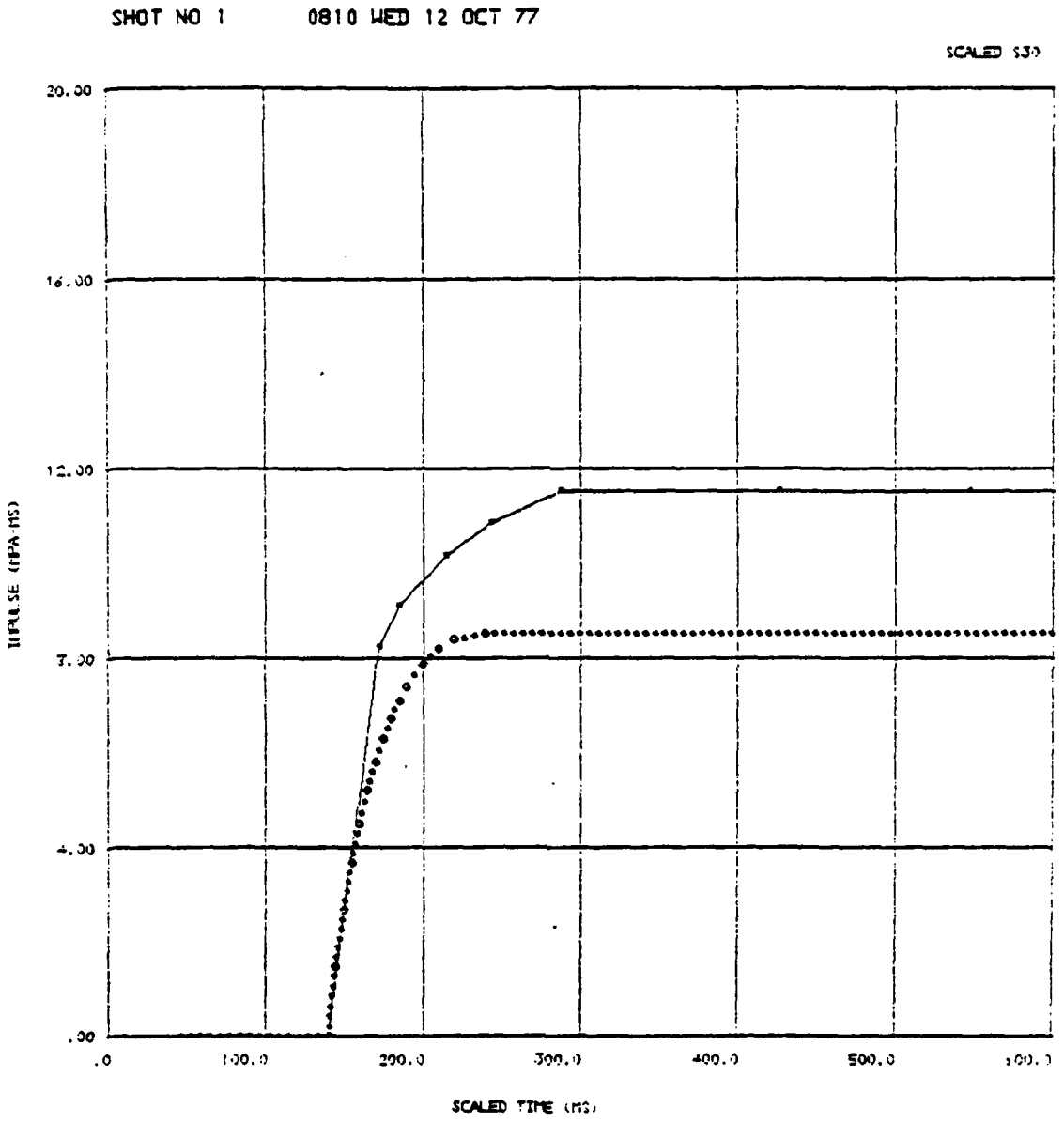
SHOT NO 1 0810 WED 12 OCT 77
SCALED S30
20.00
16.00
12.00
8.00
4.00
.00
IMPULSE (MPA-MS)
.0
100.0
200.0
300.0
400.0
500.0
SCALED TIME (MS)

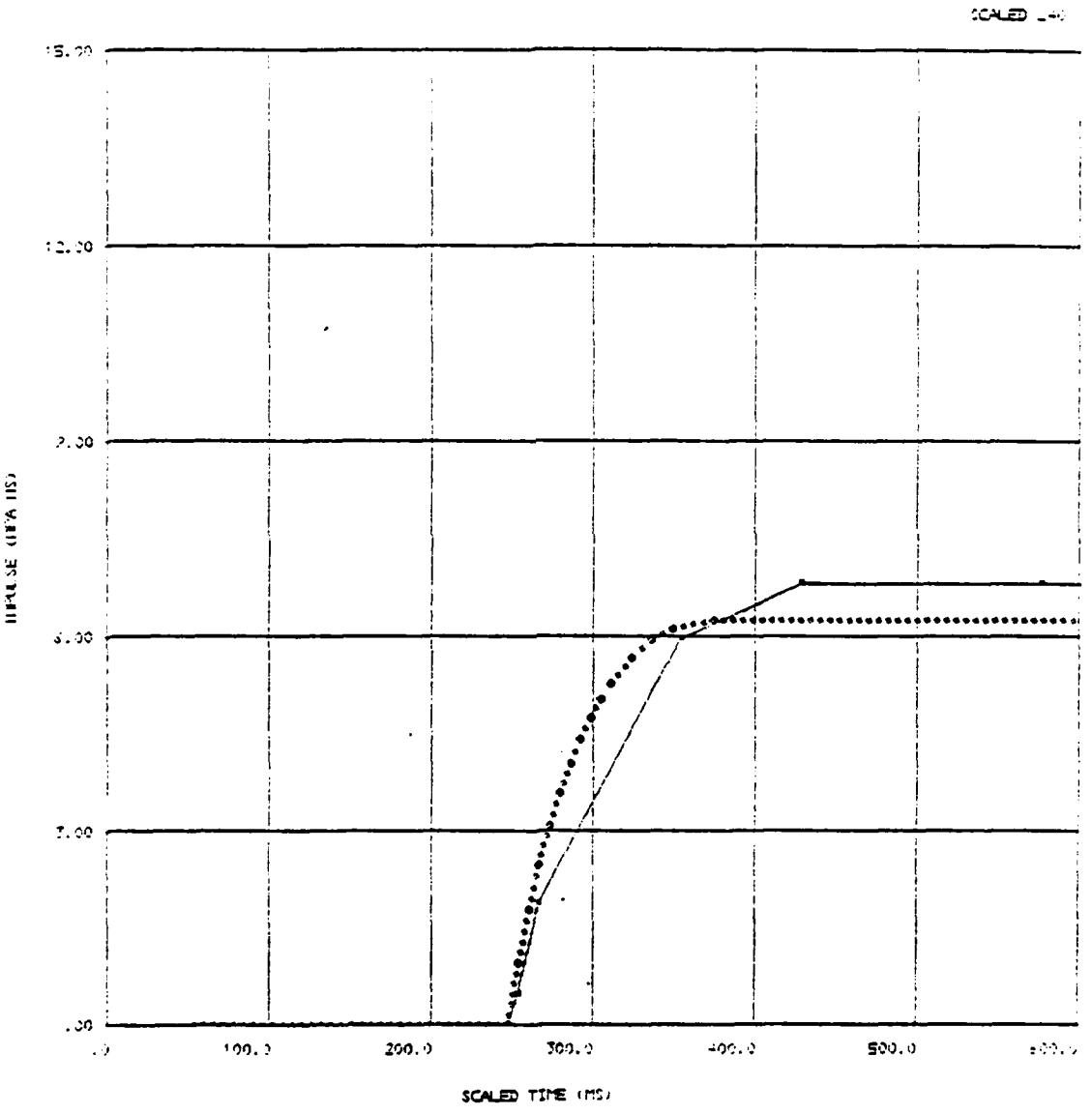
SHOT NO 1 0810 WED 12 OCT 77
SCALED
15.00
12.00
9.00
6.00
3.00
.00
100.0
200.0
300.0
400.0
500.0
SCALED TIME (MS)

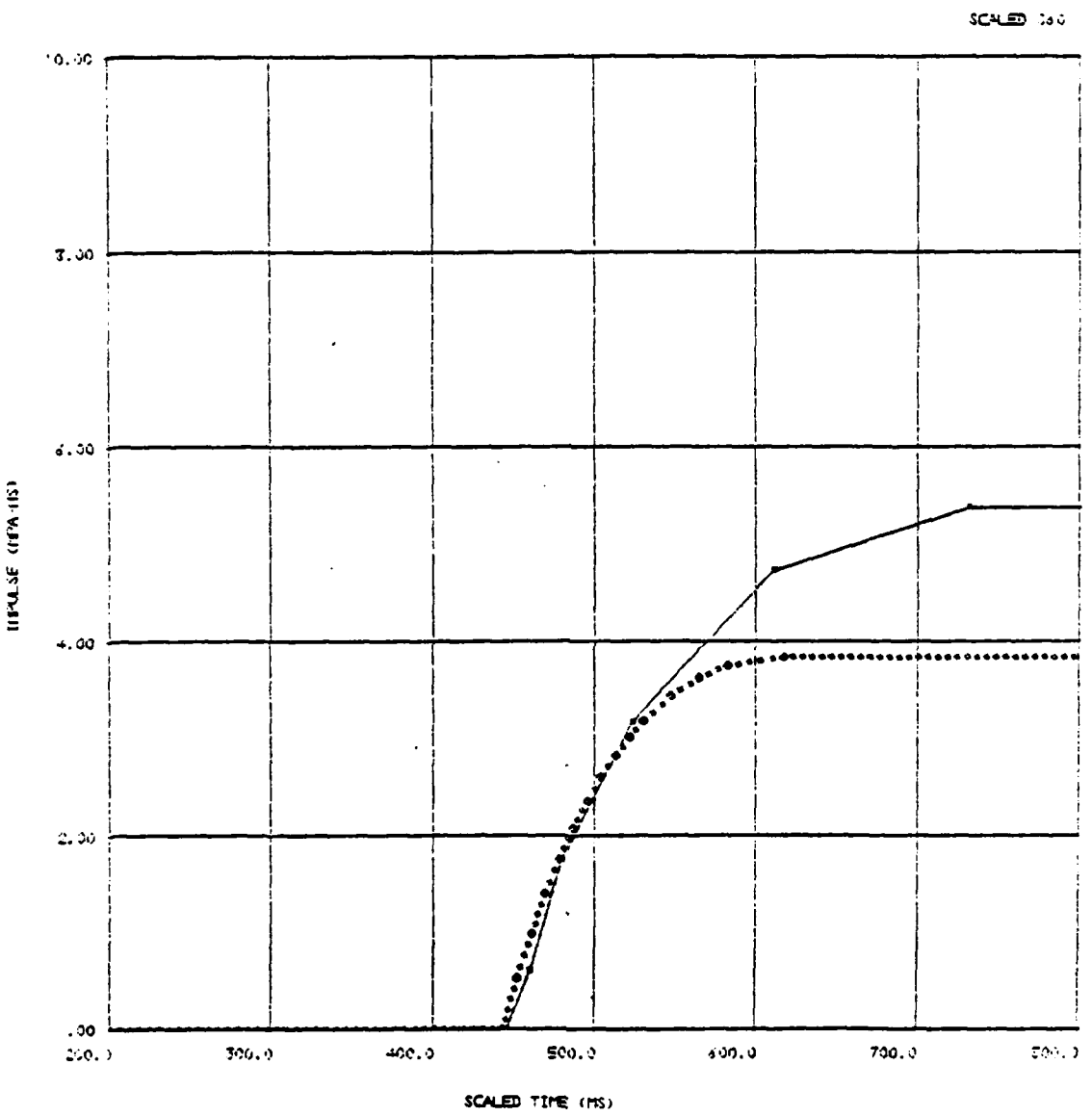
SHOT NO 1 0810 WED 12 OCT 77
SCALED
10.00
8.00
6.00
4.00
2.00
.00
300.0
400.0
500.0
600.0
700.0
SCALED TIME (MS)

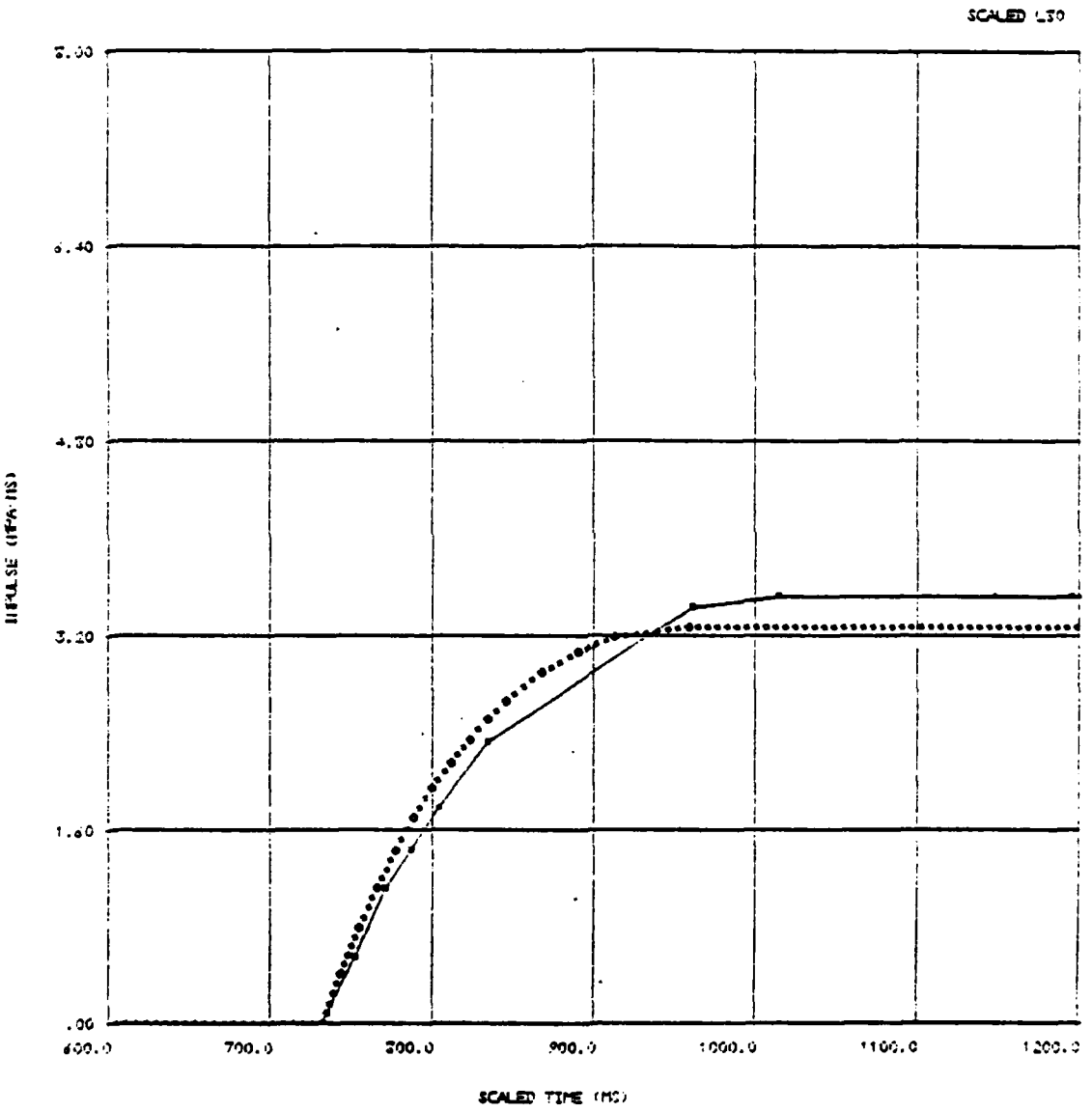
SHOT NO 1 0810 WED 12 OCT 77
SCALED I30
6.40
4.80
3.20
1.60
.00
700.0
800.0
900.0
1000.0
1100.0
SCALED TIME (MS)

APPENDIX B

COMPARISON OF SCALED EXPERIMENTAL FAE BLAST WAVEFORMS AND POSITIVE PHASE IMPULSES FOR SHOT NO. 1, 0800 THURSDAY, 13 OCTOBER 1977 WITH NUCLEAR DATA.

These plots are similar to those of Appendix A. See that appendix for a description.

SHOT NO 1 0800 THURS 13 OCT 77

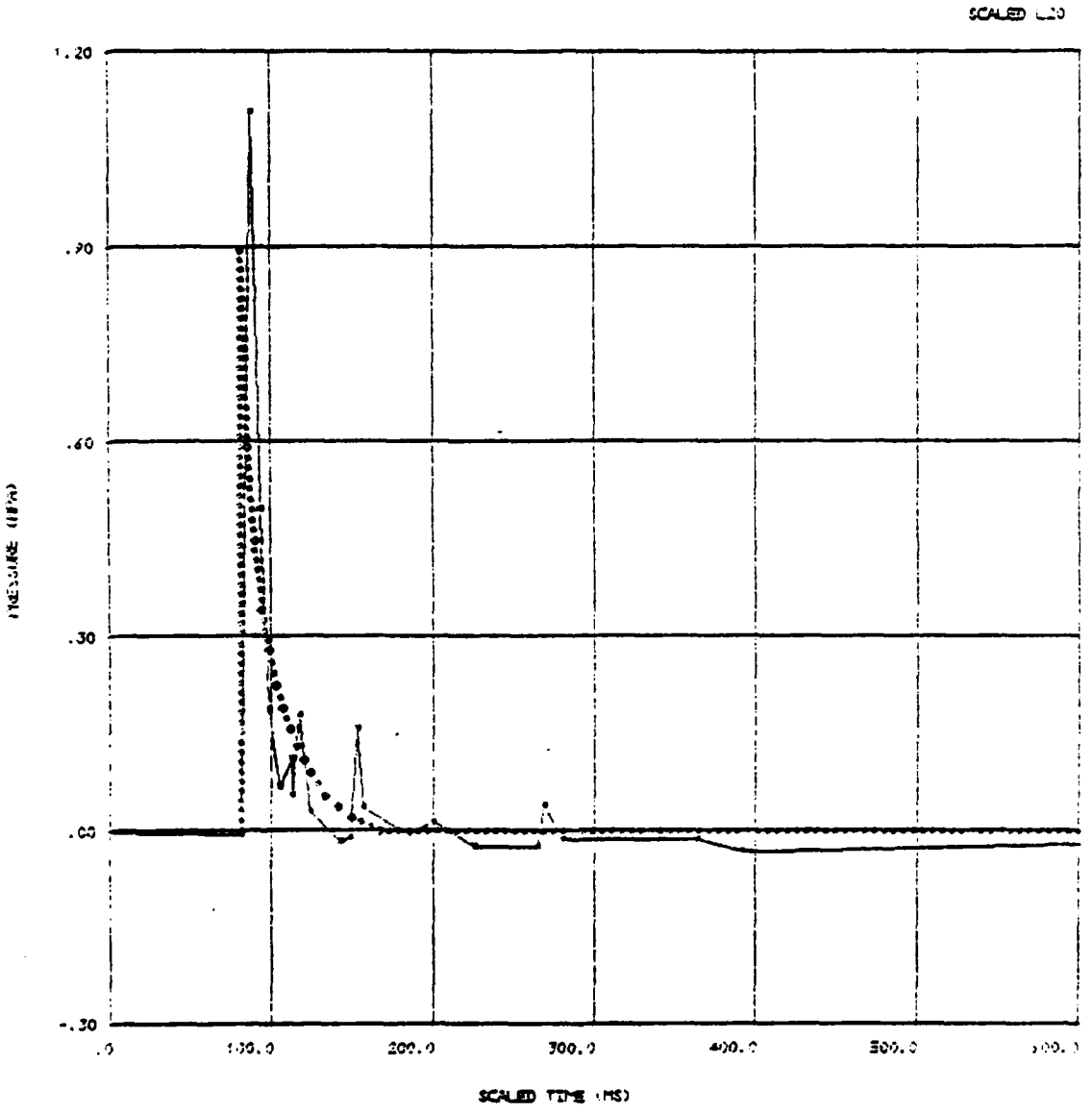

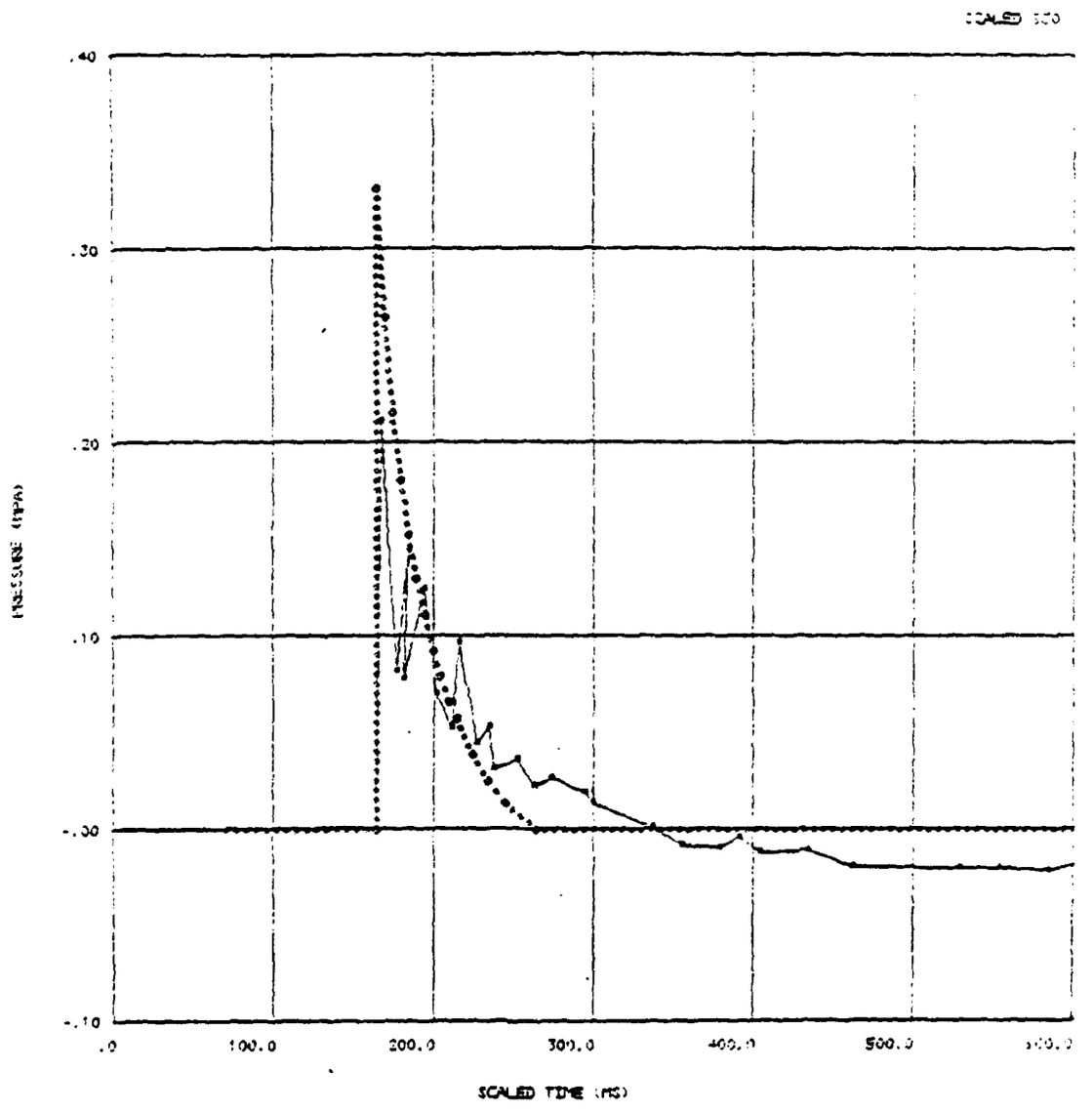
SHOT NO 1 0800 THURS 13 OCT 77
.40
.30
.20
.10
-.30
-.10
.0
100.0
200.0
300.0
400.0
500.0
SCALED TIME (MS)

SHOT NO 1 0800 THURS 13 OCT 77

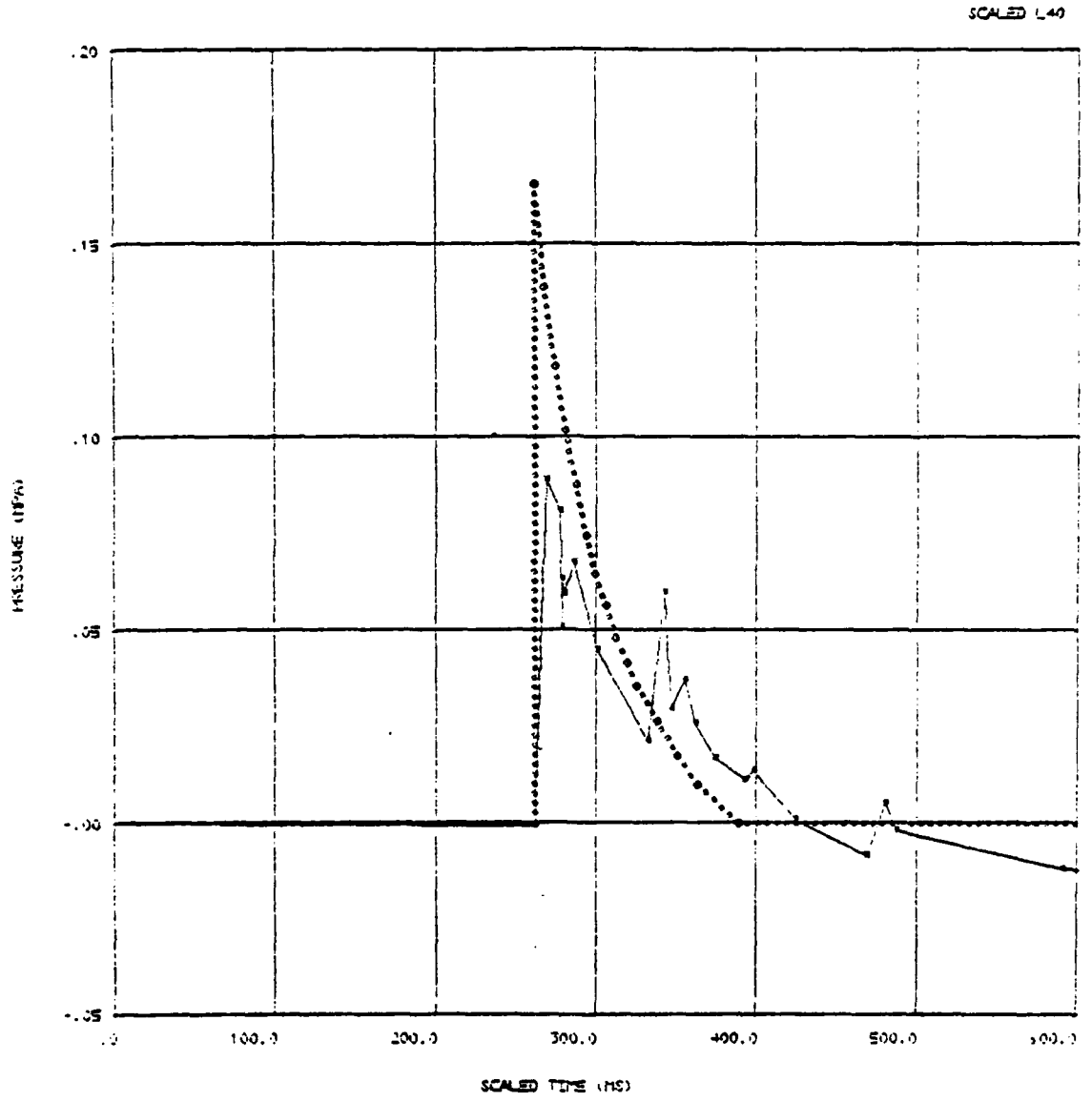

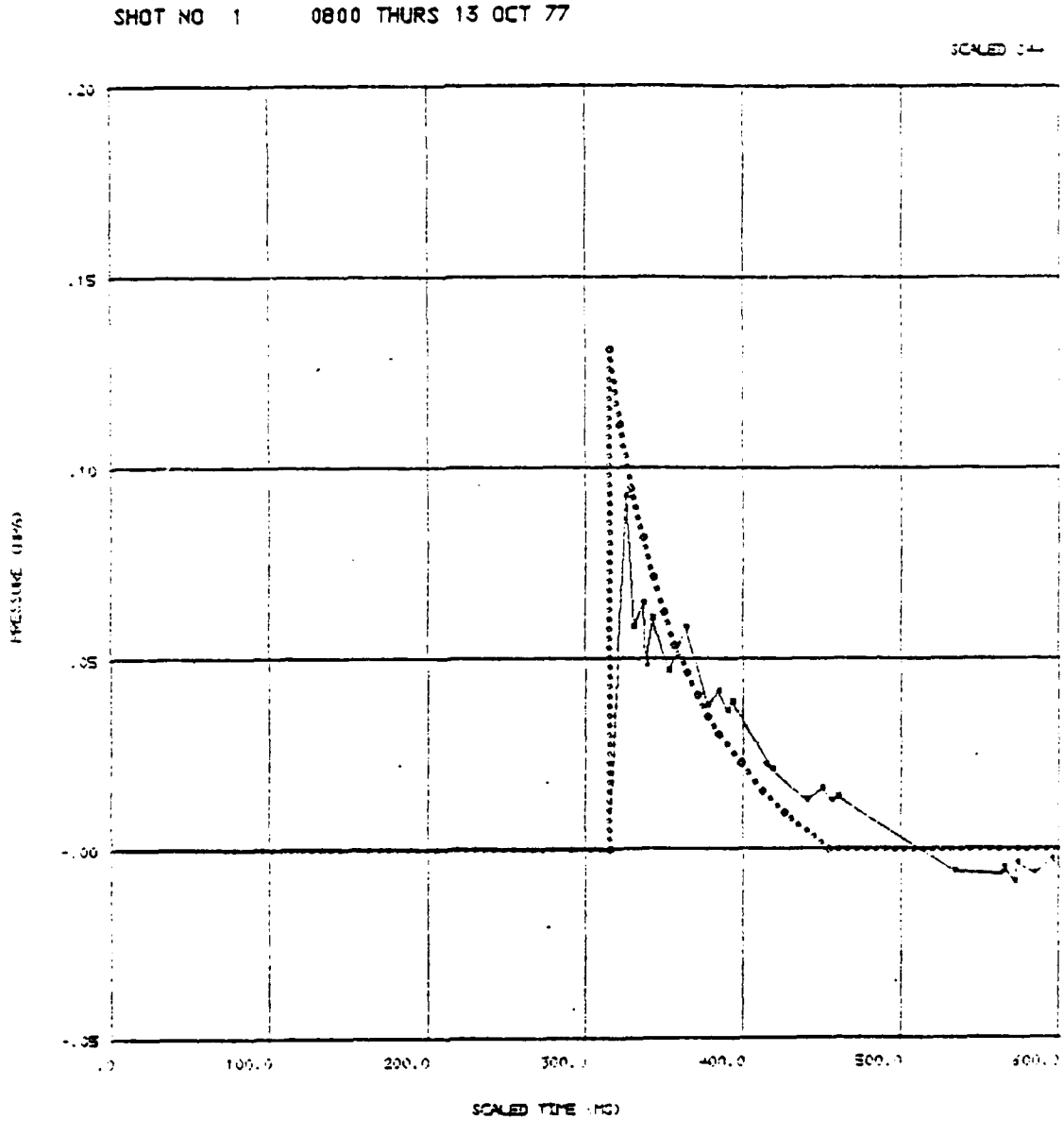
SHOT NO 1 0800 THURS 13 OCT 77
.20
.15
.10
.05
100.0
200.0
400.0
500.0

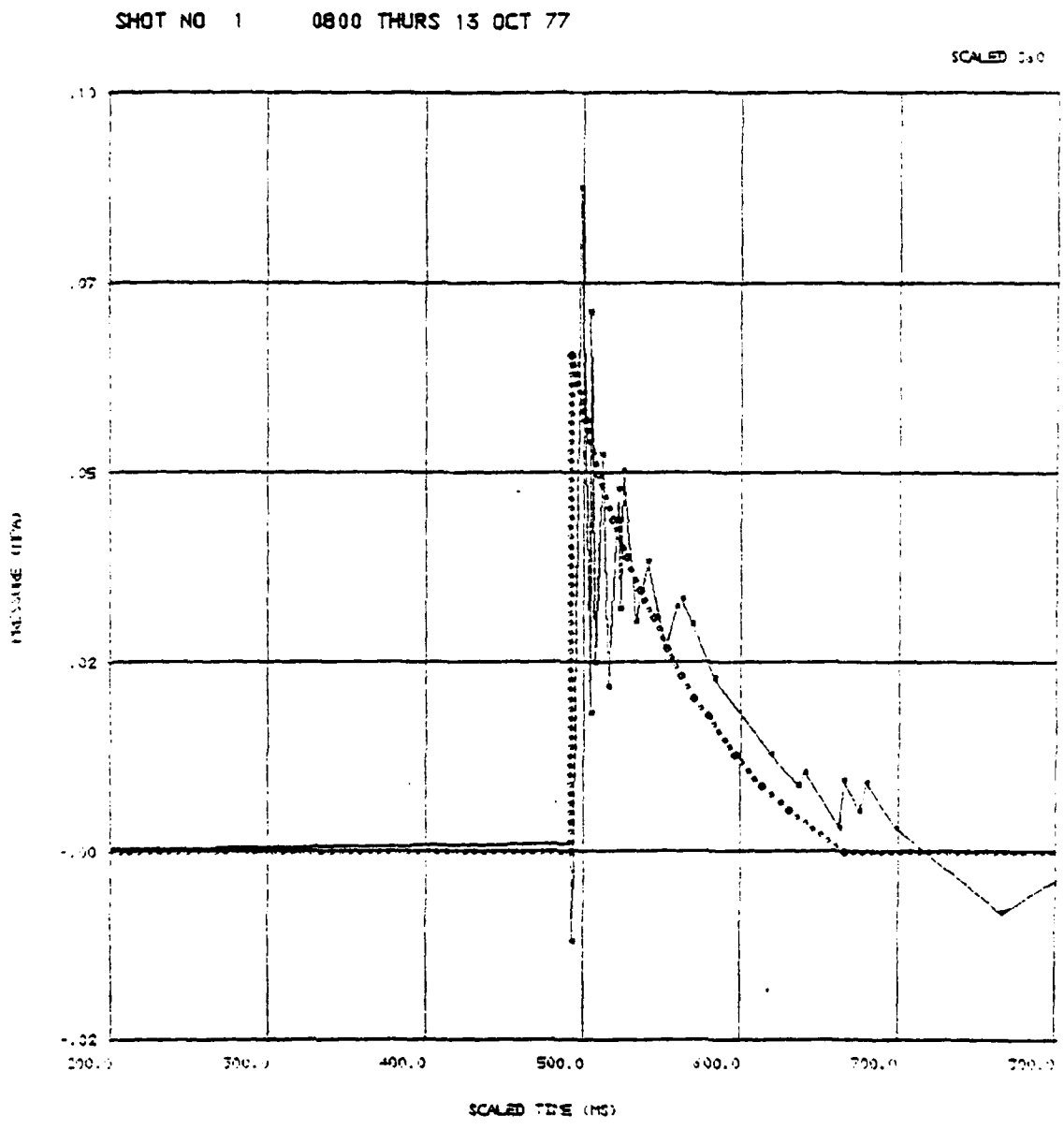
SHOT NO 1 0800 THURS 13 OCT 77
SCALED
.07
.05
.02
500.0
SCALED TIME (MS)

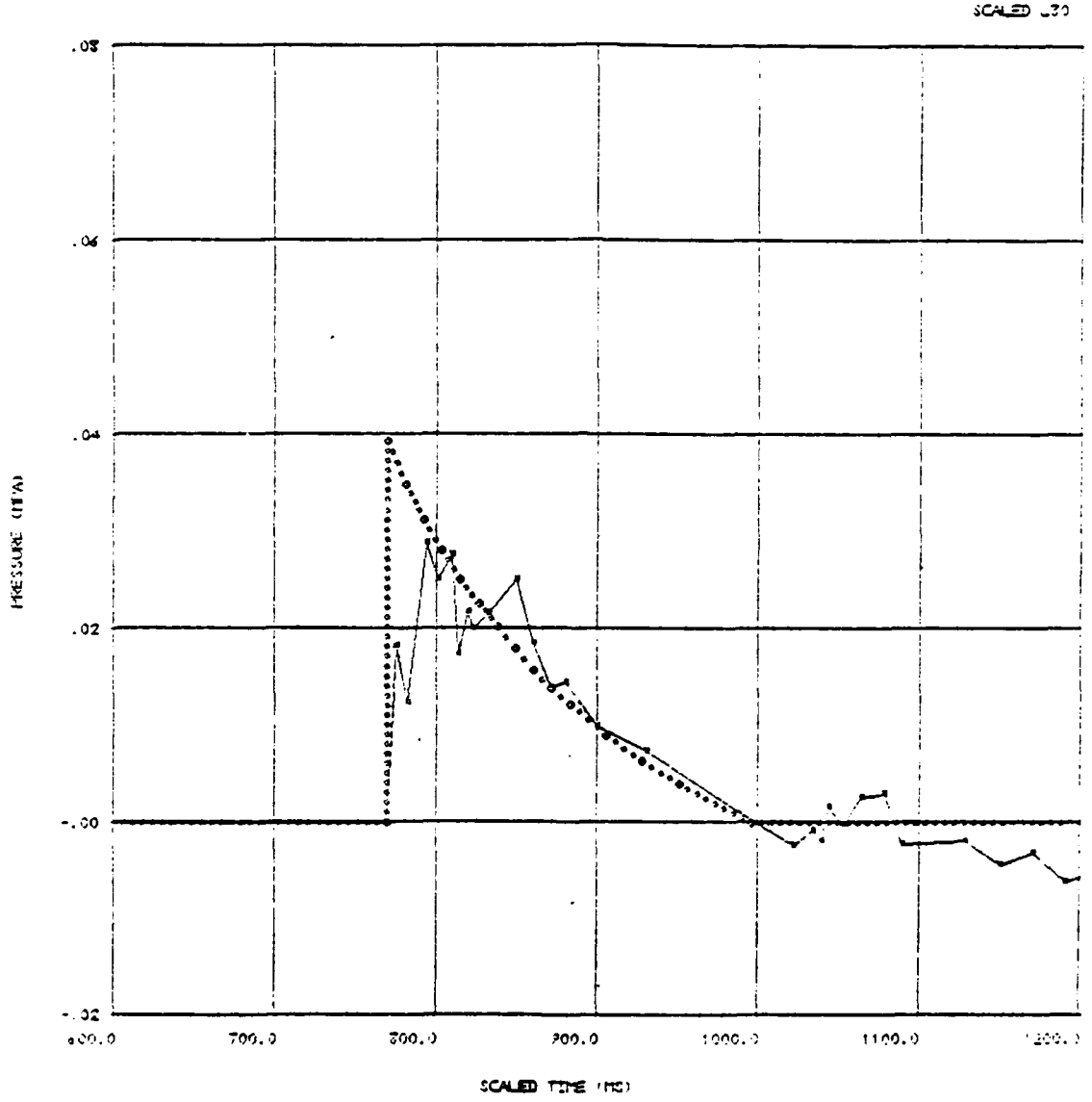
SHOT NO 1 0800 THURS 13 OCT 77
SCALED
.08
.06
.04
.02
-.00
-.02
PRESSURE (PSI)
700.0
800.0
900.0
1000.0
1100.0
SCALED TIME (MS)

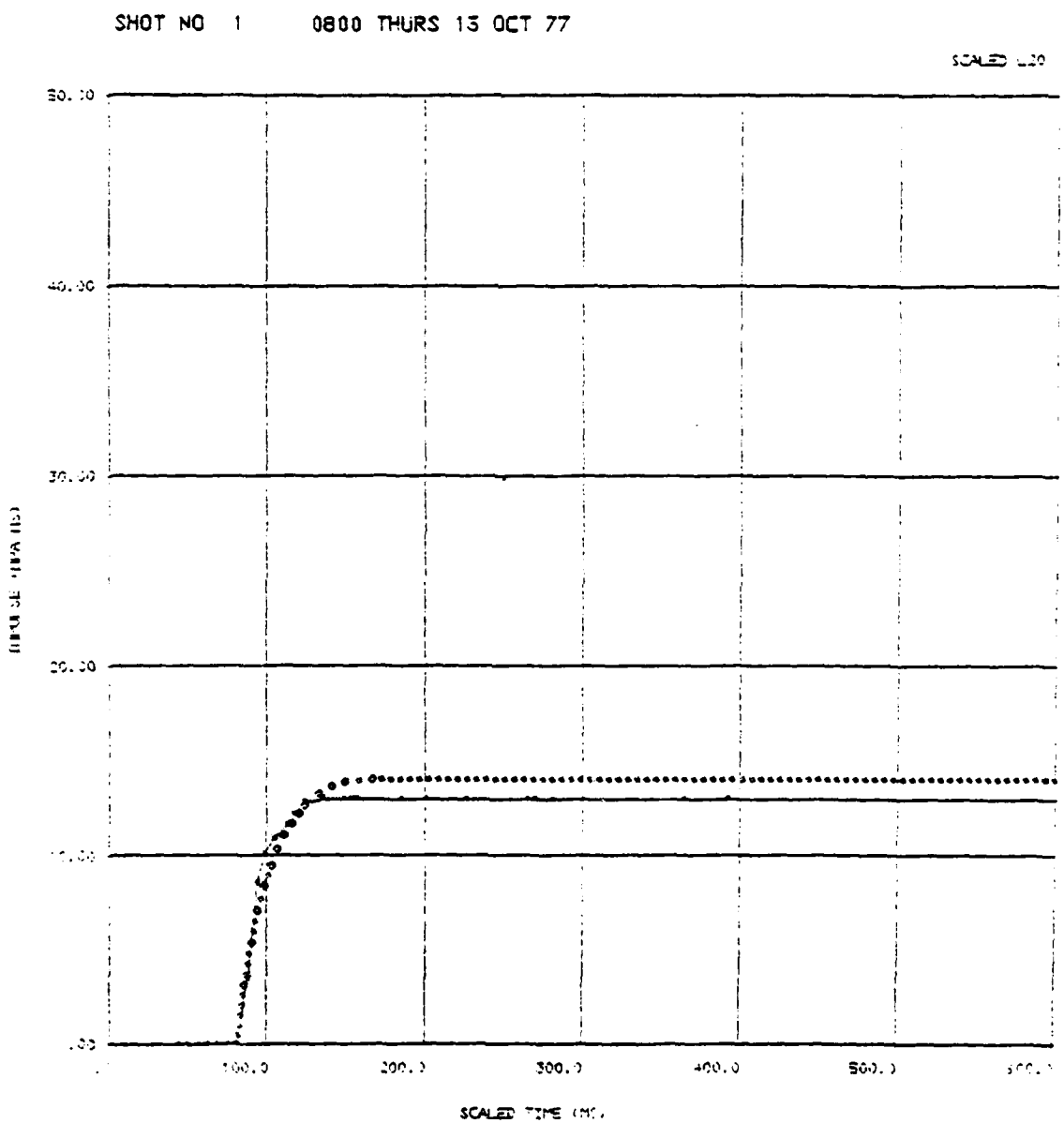
SHOT NO 1 0800 THURS 13 OCT 77
SCALED L20
50.00
40.00
30.00
20.00
.00
100.0
200.0
300.0
400.0
500.0
SCALED TIME

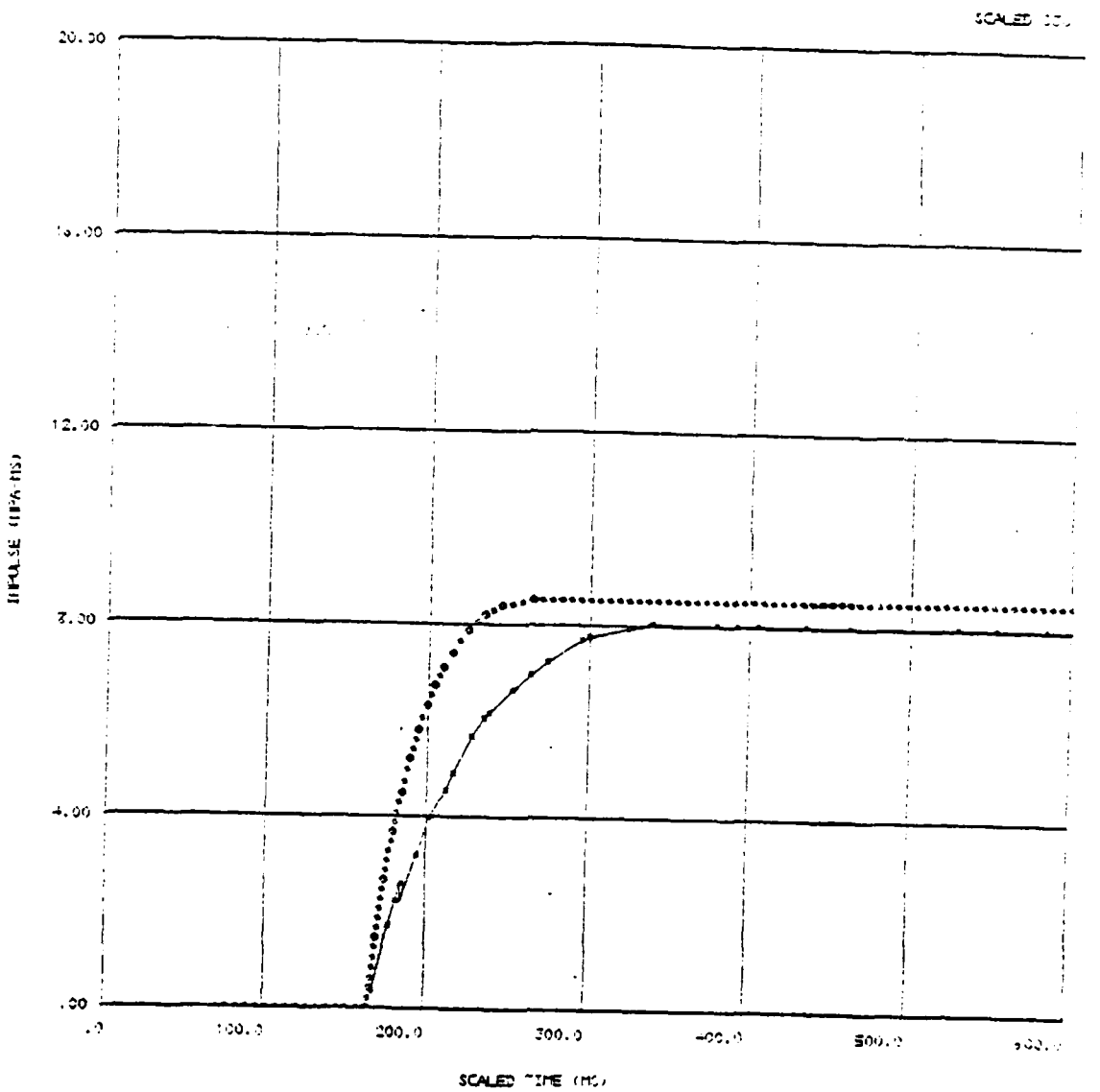
SHOT NO 1 0800 THURS 13 OCT 77
20.00
12.00
8.00
4.00
.00
100.0
200.0
300.0
500.0

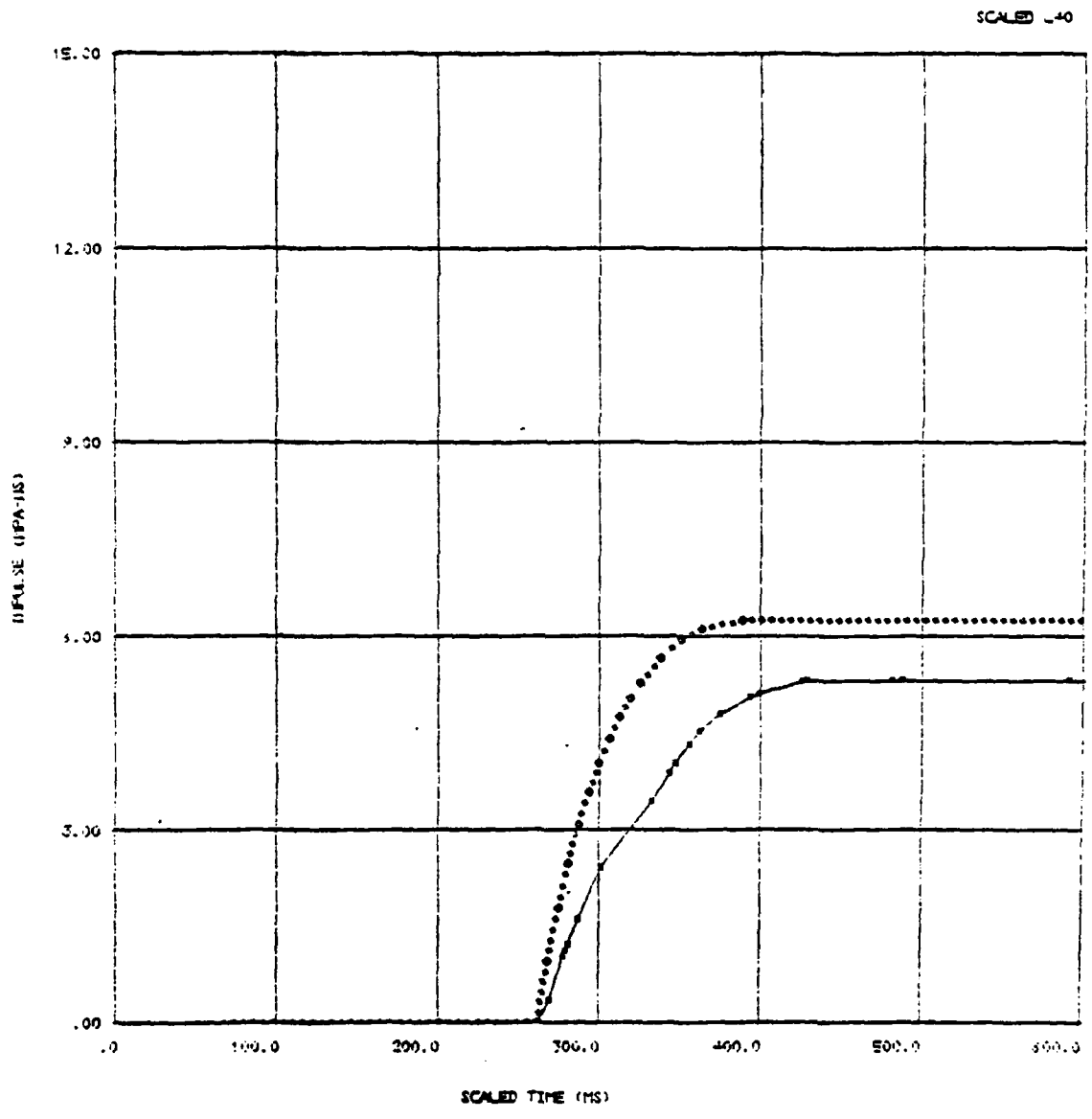
SHOT NO 1 0800 THURS 13 OCT 77
SCALED L40
15.00
12.00
9.00
6.00
3.00
.00
.0
100.0
200.0
300.0
400.0
500.0
SCALED TIME (MS)

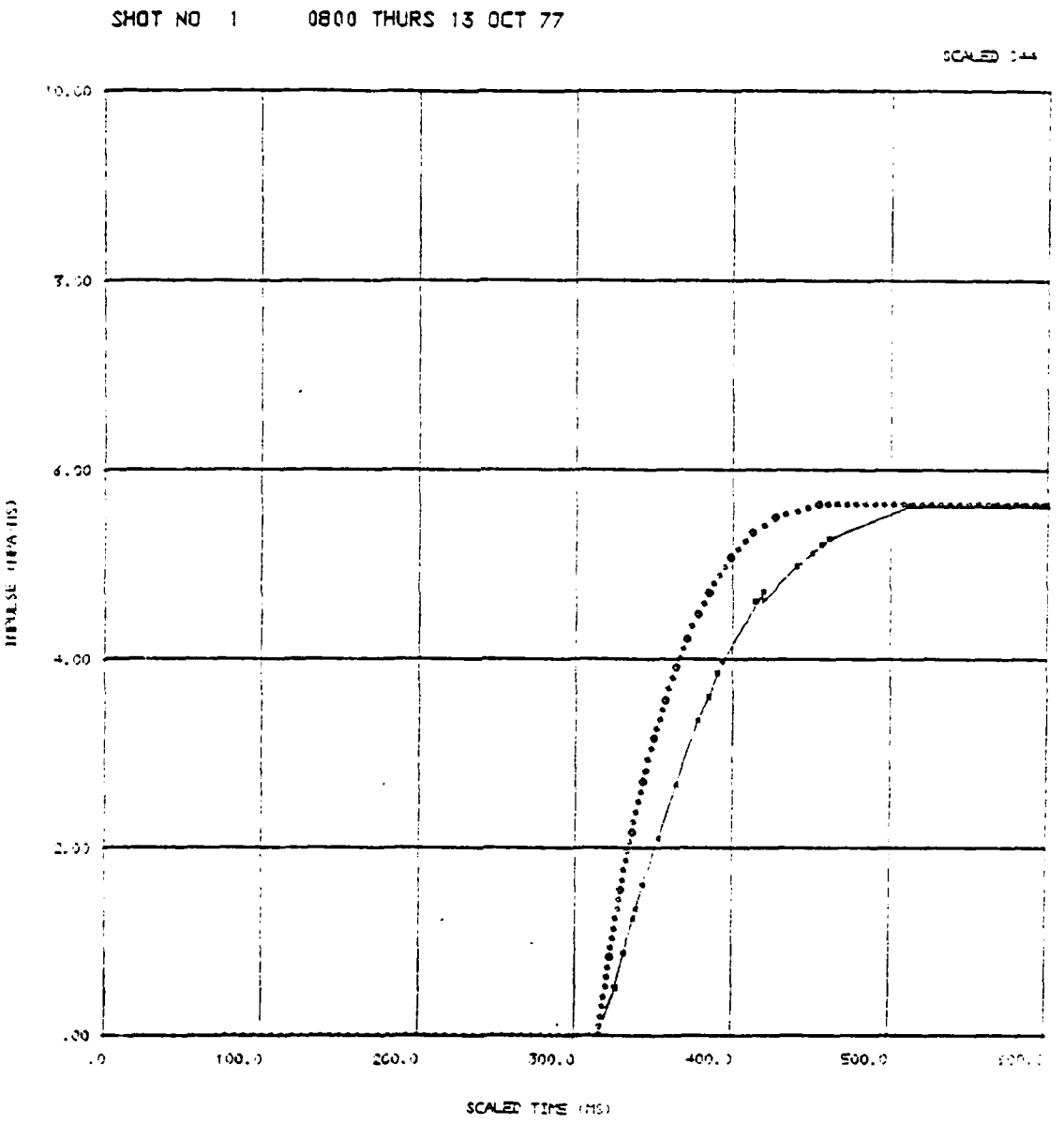
SHOT NO 1 0800 THURS 13 OCT 77
SCALED
10.00
8.00
6.00
4.00
2.00
.00
.0
100.0
200.0
300.0
400.0
500.0
SCALED TIME (MS)

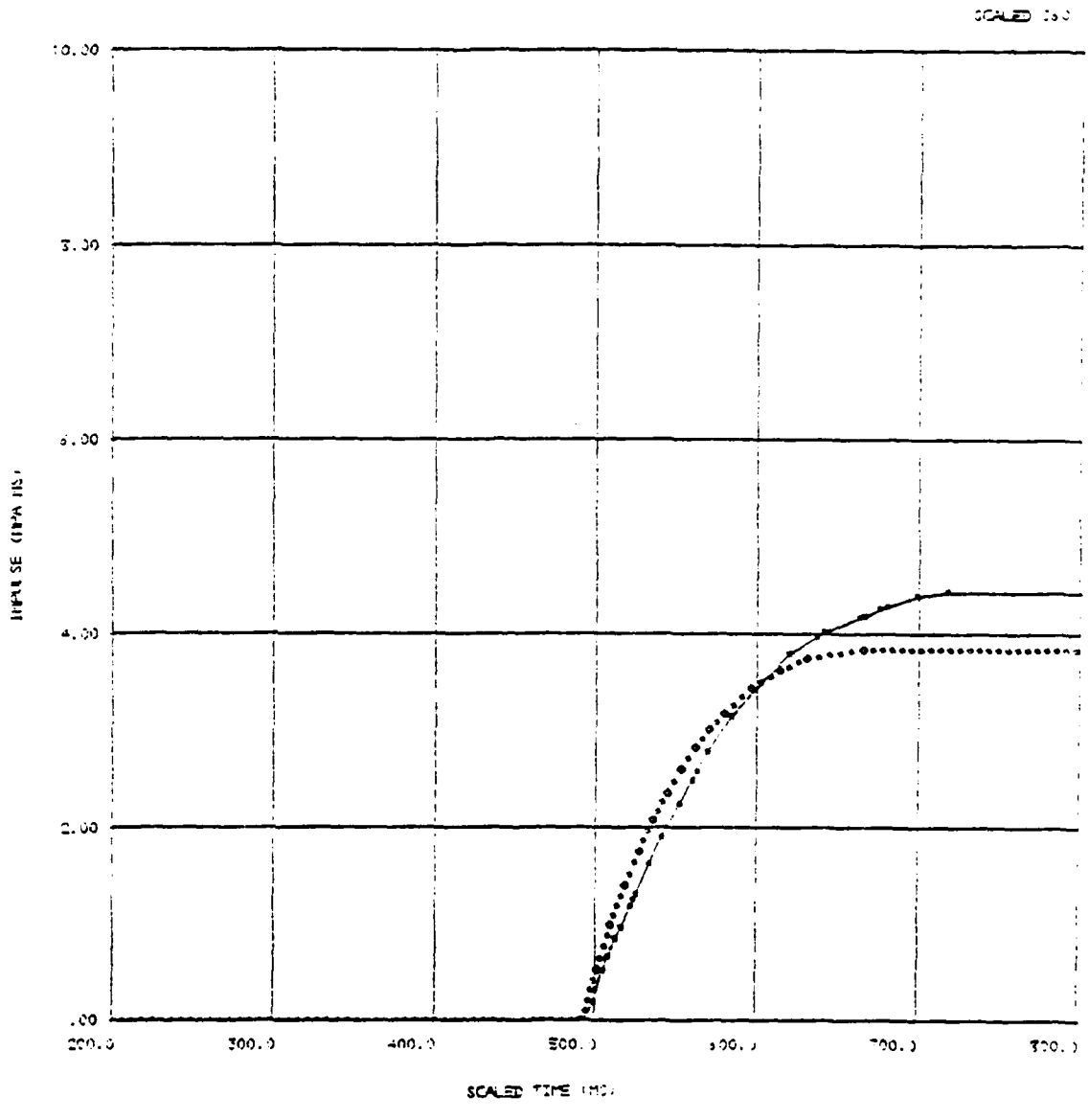
SHOT NO 1 0800 THURS 13 OCT 77
10.00
8.00
6.00
4.00
2.00
.00
200.0
300.0
400.0
500.0
600.0
700.0
800.0

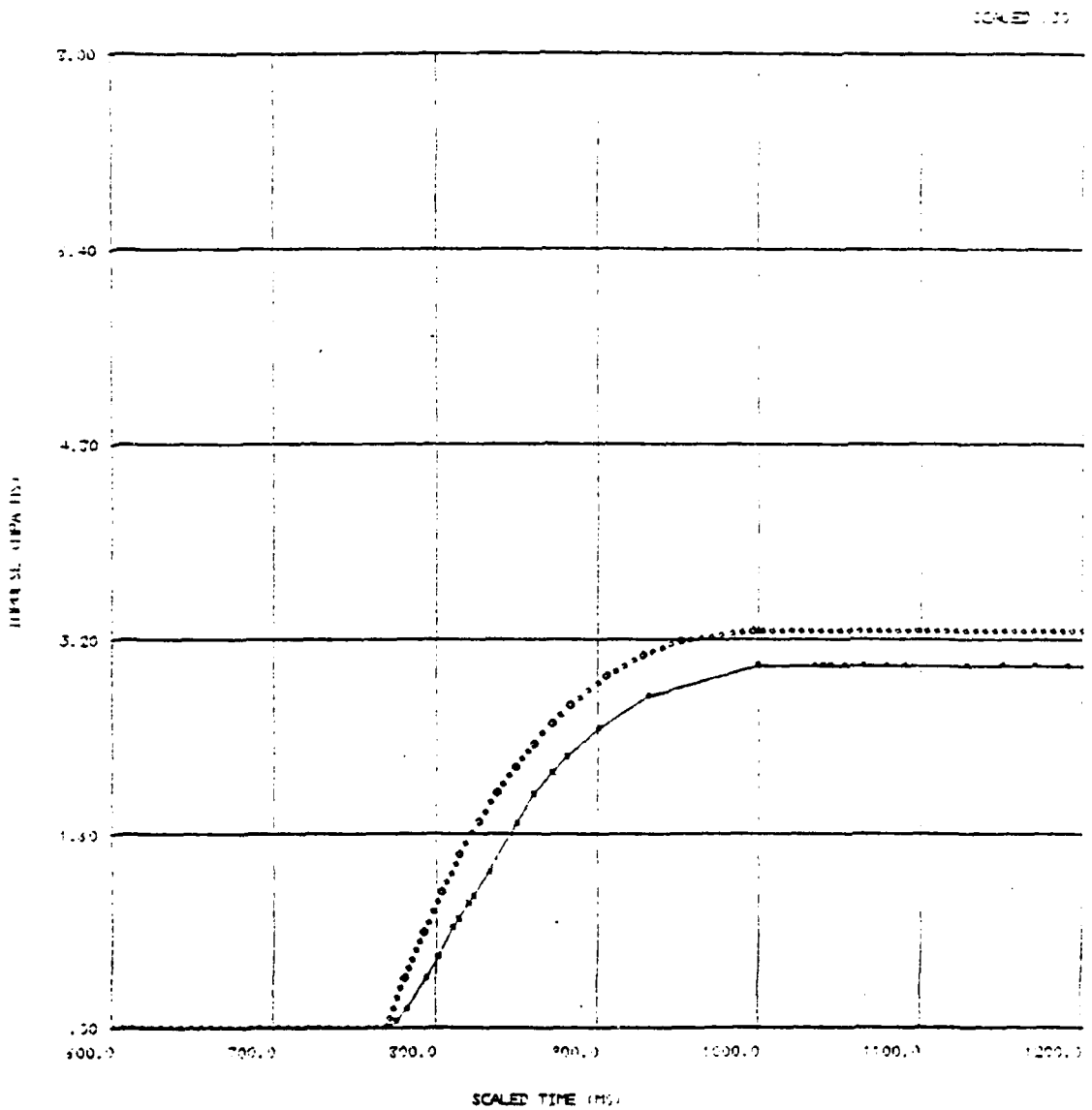
SHOT NO 1 0800 THURS 13 OCT 77
3.00
3.20
SCALED TIME

APPENDIX C

COMPARISON OF SCALED EXPERIMENTAL FAE BLAST WAVEFORMS AND POSITIVE PHASE IMPULSES FOR SHOT NO. 1, 1220 TUESDAY, 18 OCTOBER 1977 WITH NUCLEAR DATA.

These plots are similar to those of Appendix A. See that appendix for a description.

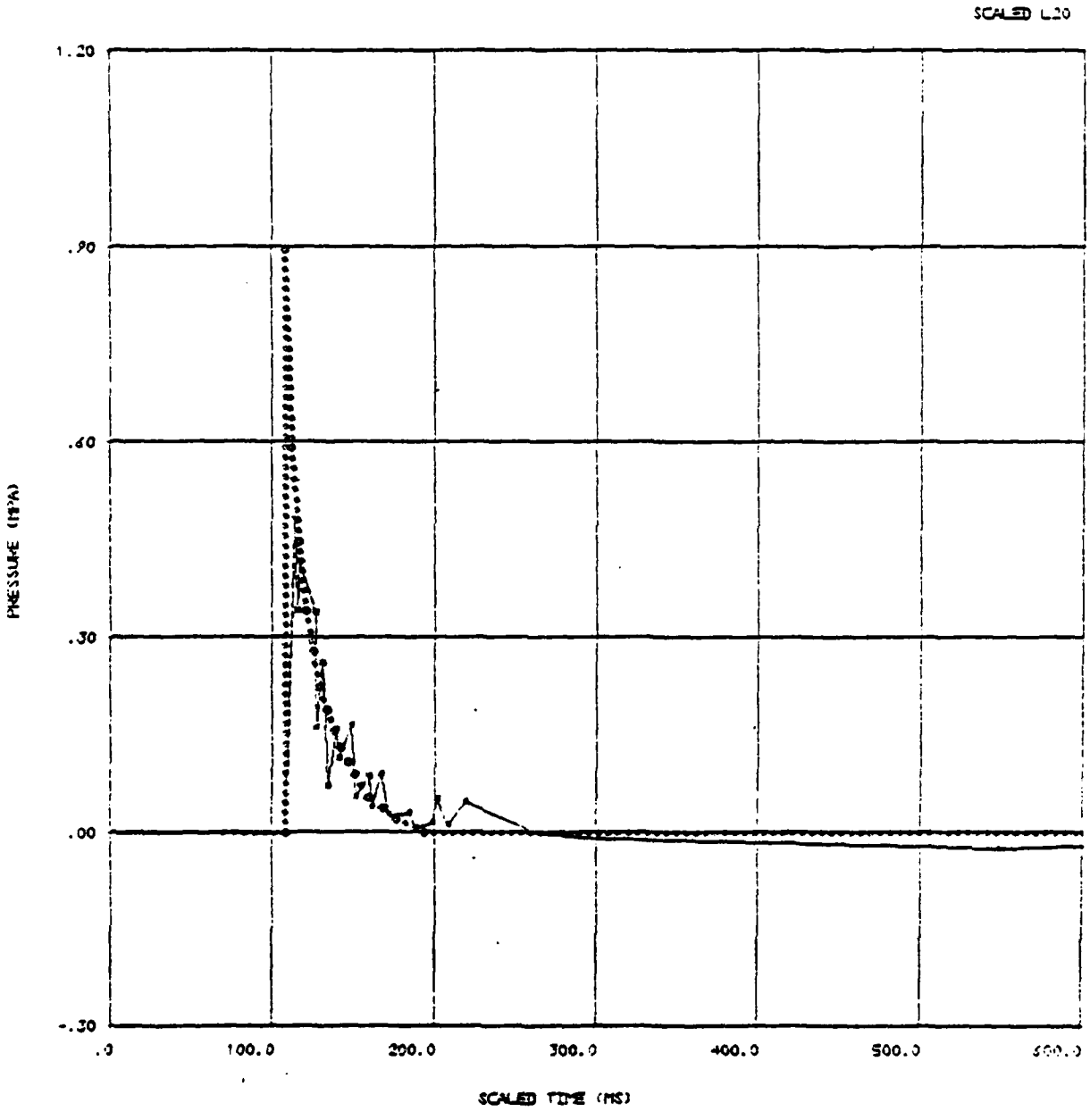
SHOT NO 1 1220 TUES 18 OCT 77
SCALED L20
1.20
.90
.60
.30
.00
-.30
PRESSURE (PSI)
.0
100.0
200.0
300.0
400.0
500.0
SCALED TIME (MS)

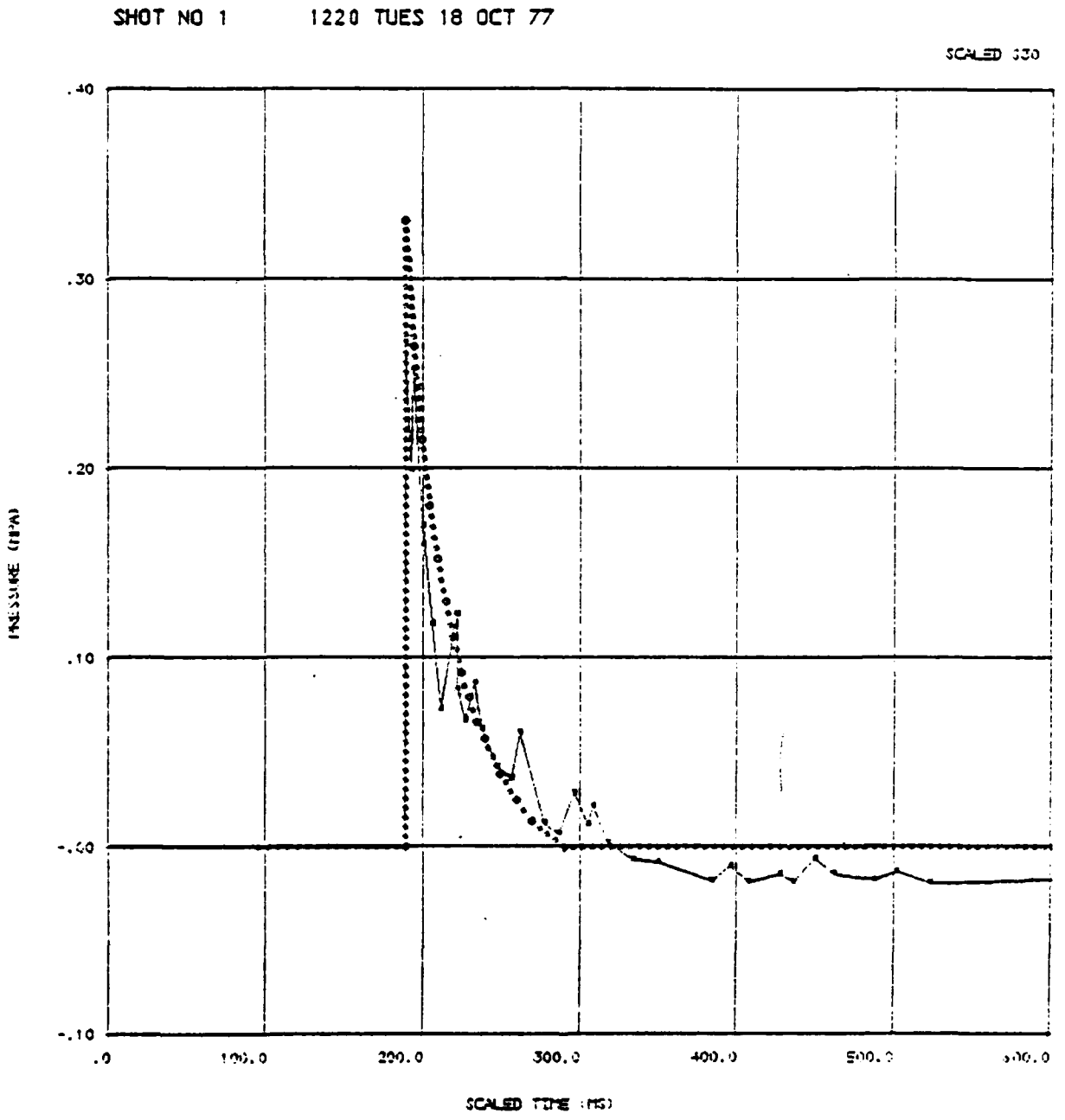
SHOT NO 1 1220 TUES 18 OCT 77
SCALED 330
.40
.30
.20
.10
-.10
.0
100.0
200.0
300.0
400.0
500.0
600.0
SCALED TIME (MS)

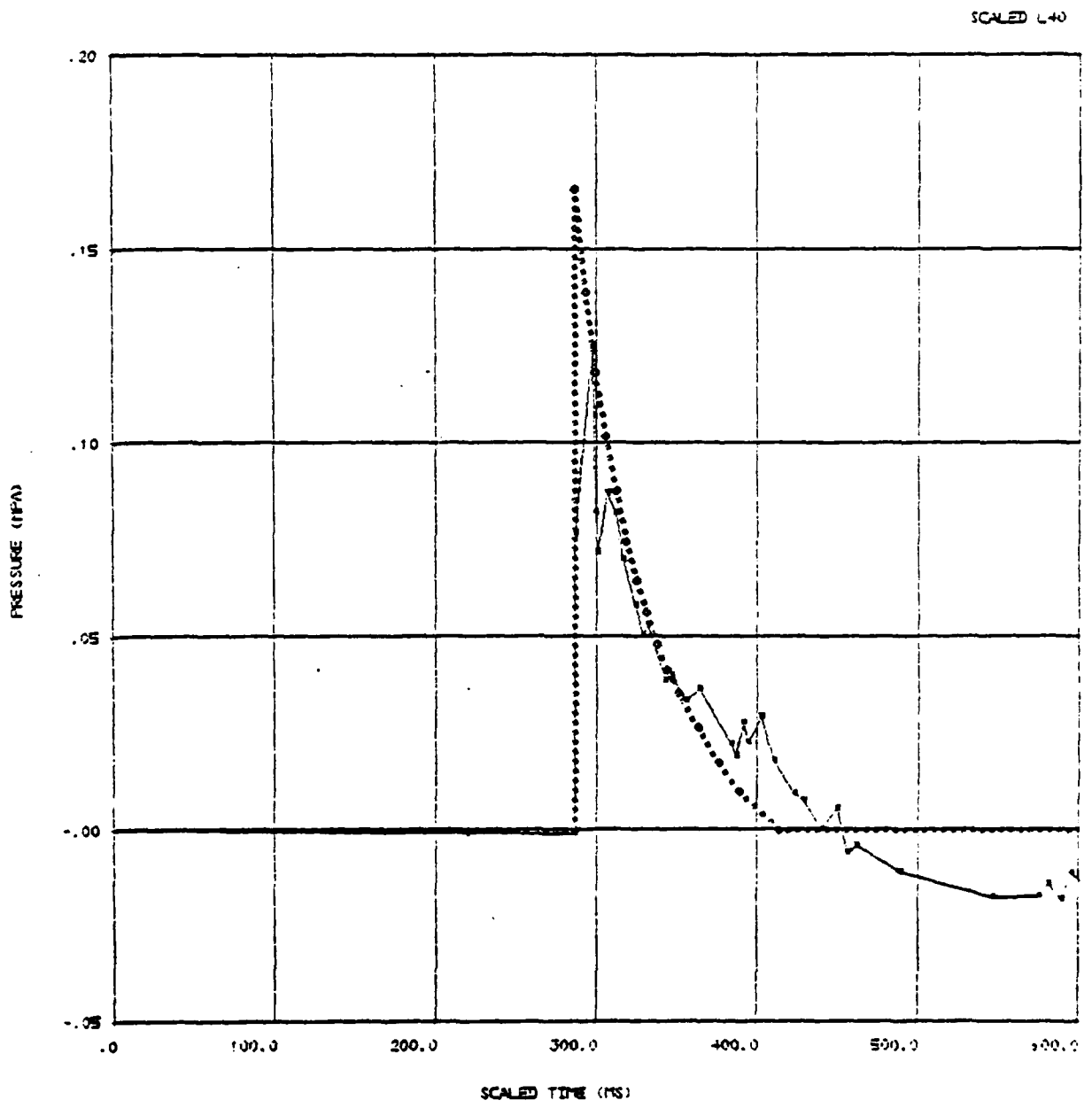
SHOT NO 1 1220 TUES 18 OCT 77
SCALED L40
.20
.15
.10
.05
-.00
-.05
PRESSURE (MPA)
.0
100.0
200.0
300.0
400.0
500.0
SCALED TIME (MS)

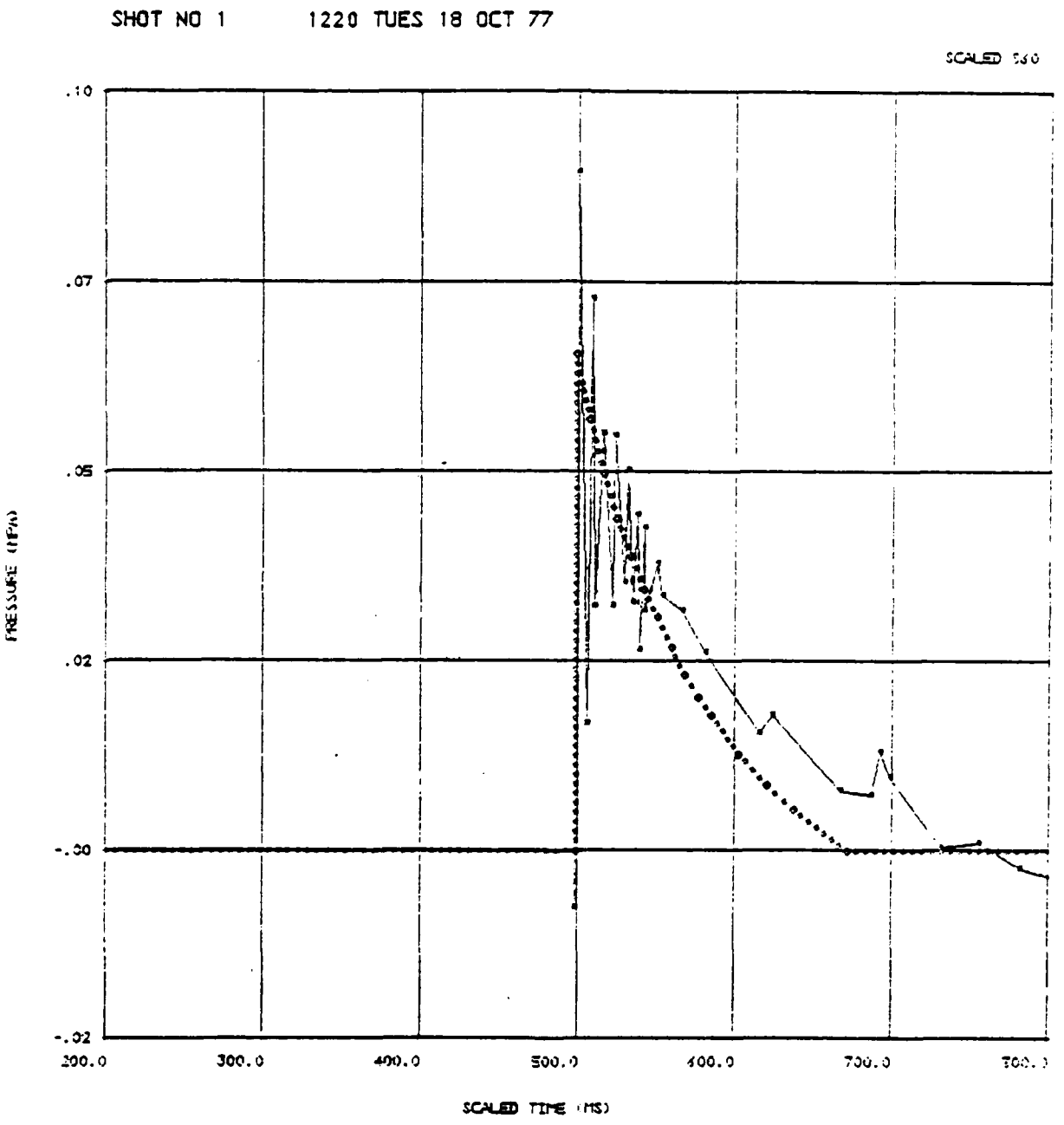
SHOT NO 1 1220 TUES 18 OCT 77
SCALED 560
.10
.07
.05
.02
-.00
-.02
200.0
300.0
400.0
500.0
600.0
700.0
SCALED TIME (MS)

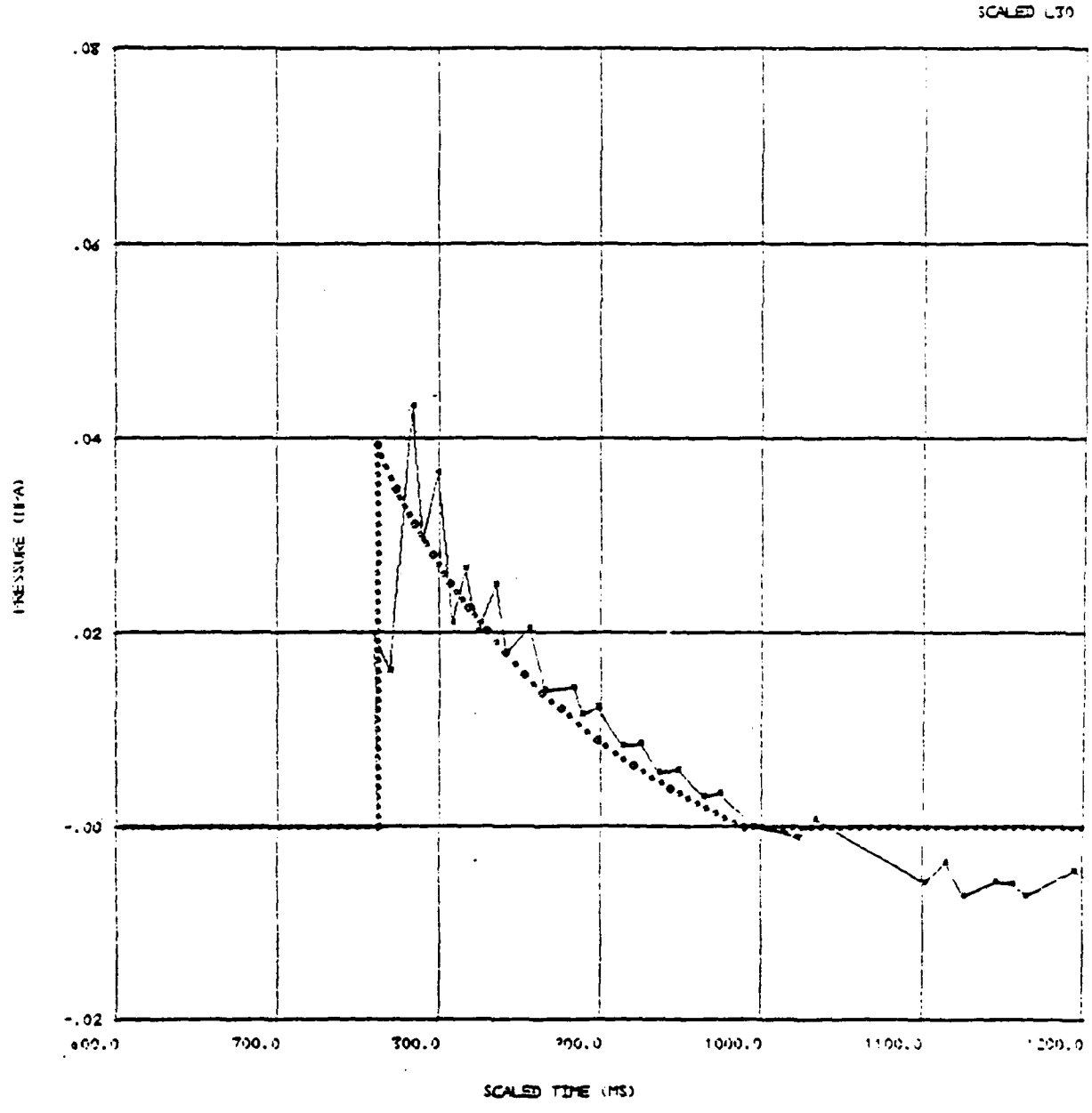
SHOT NO 1 1220 TUES 18 OCT 77
SCALED L30
.08
.06
.04
.02
-.00
-.02
PRESSURE (PSI)
700.0
900.0
1000.0
SCALED TIME (MS)

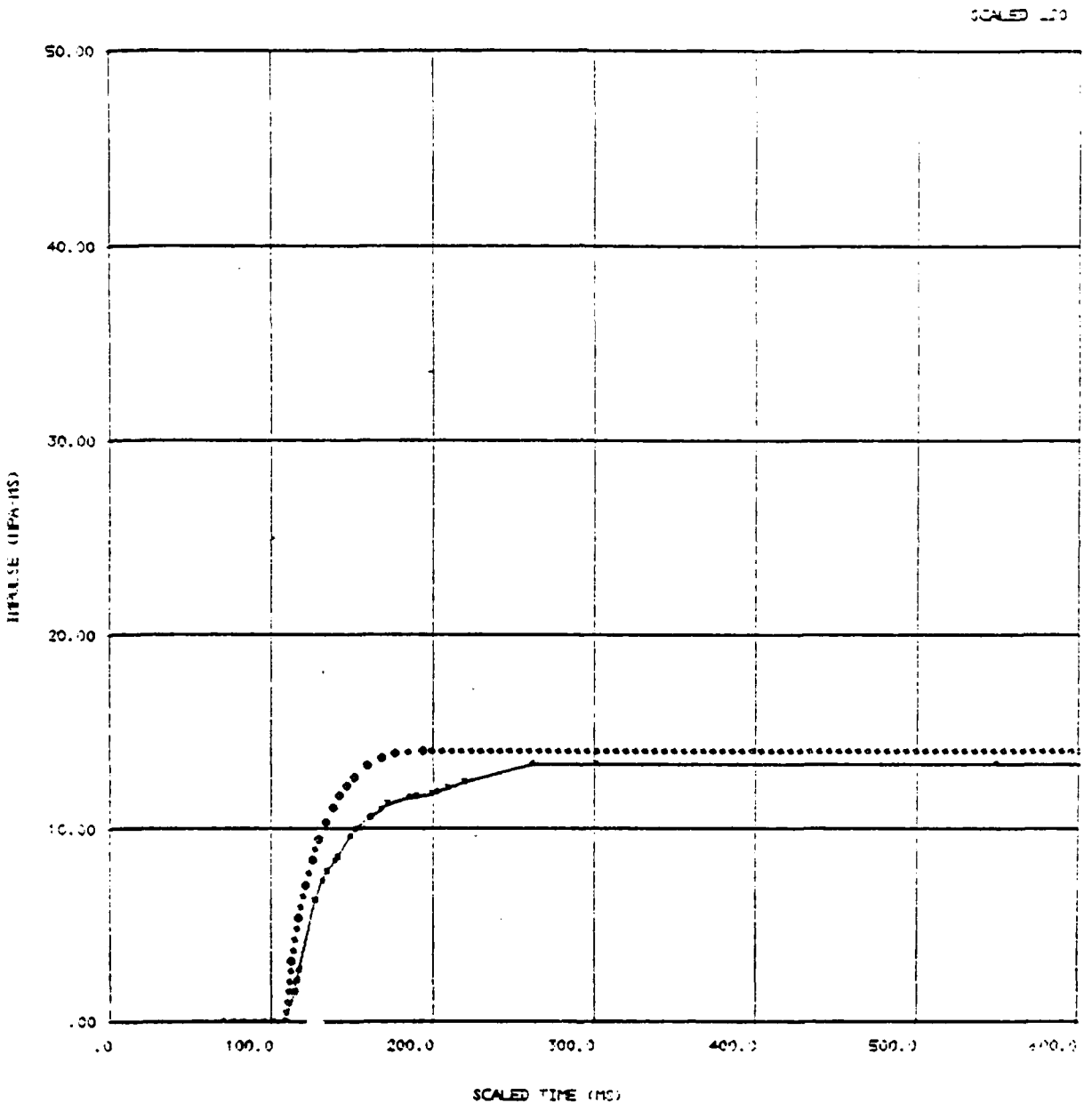
SHOT NO 1 1220 TUES 18 OCT 77
50.00
40.00
30.00
20.00
10.00
.00
.0
100.0
200.0
300.0
400.0
500.0
SCALED TIME (MS)

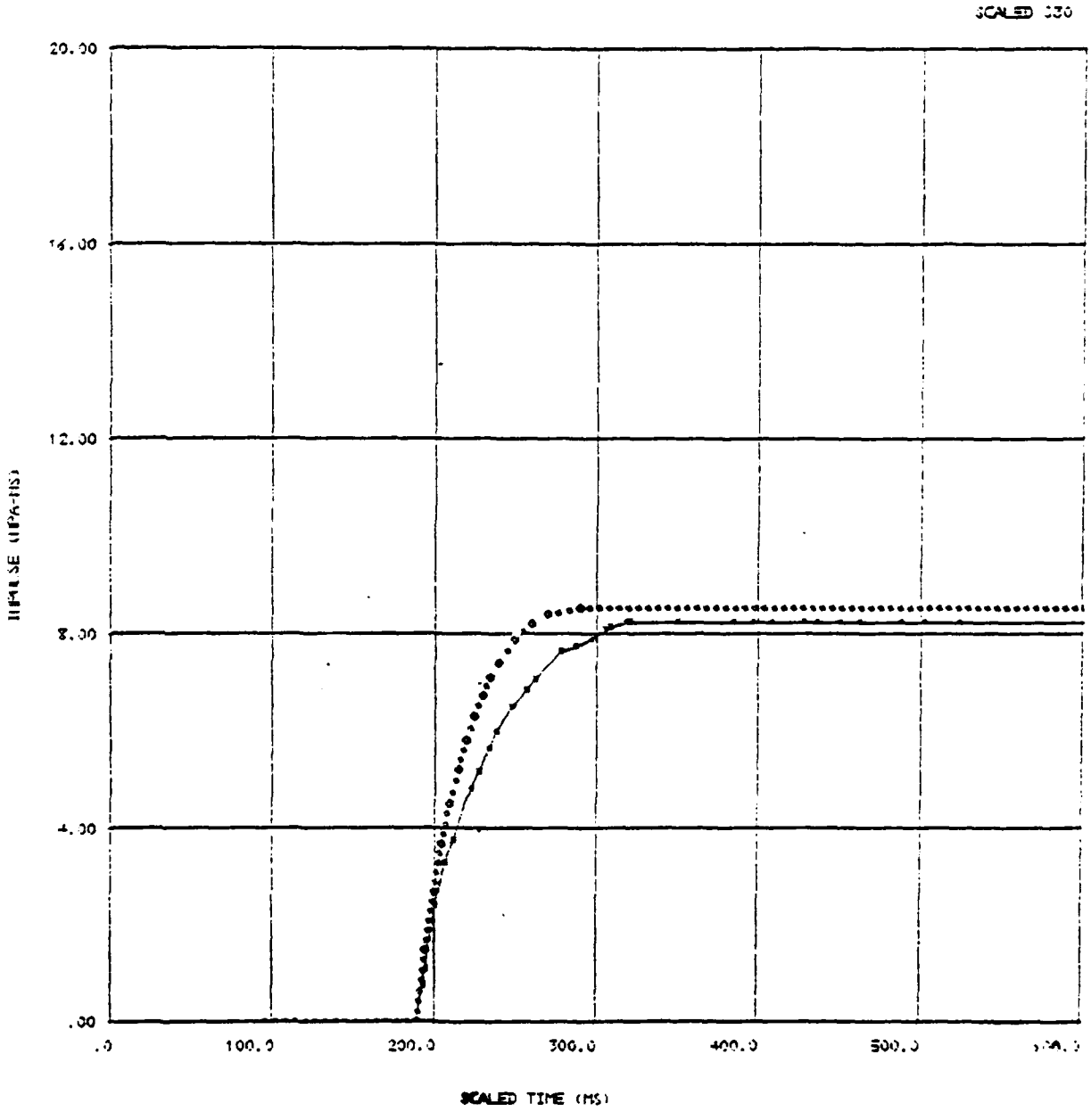
SHOT NO 1 1220 TUES 18 OCT 77
SCALED 330
20.00
16.00
12.00
8.00
4.00
.00
.0
100.0
200.0
300.0
400.0
500.0
SCALED TIME (MS)

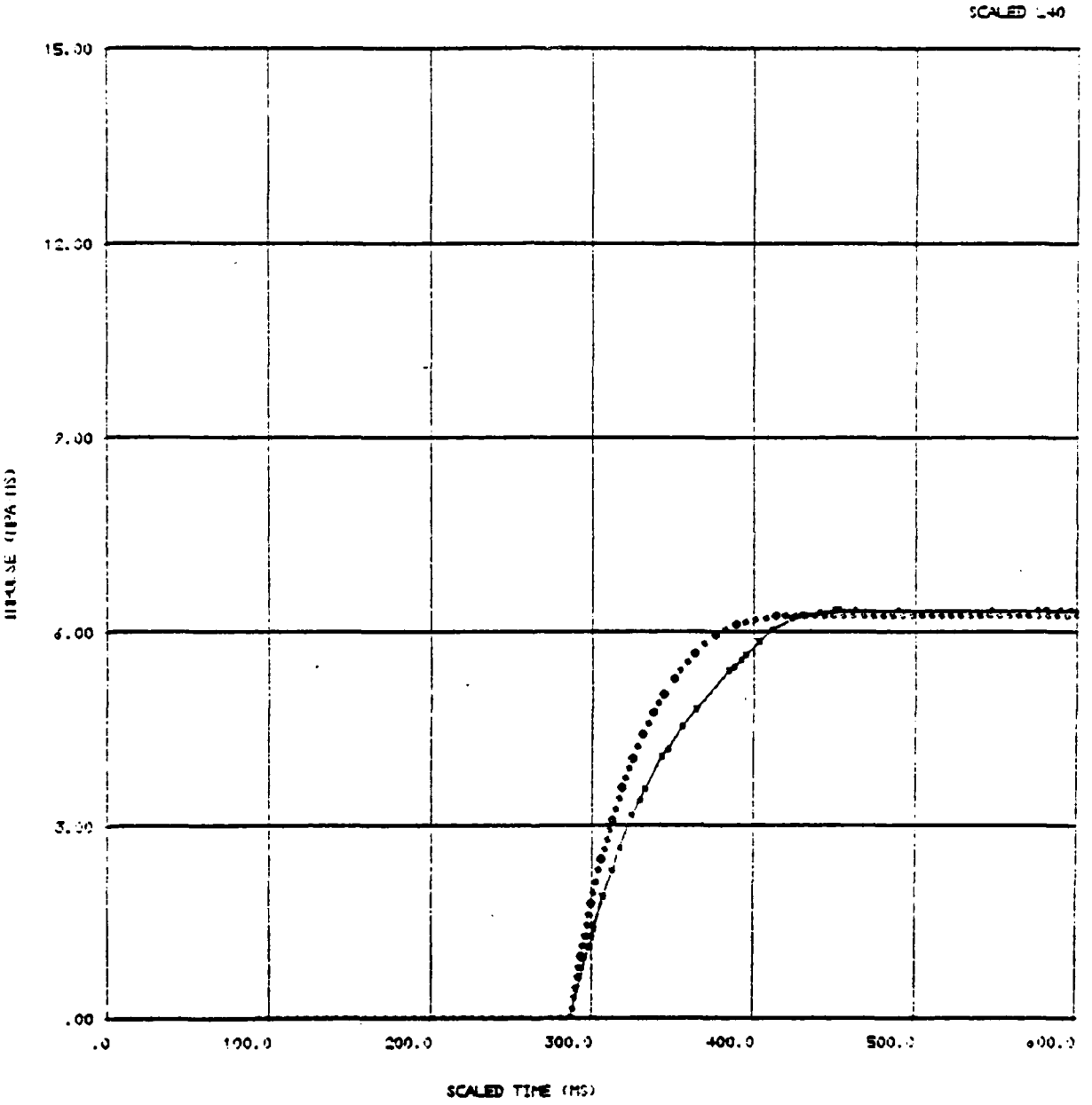
SHOT NO 1 1220 TUES 18 OCT 77
15.00
12.00
9.00
6.00
3.00
.00
.0
100.0
200.0
300.0
400.0
500.0
SCALED TIME (MS)

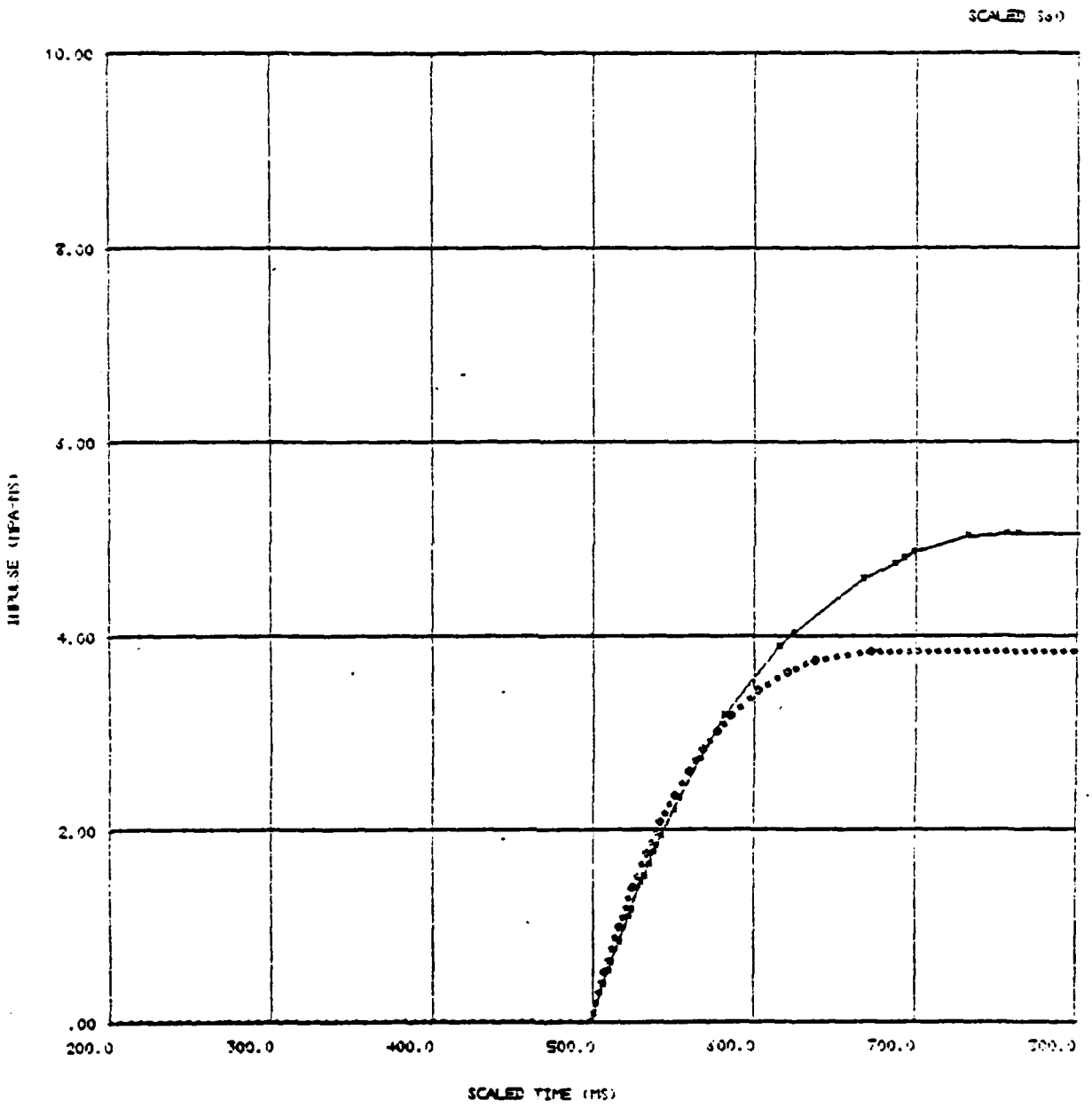
SHOT NO 1
1220 TUES 18 OCT 77
10.00
8.00
6.00
4.00
2.00
.00
200.0
300.0
400.0
500.0
600.0
700.0
SCALED TIME (MS)

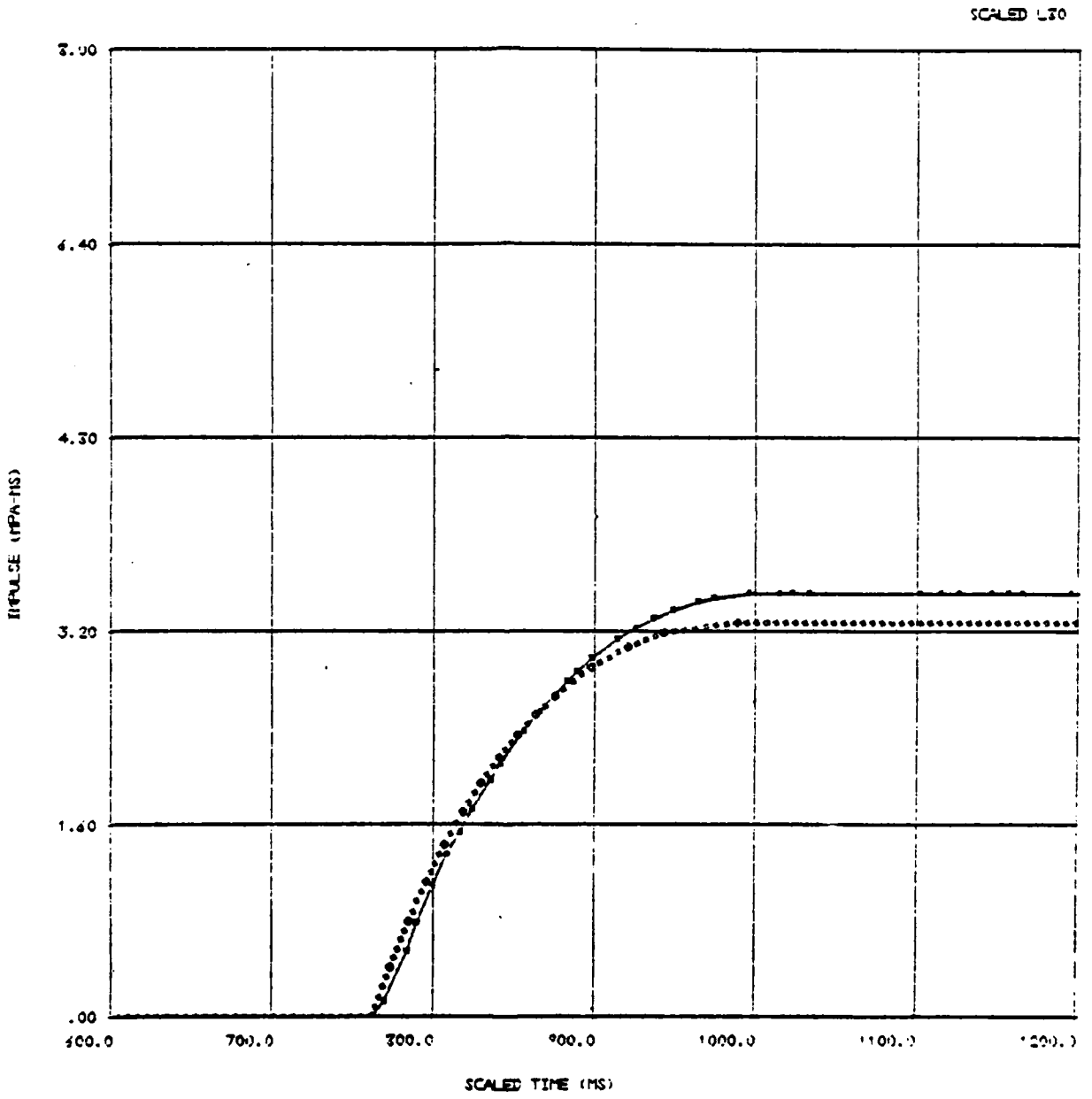
SHOT NO 1 1220 TUES 18 OCT 77
SCALED L30
8.00
6.40
4.30
3.20
1.60
.00
IMPULSE (MPA-MS)
600.0
700.0
800.0
900.0
1000.0
1100.0
1200.0
SCALED TIME (MS)

APPENDIX D

COMPARISON OF SCALED EXPERIMENTAL FAE BLAST WAVEFORMS AND POSITIVE PHASE IMPULSES FOR SHOT NO. 2, 1120 THURSDAY, 8 DECEMBER 1977 WITH NUCLEAR DATA.

These plots are similar to those of Appendix A. See that appendix for a description.

SHOT NO 2 1120 THURS 8 DEC 77

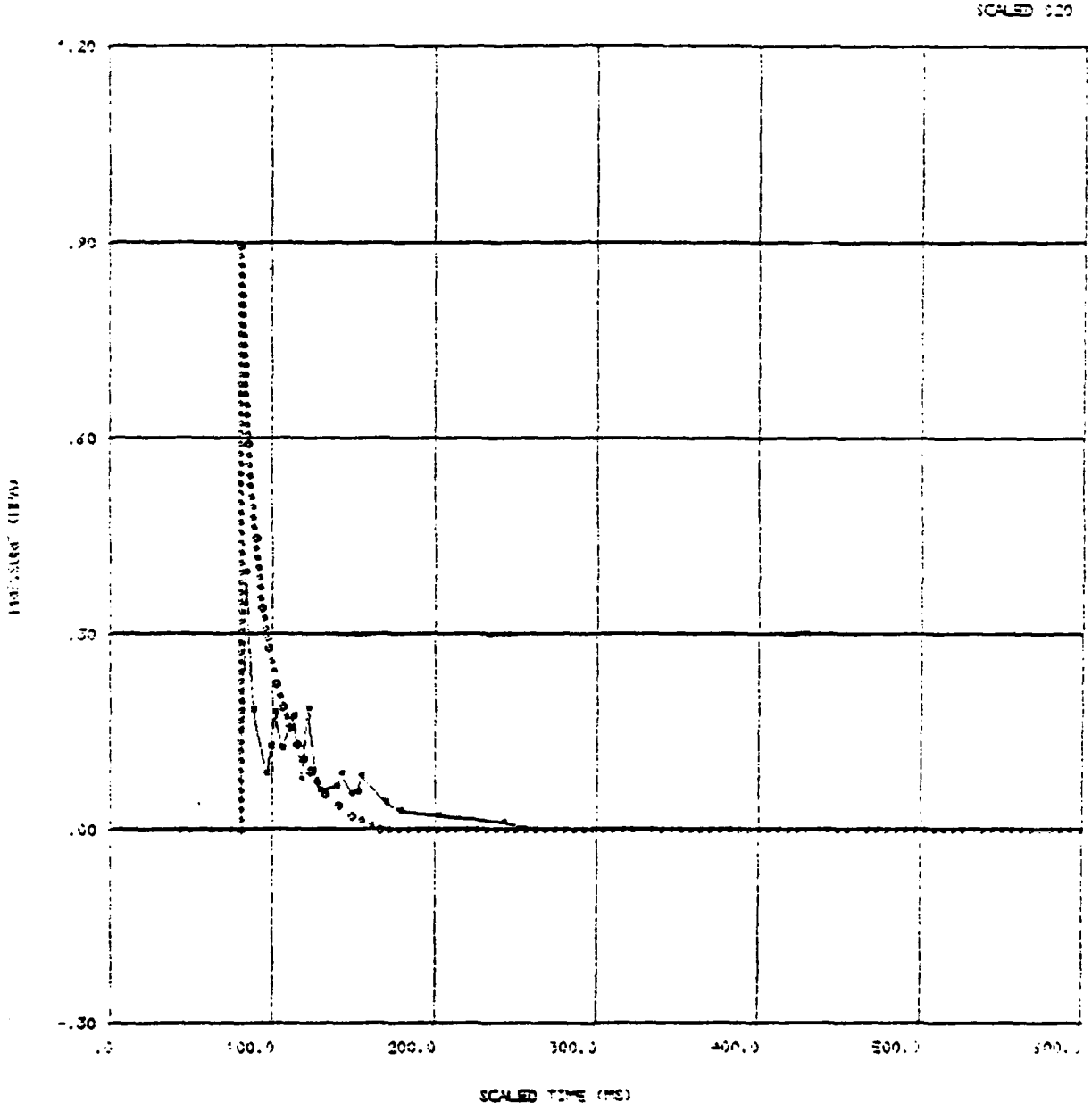

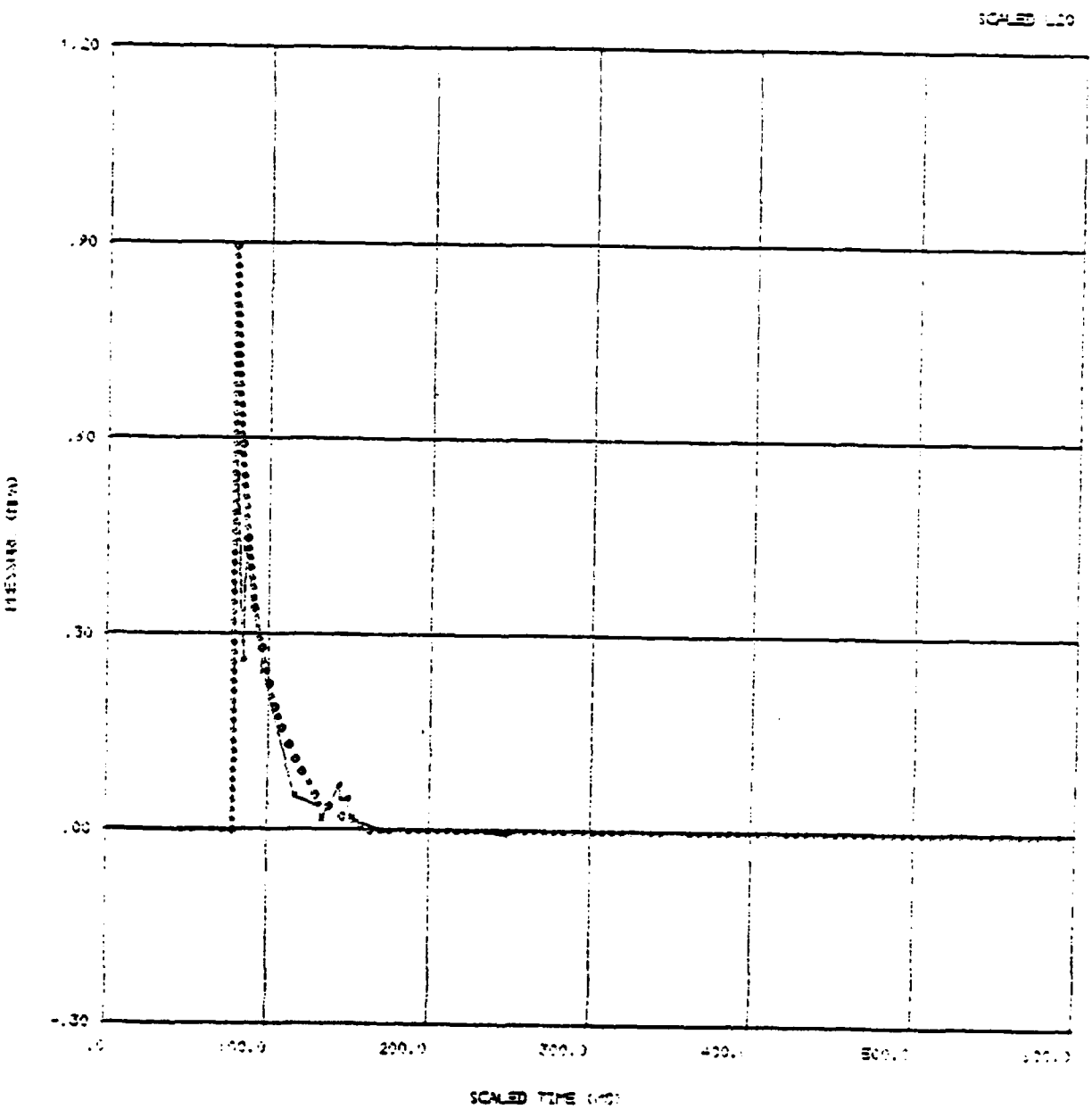
SHOT NO 2 1120 THURS 8 DEC 77
.90
.30
.00
-.30
200.0
SCALED TIME

SHOT NO 2 1120 THURS 8 DEC 77

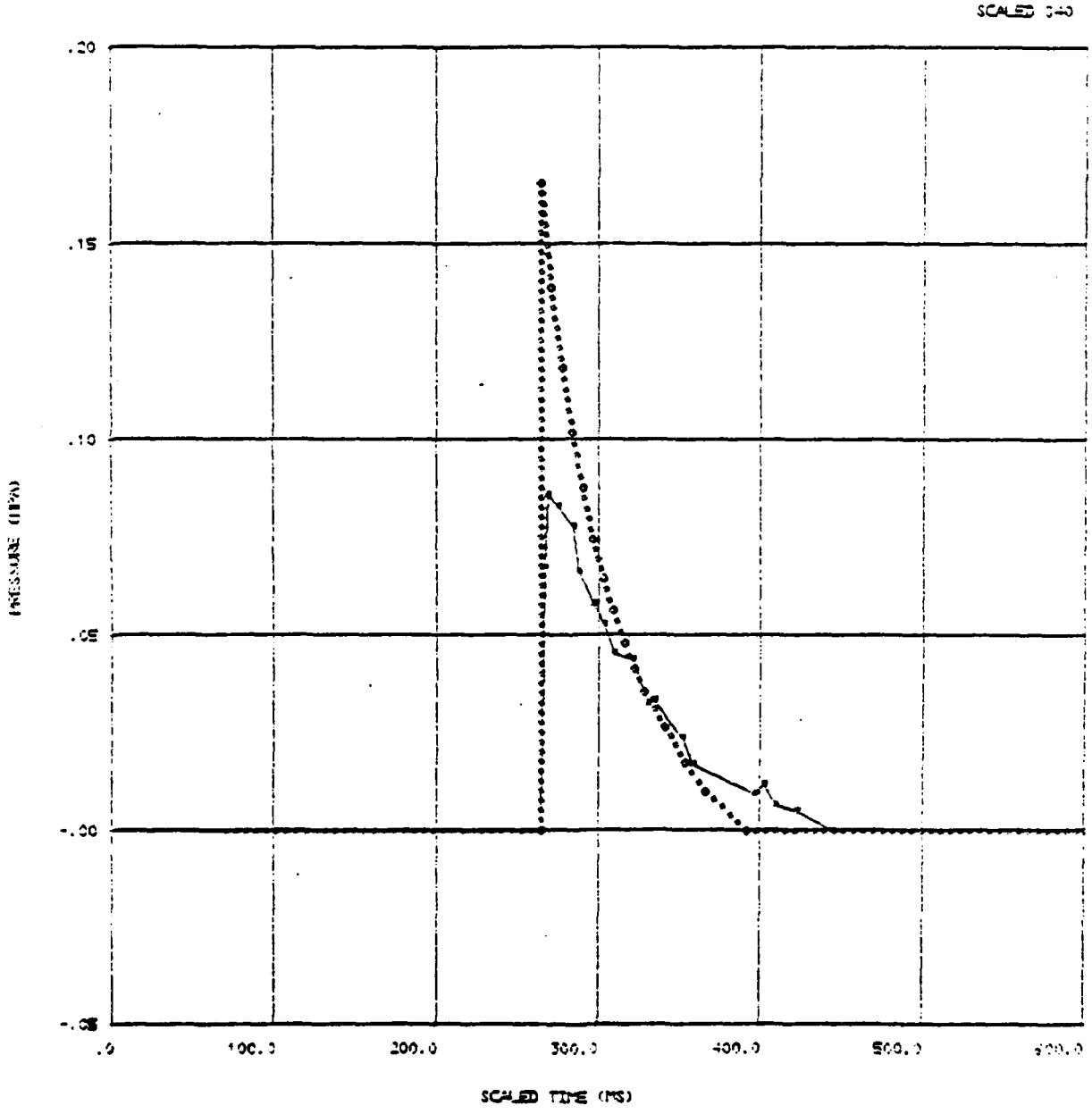

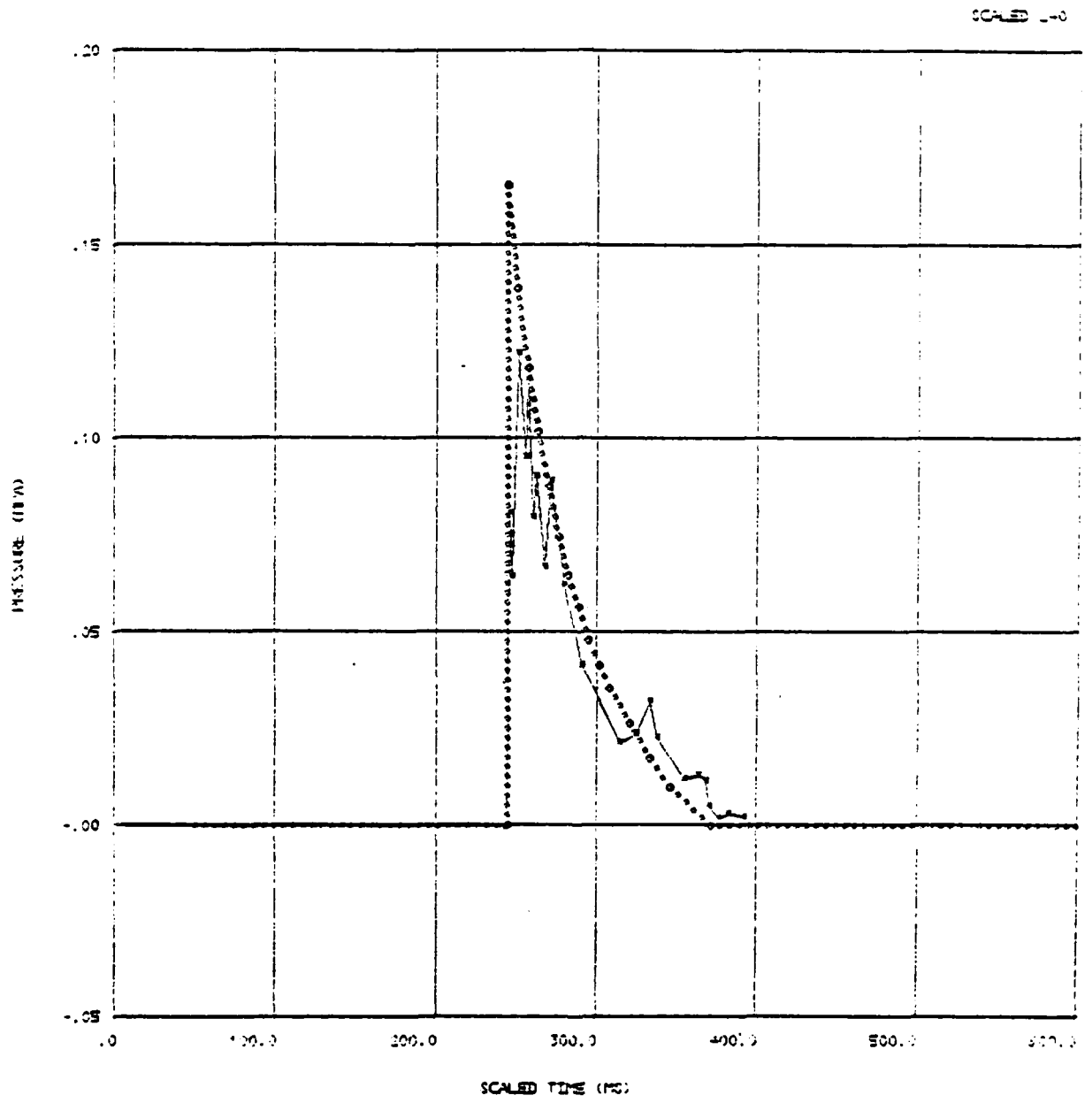
SHOT NO 2 1120 THURS 8 DEC 77
.20
.15
.10
.05
-.00
-.05
.0
200.0
300.0
500.0
SCALED TIME (MS)

SHOT NO 2 1120 THURS 8 DEC 77

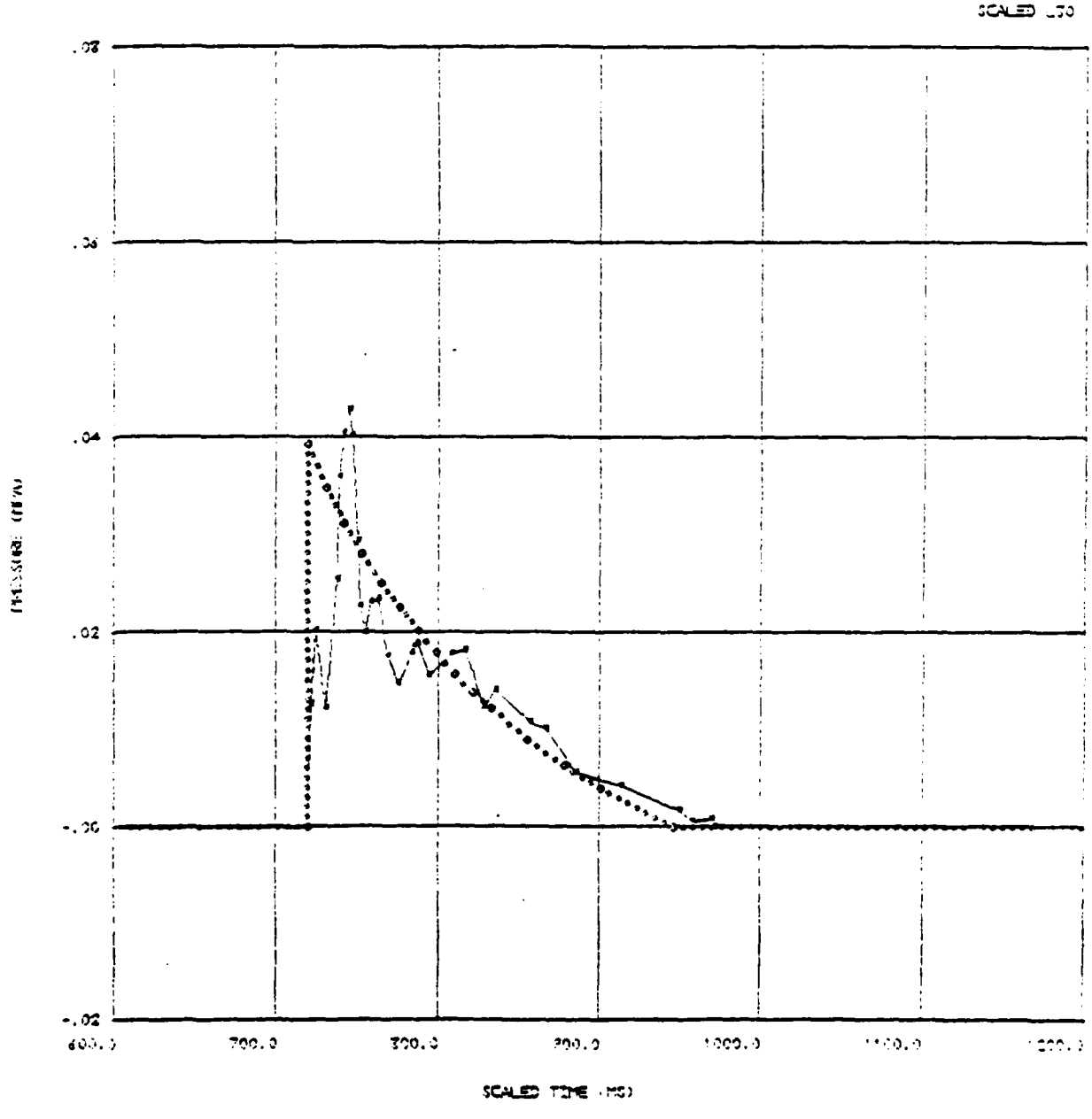

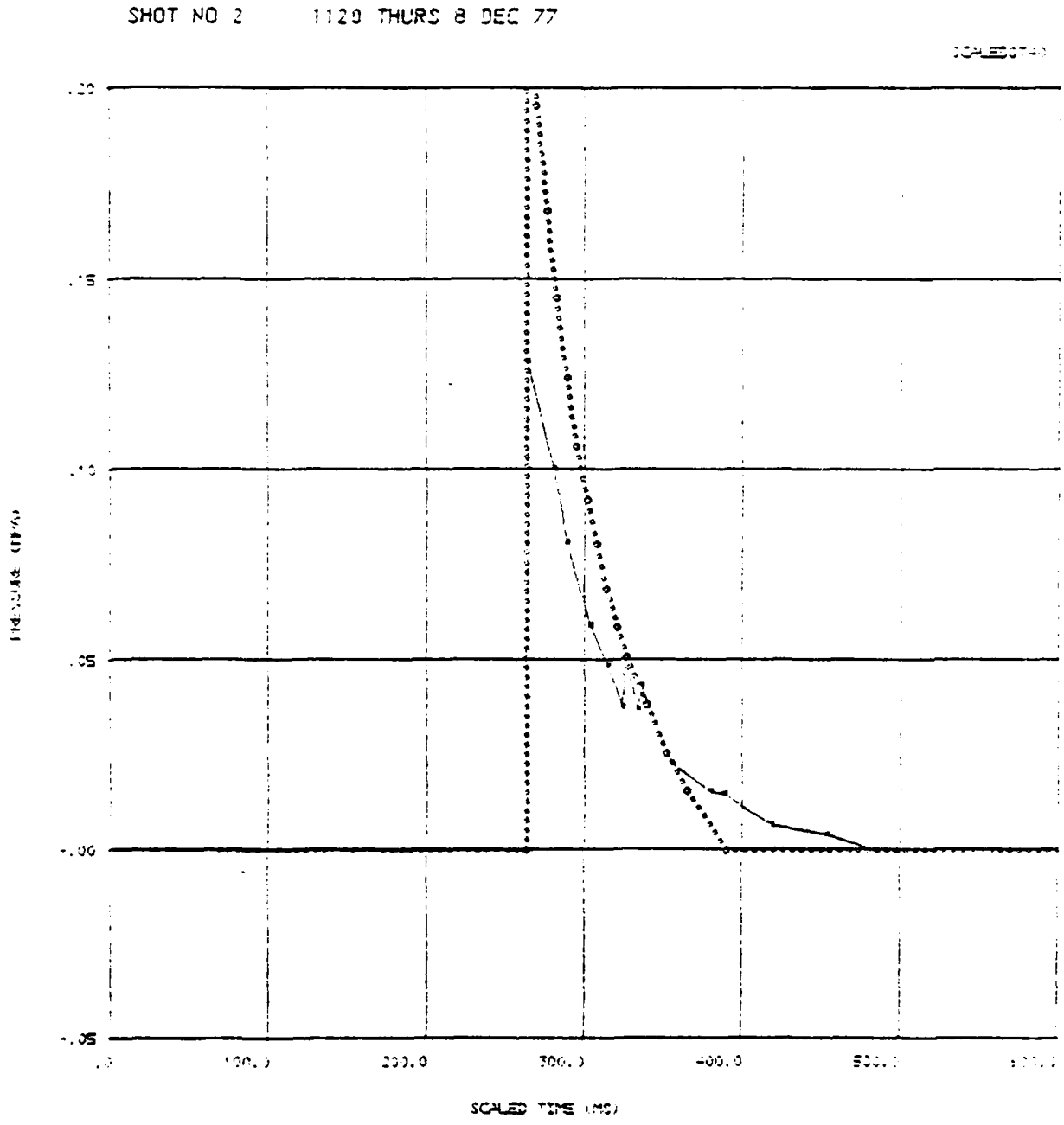
SHOT NO 2 1120 THURS 8 DEC 77
.10
.05
.00
-.05
100.0
200.0
300.0
400.0
SCALED TIME (MS)

SHOT NO 2 1120 THURS 8 DEC 77

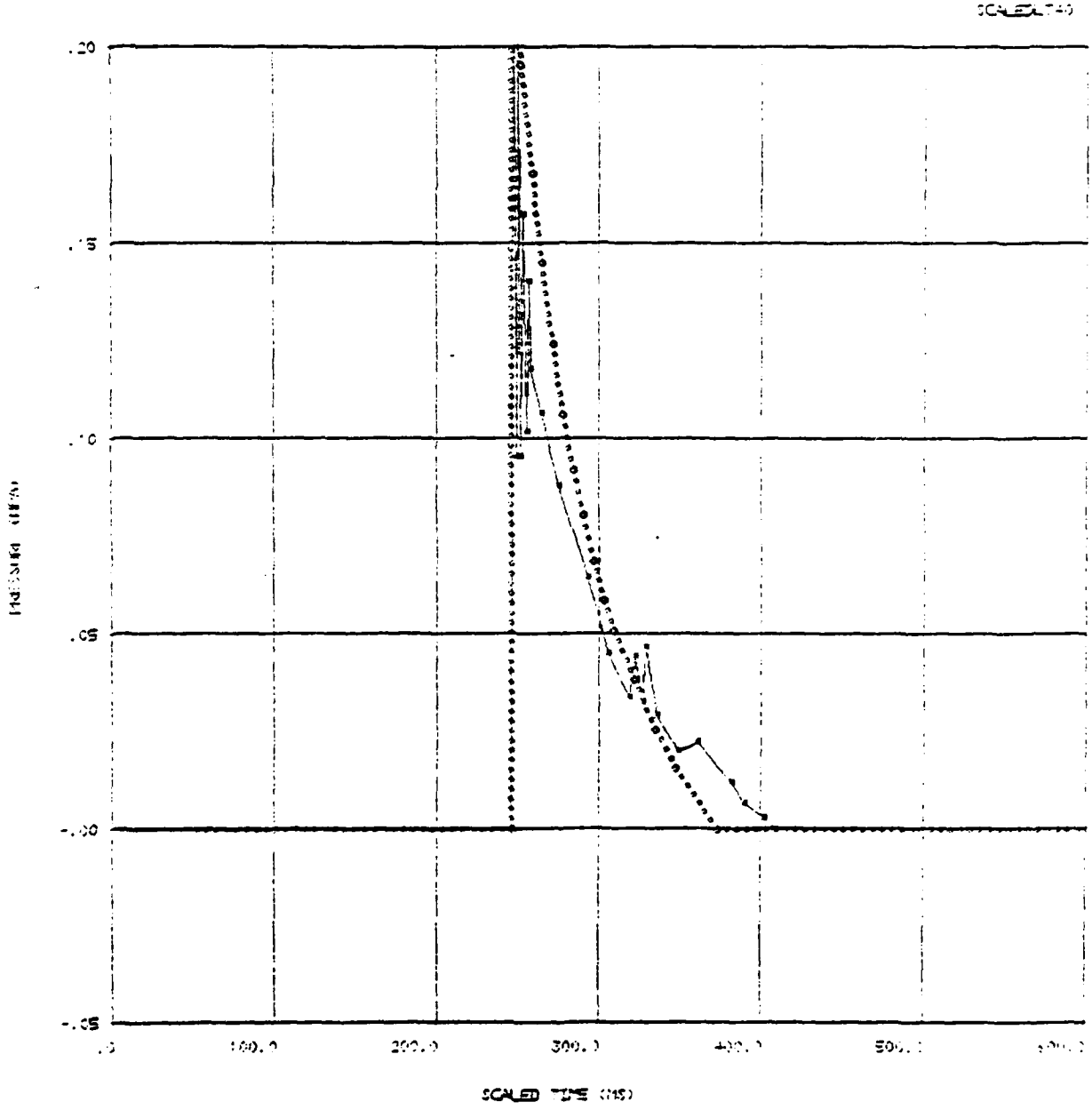

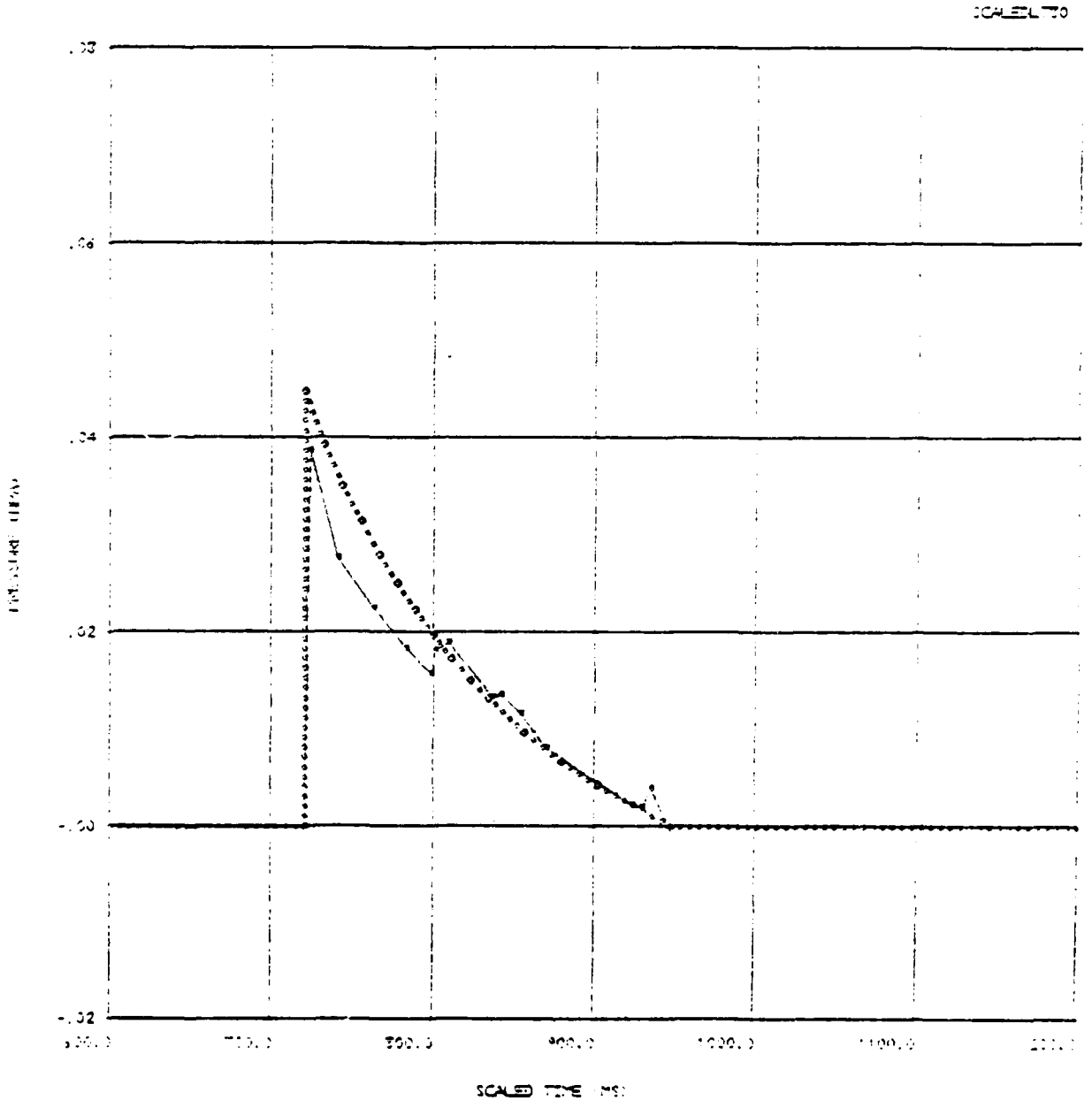
SHOT NO 2 1120 THURS 8 DEC 77
.06
.04
.02
-.02
SCALED TIME (MS)

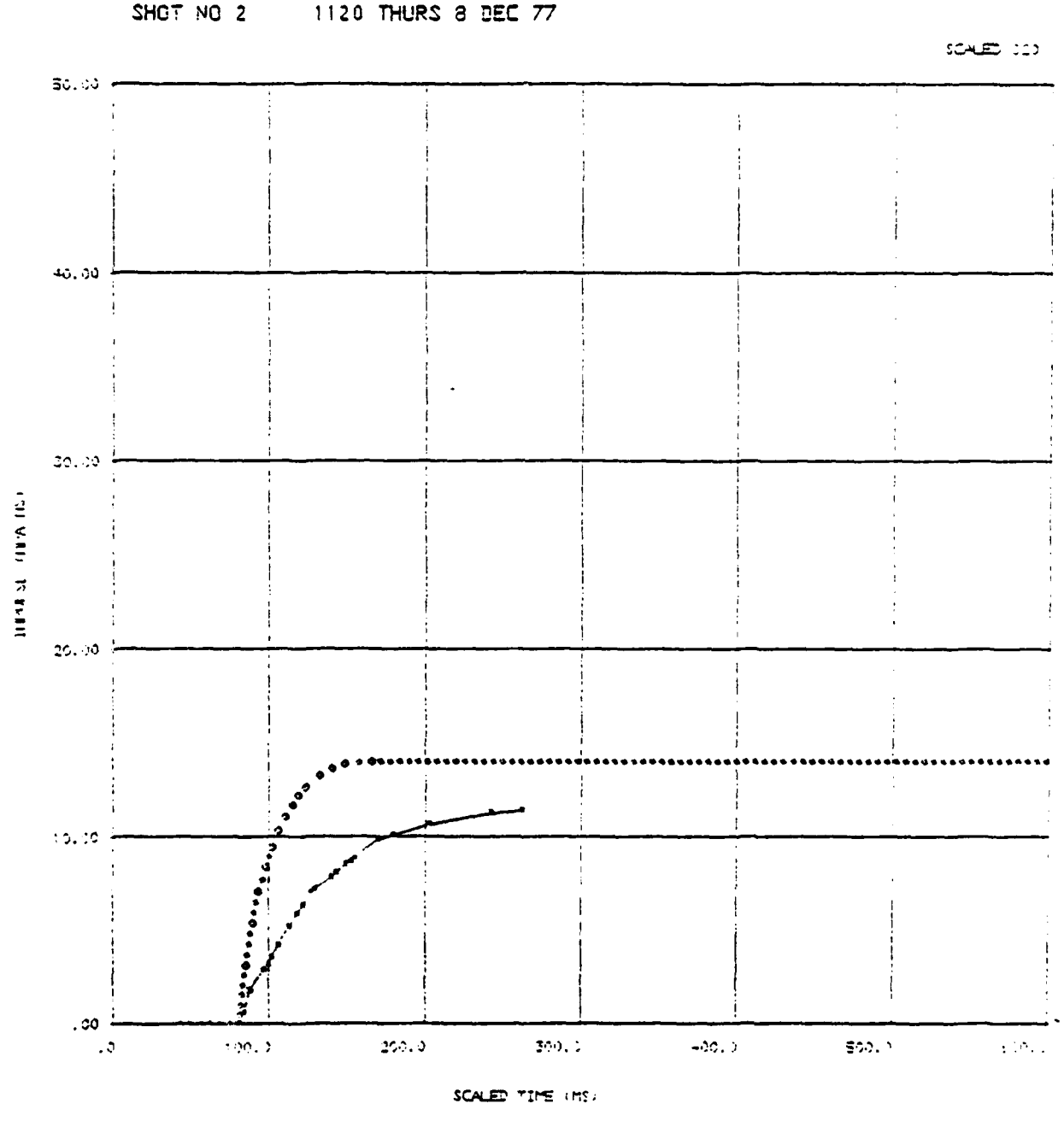
SHOT NO 2 1120 THURS 8 DEC 77
50.00
40.00
30.00
20.00
10.00
.00
SCALED TIME (MS)

SHOT NO 2 1120 THURS 8 DEC 77

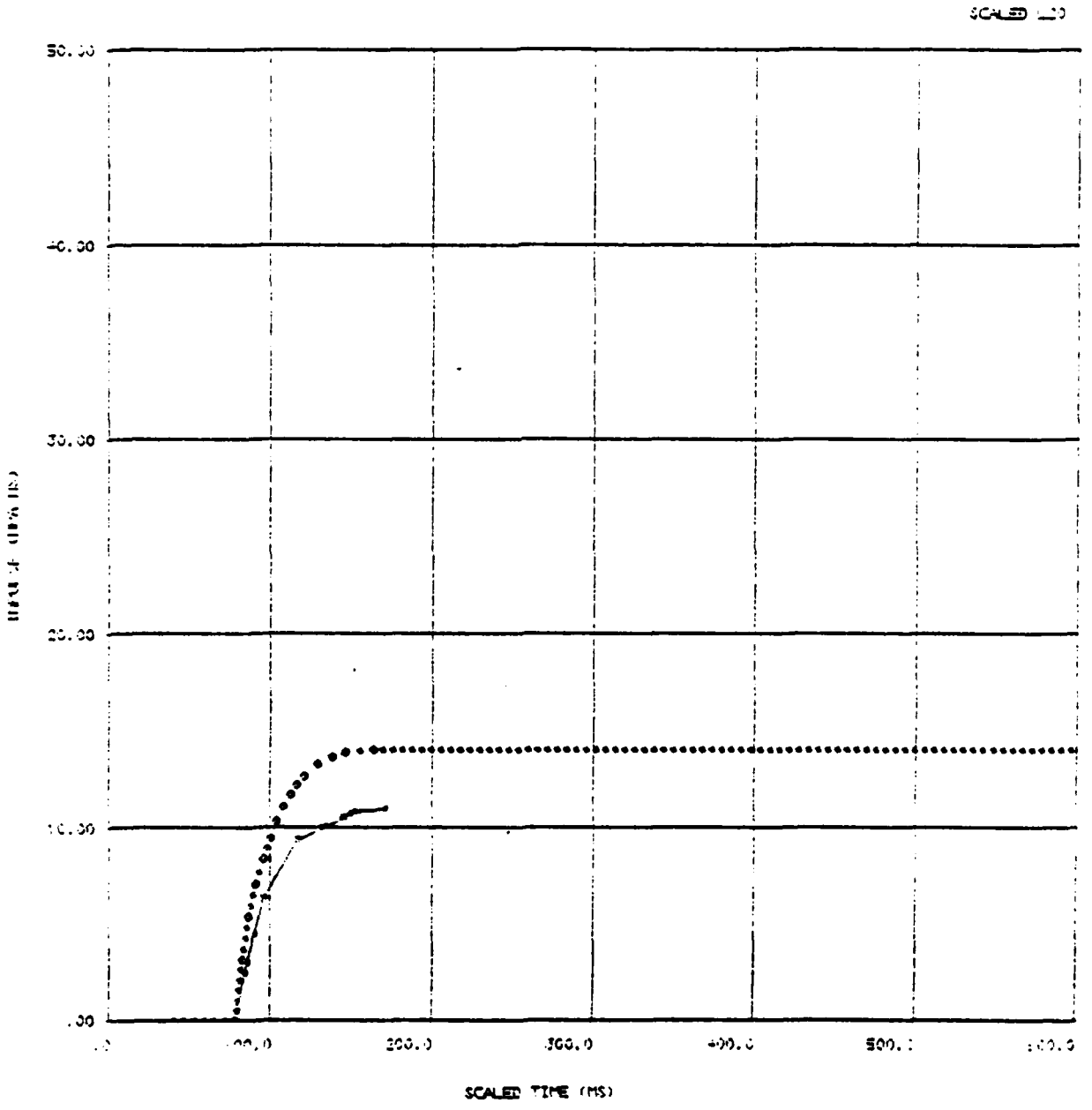

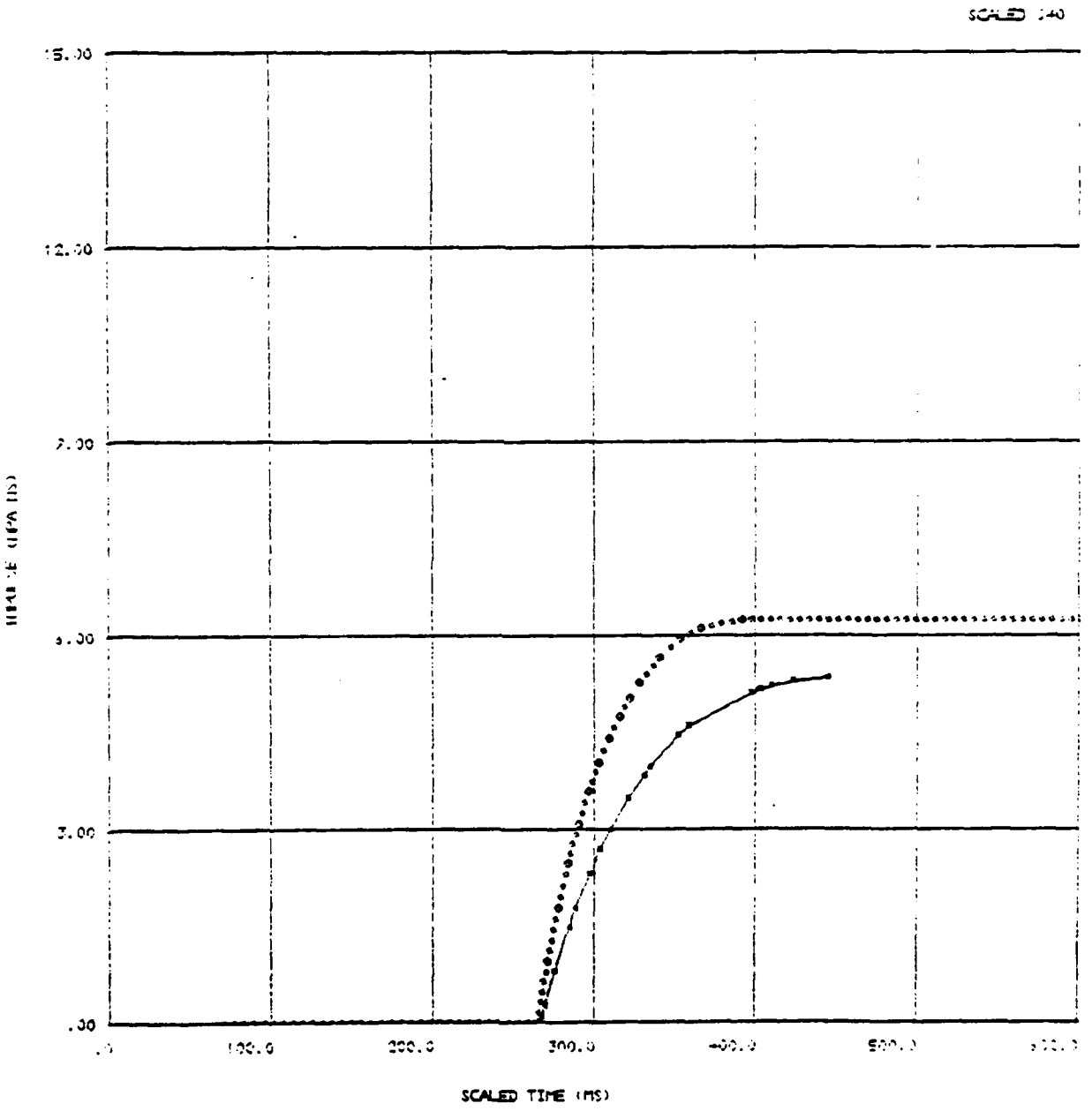
SHOT NO 2 1120 THURS 8 DEC 77
15.00
12.00
9.00
6.00
3.00
.00
300.0
SCALED TIME (MS)

SHOT NO 2 1120 THURS 8 DEC 77

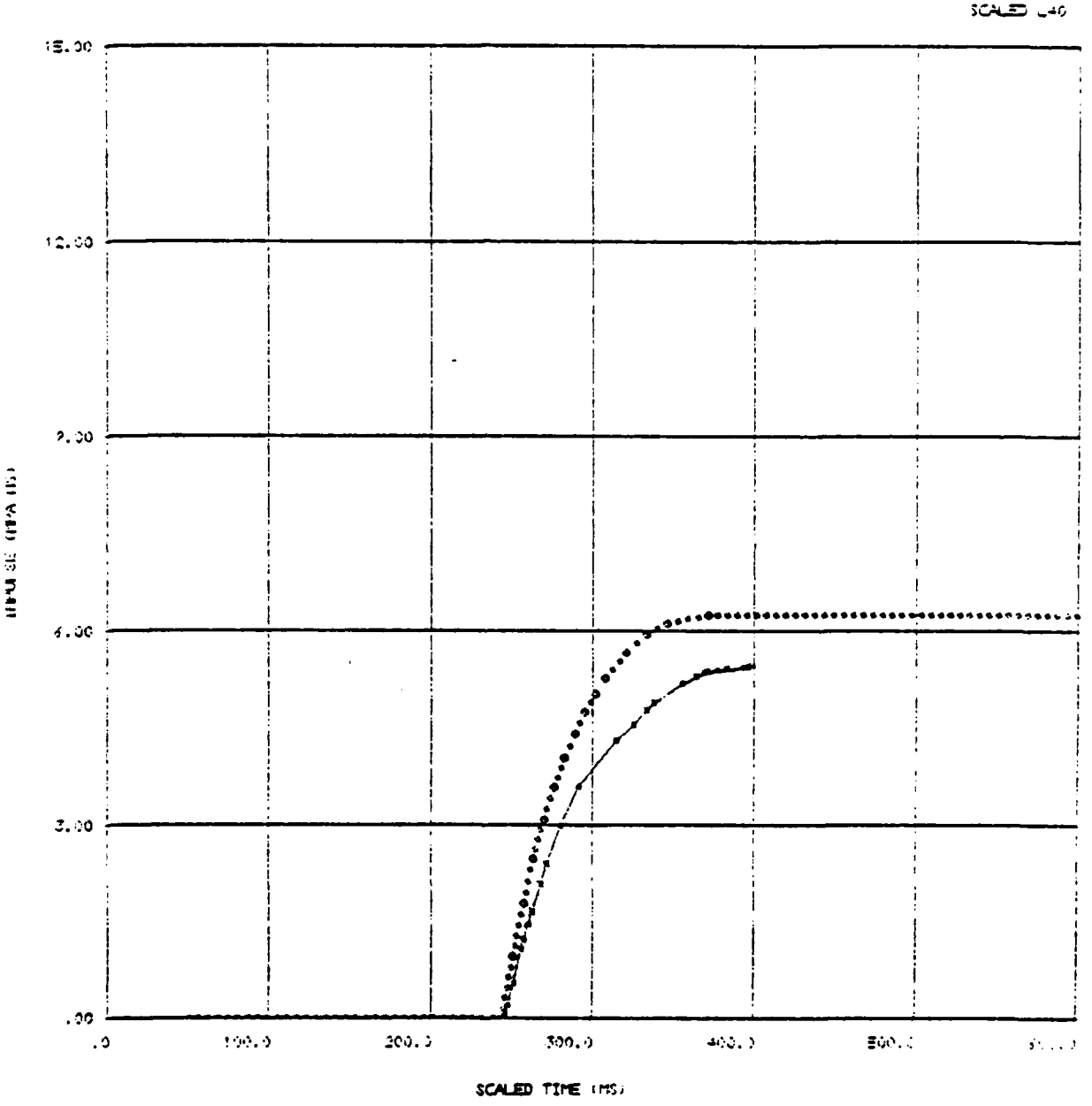

SHOT NO 2 1120 THURS 8 DEC 77

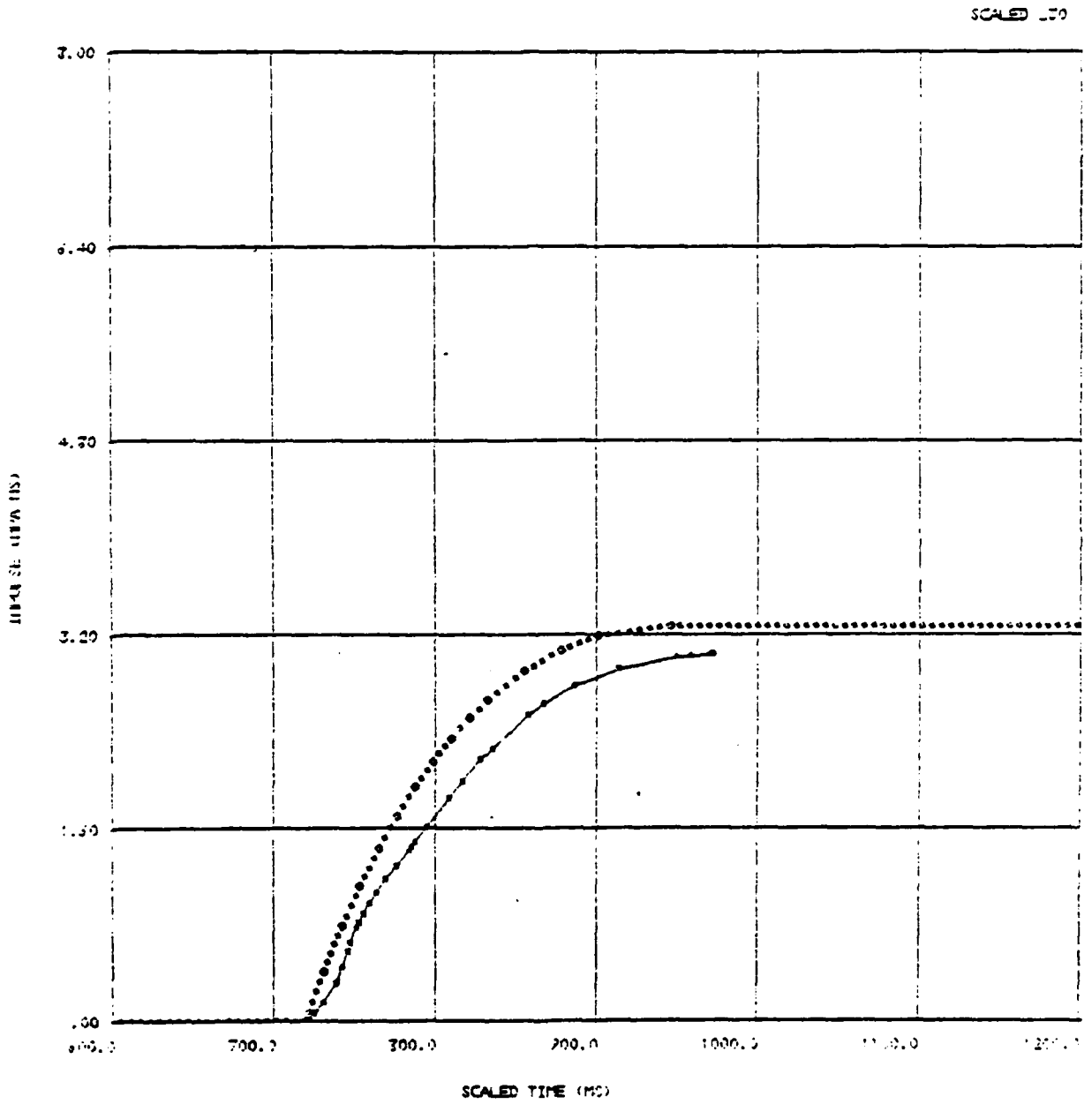

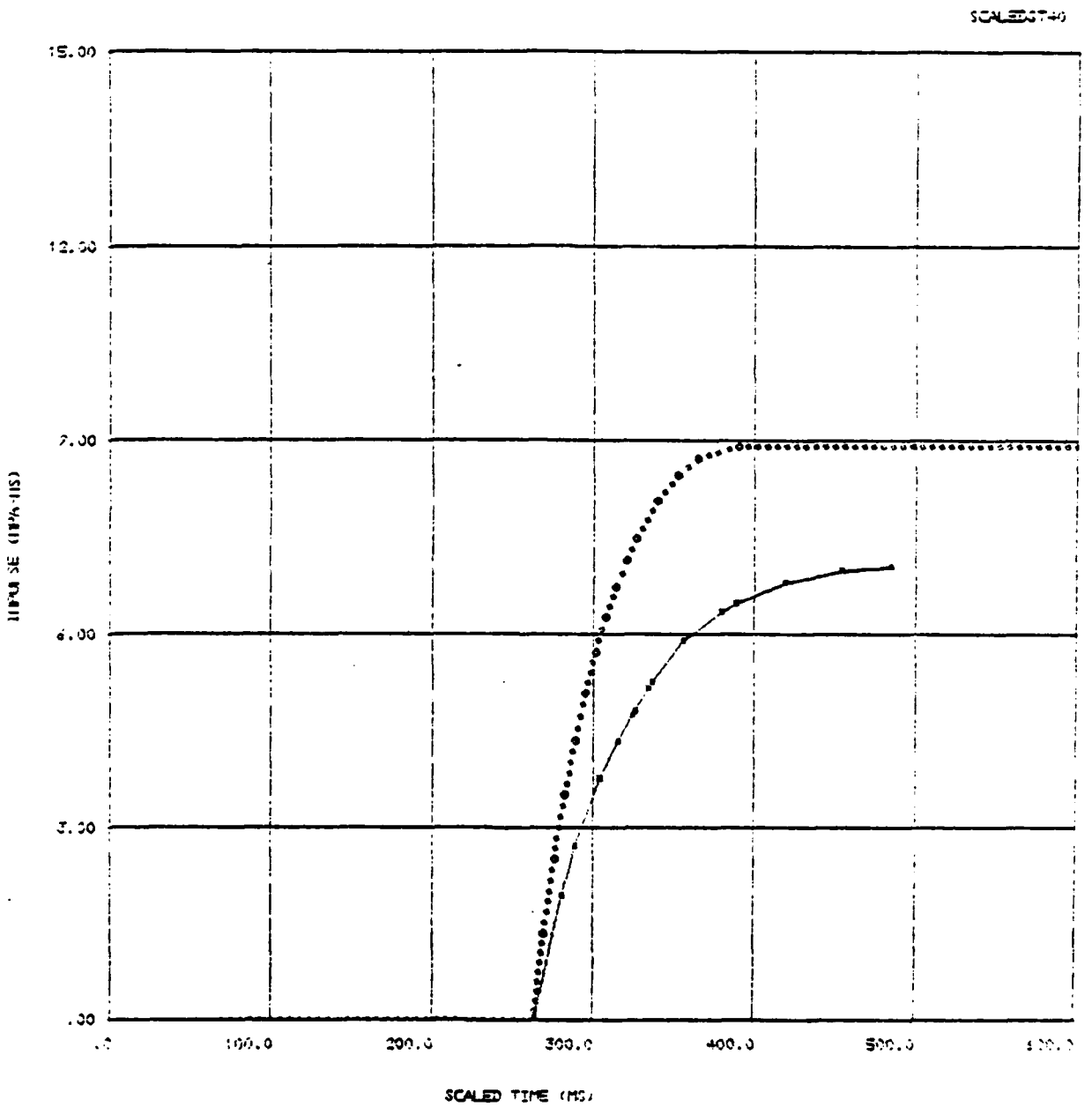
SHOT NO 2 1120 THURS 8 DEC 77
15.00
12.00
9.00
6.00
3.00
.00
100.0
200.0
300.0
400.0
500.0
SCALED TIME (MS)

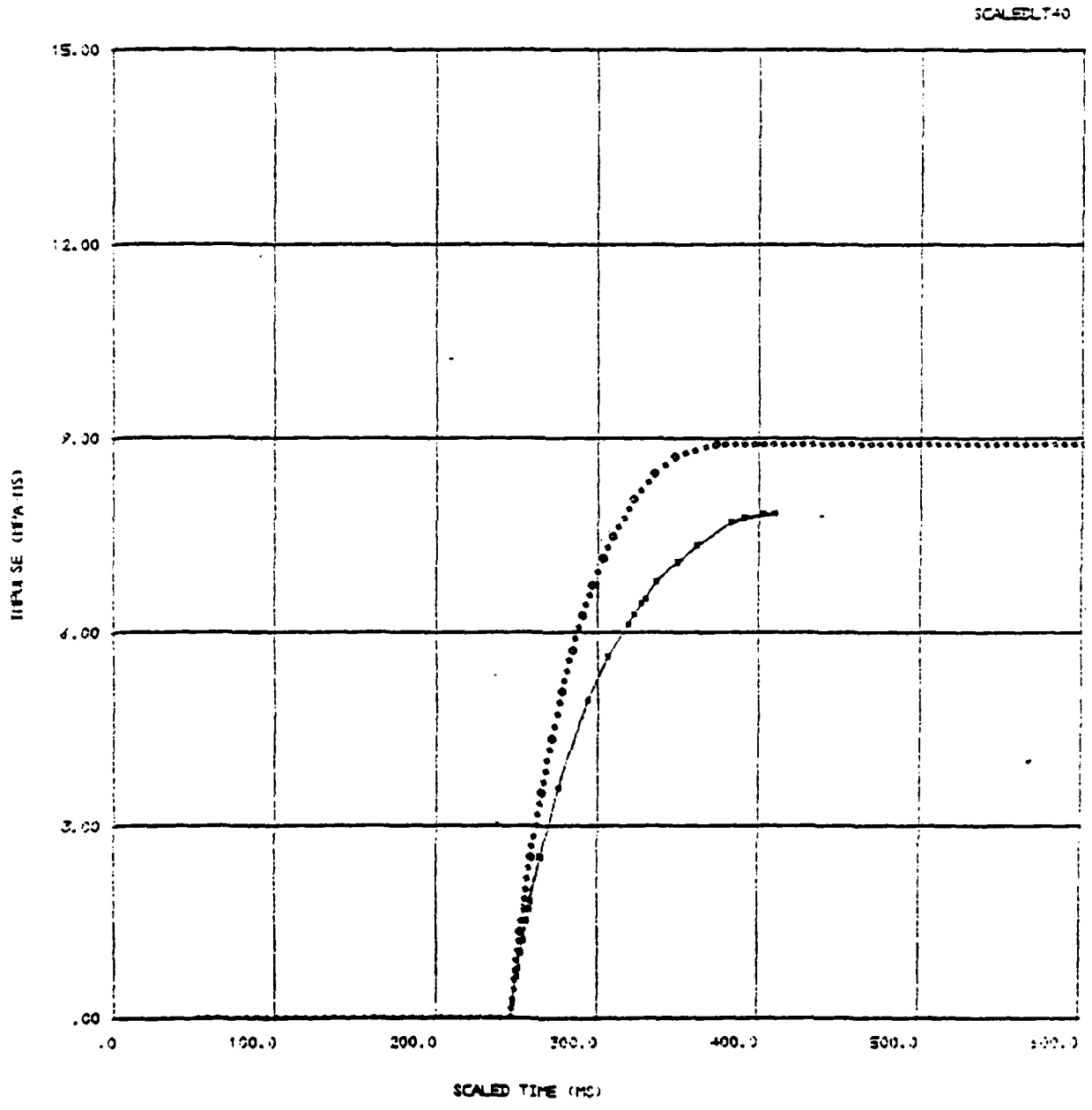
SHOT NO 2 1120 THURS 8 DEC 77
SCALED T40
15.00
12.00
9.00
6.00
3.00
.00
.0
100.0
200.0
300.0
400.0
500.0
SCALED TIME (MS)

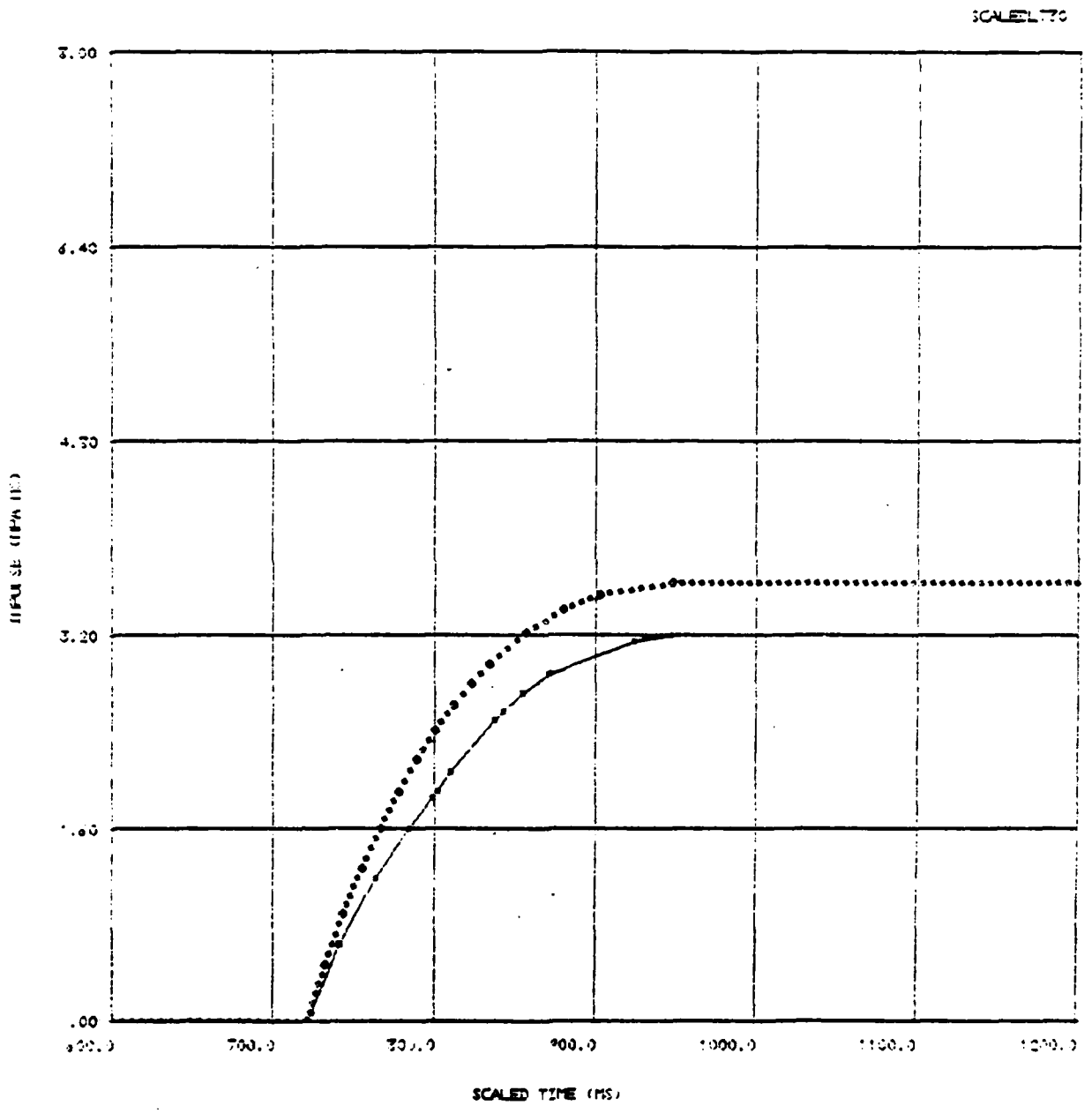
SHOT NO 2 1120 THURS 8 DEC 77
8.00
6.40
4.80
3.20
1.60
.00
700.0
900.0
1000.0
SCALED TIME (MS)

DISTRIBUTION LIST

DEPARTMENT OF DEFENSE

Assistant to the Secretary of Defense
Atomic Energy
ATTN: Executive Assistant

Defense Advanced Rsch. Proj. Agency
ATTN: TIO

Defense Intelligence Agency
ATTN: DT-1C
ATTN: DB-4C, E. O'Farrell
ATTN: DT-2

Defense Nuclear Agency
ATTN: SPTD
ATTN: SPAS
2 cy ATTN: SPSS
4 cy ATTN: TITL

Defense Technical Information Center
12 cy ATTN: DD

Department of Defense Explo. Safety Board
ATTN: Chairman

Field Command
Defense Nuclear Agency
ATTN: FCT
ATTN: FCPR
ATTN: FCTMOF

Field Command
Defense Nuclear Agency
Livermore Division
ATTN: FCPRL

Field Command Test Directorate
ATTN: FCTC

NATO School (SHAPE)
ATTN: U.S. Documents Officer

Undersecretary of Defense for Rsch. & Engrg.
ATTN: Strategic & Space Systems (OS)

DEPARTMENT OF THE ARMY

Chief of Engineers
Department of the Army
ATTN: DAEN-RDM
ATTN: DAEN-MCE-D

Deputy Chief of Staff for Ops. & Plans
Department of the Army
ATTN: MOCA-ADL

Harry Diamond Laboratories
Department of the Army
ATTN: DELHD-N-P
ATTN: DELHD-I-TL

U.S. Army Ballistic Research Labs.
ATTN: DRDAR-BLE, J. Keefer
ATTN: DRDAR-TSB-S
ATTN: DRDAR-BLT, W. Taylor
ATTN: DRDAR-BLV

DEPARTMENT OF THE ARMY (Continued)

U.S. Army Engr. Waterways Exper. Station
ATTN: Library
ATTN: WESSD, G. Jackson
ATTN: WESSA, W. Flathau
ATTN: J. Strange

U S. Army Material & Mechanics Rsch. Ctr.
ATTN: Technical Library

U.S. Army Materiel Dev. & Readiness Cmd.
ATTN: DRXAM-TL

U.S. Army Missile Command
ATTN: RSIC

U.S. Army Mobility Equip. R&D Cmd.
ATTN: DRDME-WC

U.S. Army Nuclear & Chemical Agency
ATTN: Library

XVIII Airborne Corps
Department of the Army
ATTN: F. Ford

DEPARTMENT OF THE NAVY

David Taylor Naval Ship R&D Ctr.
ATTN: Code L42-3
ATTN: Code 1844
ATTN: Code 17
2 cy ATTN: Code 1740.5, B. Whang

Naval Construction Battalion Center
ATTN: Code L51, R. Odello
ATTN: Code L08A

Naval Electronic Systems Command
ATTN: PME 117-21

Naval Facilities Engineering Command
ATTN: Code 04B
ATTN: Code 03T
ATTN: Code 09M22C

Naval Material Command
ATTN: MAT 08T-22

Naval Research Laboratory
ATTN: Code 8440, G. O'Hara
ATTN: Code 2627

Naval Sea Systems Command
ATTN: SEA-09G53
ATTN: SEA-0351
2 cy ATTN: SEA-0322

Naval Surface Weapons Center
ATTN: Code R14
ATTN: Code R14, I. Blatstein
ATTN: Code F31

Naval Surface Weapons Center
ATTN: Tech. Library & Info. Services Branch

DEPARTMENT OF THE NAVY (Continued)

Office of Naval Research
ATTN: Code 715
ATTN: Code 474, N. Perrone

Office of the Chief of Naval Operations
ATTN: OP 03EG
ATTN: OP 981

Strategic Systems Project Office
Department of the Navy
ATTN: NSP-43
ATTN: NSP-272

DEPARTMENT OF THE AIR FORCE

Air Force Geophysics Laboratory
ATTN: LWW, K. Thompson

Air Force Institute of Technology
ATTN: Library

Air Force Systems Command
2 cy ATTN: DLW

Air Force Weapons Laboratory
Air Force Systems Command
ATTN: SUL
ATTN: NTE, M. Plamondon
ATTN: NTES-C, R. Henny
ATTN: DEX

Assistant Chief of Staff
Intelligence
Department of the Air Force
ATTN: INT

Deputy Chief of Staff
Research, Development, & Acq.
Department of the Air Force
ATTN: AFRDQSM

Strategic Air Command
Department of the Air Force
ATTN: NRI-STINFO Library

DEPARTMENT OF ENERGY

Department of Energy
Albuquerque Operations Office
ATTN: CTID

Department of Energy
ATTN: OMA/RD&T

Department of Energy
Nevada Operations Office
ATTN: Mail & Records for Technical Library

DEPARTMENT OF ENERGY CONTRACTORS

Lawrence Livermore Laboratory
ATTN: Document Control for Technical Information Dept. Library
ATTN: Document Control for L-96, L. Woodruff

Los Alamos Scientific Laboratory
ATTN: Document Control for MS 364

DEPARTMENT OF ENERGY CONTRACTORS (Continued)

Sandia Laboratories
Livermore Laboratory
ATTN: Document Control for Library and Security Classification Division

Sandia Laboratories
ATTN: Document Control for 3141

OTHER GOVERNMENT AGENCY

Federal Emergency Management Agency
ATTN: Hazard Eval. & Vul. Red. Div., G. Sisson

DEPARTMENT OF DEFENSE CONTRACTORS

Aerospace Corp.
ATTN: Technical Information Services

BDM Corp.
ATTN: T. Neighbors
ATTN: Corporate Library

Boeing Co.
ATTN: Aerospace Library

California Research & Technology, Inc.
ATTN: M. Rosenblatt

California Research & Technology, Inc.
ATTN: D. Orphal

Civil Systems, Inc.
ATTN: J. Bratton

EG&G Washington Analytical Services Center, Inc.
ATTN: Library

Eric H. Wang
Civil Engineering Rsch. Fac.
ATTN: N. Baum

General Electric Company-TEMPO
ATTN: DASIAC

Geocenter, Inc.
ATTN: E. Marram

H-Tech Labs., Inc.
ATTN: B. Hartenbaum

IIT Research Institute
ATTN: Documents Library

Institute for Defense Analyses
ATTN: Library

JAYCOR
ATTN: H. Linnerud

Kaman Sciences Corp.
ATTN: Library

Lockheed Missiles & Space Co., Inc.
ATTN: T. Geers
ATTN: Technical Library

DEPARTMENT OF DEFENSE CONTRACTORS (Continued)

Lockheed Missiles & Space Co., Inc.
ATTN: TIC, Library

Lovelace Biomedical & Environmental Rsch. Inst., Inc.
ATTN: D. Richmond

Merritt CASES, Inc.
ATTN: J. Merritt

University of New Mexico
ATTN: CERF, G. Leigh
ATTN: CERF, N. Baum

Pacifica Technology
ATTN: J. Kent

Physics Applications, Inc.
ATTN: F. Ford

Physics International Co.
ATTN: F. Sauer
ATTN: E. Moore
ATTN: Technical Library

R & D Associates
ATTN: C. MacDonald
ATTN: J. Lewis
ATTN: R. Port
ATTN: Technical Information Center

Science Applications, Inc.
ATTN: Technical Library

Science Applications, Inc.
ATTN: J. Dishon

DEPARTMENT OF DEFENSE CONTRACTORS (Continued)

Science Applications, Inc.
ATTN: M. Knasel

Southwest Research Institute
ATTN: A. Wenzel
ATTN: W. Baker

SRI International
ATTN: G. Abrahamson
ATTN: B. Gasten

Systems, Science & Software, Inc.
ATTN: Library
ATTN: D. Grine
ATTN: R. Herrmann
ATTN: T. Pierce
5 cy ATTN: R. Sedgwick

TRW Defense & Space Sys. Group
ATTN: Technical Information Center
ATTN: D. Baer
2 cy ATTN: P. Dai

TRW Defense & Space Sys. Group
ATTN: E. Wong

Weidlinger Assoc., Consulting Engineers
ATTN: M. Baron

Weidlinger Assoc., Consulting Engineers
ATTN: J. Isenberg

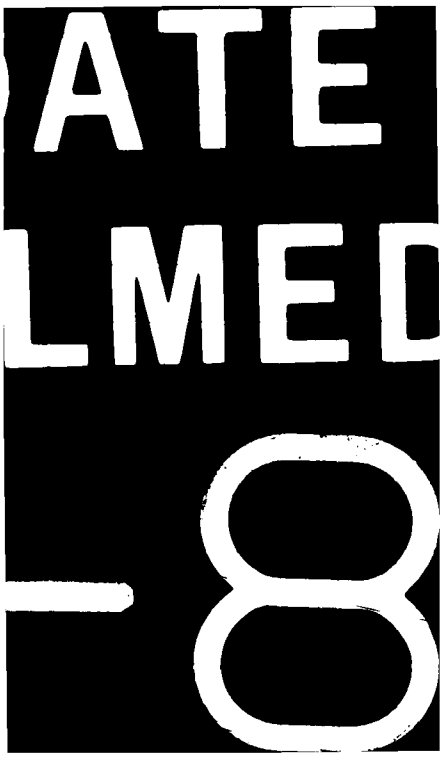
ATE
LMED
8